Summer 2014

Analysis and implementation of PM sampling methodology protocols to aid in the development of an ARP (Aerospace Recommended Practice) for aircraft non-volatile PM measurements

Brian Lowell Catron

Department:

ANALYSIS AND IMPLEMENTATION OF PM SAMPLING METHODOLOGY PROTOCOLS TO AID IN THE DEVELOPMENT OF AN ARP (AEROSPACE RECOMMENDED PRACTICE) FOR AIRCRAFT NON-VOLATILE PM MEASUREMENTS

by

BRIAN LOWELL CATRON

A THESIS

Presented to the Faculty of the Graduate School of the

MISSOURI UNIVERSITY OF SCIENCE AND TECHNOLOGY

In Partial Fulfillment of the Requirements for the Degree

MASTER OF SCIENCE IN AEROSPACE ENGINEERING

2014

Approved by

Dr. Umit O. Koylu, Co-advisor
Dr. Philip D. Whitefield, Co-advisor
Dr. Donald E. Hagen

ABSTRACT

Due to the growing concerns that particulate matter (PM) have on health and the environment, there is a need to include mass and number non-volatile PM measurements to current jet engine certification. This thesis looks at the necessary work required to help produce recommendations and perform background research to aid in the creation of an improved Aerospace Recommended Practice (ARP) (by the SAE E-31 Committee). This work addressed the following issues. The investigation began in the Missouri S&T Center of Excellence for Aerospace Particulate Emissions Reduction Research (COE) laboratory with an examination of the jet engine surrogate used, the miniCAST, as well as integrating it into the COE's PM measurement system. A clean PM sample line was aged by running a PM source through it until a steady state signal was measured by the instruments in order to make a recommended procedure for line conditioning as well as reconditioning. Several eductors were studied for their performance characteristics and compared against desired characteristics, which suggested a need to include a pressure relief valve to cap the sample pressure at the eductor entrance. A volatile particle remover (VPR) was studied for penetration and ability to remove volatile material. A prototype E-31 system was setup at the second alternative aviation fuel experiment (AAFEX II), which provided a direct comparison of probe tip dilution and downstream dilution and found comparable results when line loss was taken into account. Also performed at AAFEX II was a study that compared measured sample line penetration with theoretical calculations finding that theoretical calculations were an accurate alternative of measuring line loss. Two PM sampling systems were setup at an ARP demonstration and both system had similar results for both number and mass measurement. An instrument comparison was also performed that included an examination of condensation particle counter (CPC) cutoff size. It was also determined that a VPR was necessary to ensure that number instrument devices were only measuring non-volatile PM.

ACKNOWLEDGMENTS

I would like to dedicate this to my family and friends, whose unwavering support for my pursuits helped get me through hard times. To the University of Missouri - Rolla (as I originally knew it) Center of Excellence, thank you for your support, both financially and for your guidance since I started working back during my freshman year of college. To my advisers, Drs. Koylu, Whitefield, and Hagen, as well as Mr. Lobo, your help has been instrumental in helping me put this thesis together and ironing out its issues. I would also like to think the many people of the SAE E-31 committee, no matter how much or little they may have contributed to this endeavor. And to my painfully optimistic friend, your constant encouragement and cheerleading are always appreciated.

TABLE OF CONTENTS

Page

LIST OF ILLUSTRATIONS

Figure Page

LIST OF TABLES

1. INTRODUCTION

Due to concerns of health and environmental impacts from particulate matter (PM) emissions, there is a desire to have number and mass emissions reported for jet engines along side gaseous emissions that are currently required for engine certification in the aviation/aircraft industry. This thesis discusses the necessary work for a ARP to be developed in order to measure number and mass emissions. This work began by checking component performance and determining operating procedures. A couple of trial systems were then tested on jet engines, the first being compared to probe tip dilution and the second time consisting of two sampling system compared to one another.

The thesis begins with a review in Section 2 of current engine certification protocol. It then discusses briefly what is known on the health and environmental impacts of particulate matter emissions along with their relevant parameters. The discussion then moves to the current methodology along with instrumentation used for jet engine PM emissions measurement in a typical research setting. The last portion of the review examines current engine certification of diesel engine emissions. Section 3 discusses a conceptual PM emissions system merged with the current gaseous measurement system. This concept system utilizes the current probe setup to greatly reduce the cost of implementation.

The series of experiments begins in Section 4, with a series of experiments conducted in the Missouri S&T Center of Excellence for Aerospace Particulate Emissions Reduction Research laboratory. This section begins with a look at the jet engine surragate used in the proceeding experiments conducted at Missouri S&T. The remaining experiments focus on component checks of sample line performance, eductor selection and performance, and the use of a catalytic stripper to remove volatile PM

emissions. Section 5 examines a prototype E-31 PM sampling setup using a jet engine as the source performed at AAFEX II. This section focuses on a probe tip vs. downstream dilution study as well as a comparison of measured and theoretical line loss. The final section of the experiment series, Section 6, looks at the results of two different E-31 setups at SR Technics in Zurich, Switzerland, and their agreements with each other. It also looks at an instrument comparison, examining the agreement of several types of mass and number instrument likely to be used in an E-31 deployment.

2. LITERATURE REVIEW

This section examines the current state of research relevant to PM measurement methodology and impact of PM emissions on health effects and environmental issues. Current aircraft engine certification protocol for gaseous pollutants emissions and smoke number, exhaust plum visibility, are discussed first. Next, the impact of PM on local environment and human health will be discussed along with how smoke number fails to provide any meaningful insight to how aircraft smoke emissions affect these delicate issues. This leads into discussion of a new protocol for measure of mass, number, size, and composition of aircraft PM emissions. The last section examines current diesel engine PM measurement techniques, a comparison of diesel and aircraft PM emissions, and how some of some of these techniques could be used for aircraft PM emissions in terms developing the sampling and measurement protocols.

2.1. ICAO AIRCRAFT ENGINE EMISSIONS CERTIFICATION

Aircraft engines, both for subsonic and supersonic propulsion, are certified based on a variety of criteria including but not limited to noise and emissions. The International Civil Aviation Organization defines the international standards and recommends practices for emissions certification in Annex 16 To The Convention On International Civil Aviation - Volume II [1]. Annex 16 sets regulatory limits for PM emissions (covered in Annex 16 as smoke) and gaseous emissions. Both smoke and gaseous emissions measurements can be performed simultaneously provided it is shown to be valid when compared to sequential measurements. Engines are certified for emissions at levels corresponding to the landing take-off (LTO) cycle, which approximates engine power conditions typical at an airport from aircraft landing through subsequent take-off. This LTO cycle gives an idea of local impact by aircraft

operations. For subsonic propulsion the LTO cycle consists of four operation modes: take-off (100% of F_{00} for 0.7 minutes), climb (85% of F_{00} for 2.2 minutes), approach (30% of F_{00} for 4.0 minutes), and taxi/ground idle (7% of F_{00} for 26.0 minutes), where F_{00} is the rated power output.

2.1.1. Gaseous Emissions. Annex 16 [1] regulates the gaseous emissions of unburned hydrocarbons (UHC), carbon monoxide (CO), and oxides of nitrogen (NO_X). These emissions levels are based on whether the engine is intended for subsonic or supersonic propulsion, date of manufacture (only used for NO_X), engine pressure ratio, and maximum rated thrust. Although not regulated, carbon dioxide (CO_2) is also measured for the purposes of performing a carbon balance check. The regulated emissions levels of NO_X as shown in Figure 2.1, were originally set by ICAO in 1986 and have subsequently been lowered by ICAO Committee on Aviation Environmental Protection (CAEP) as part of CAEP/2, CAEP/4, CAEP/6 in 1991, 1998, and 2004, respectively. The emission level of NO_X will be further lowered in 2014 as part of CAEP/8.

The gaseous emissions sampling and measurement system is shown in Figure 2.2. The probe assembly must have at least 80% of the pressure drop occur at the orifices with a minimum of 12 sampling points within half a nozzle diameter of the exhaust plane. The sample line must have a transient time less than 10 seconds and be maintained at a temperature of 160°C [1].

2.1.2. Smoke Emissions. Aircraft smoke emissions are represented by a parameter called smoke number (SN) as defined in SAE ARP1179 [2]. Smoke number is a means to quantify plume visibility and provides a regulatory standard to reduce plume visibility. Engine characteristic smoke numbers [3] have decreased over time as shown in Figure 2.3. While a 40% reduction in characteristic smoke number is shown, the uncertainty in the smoke number measurement method is reported as ±3 [2], resulting in no statistically meaningful reduction in characteristic smoke number.

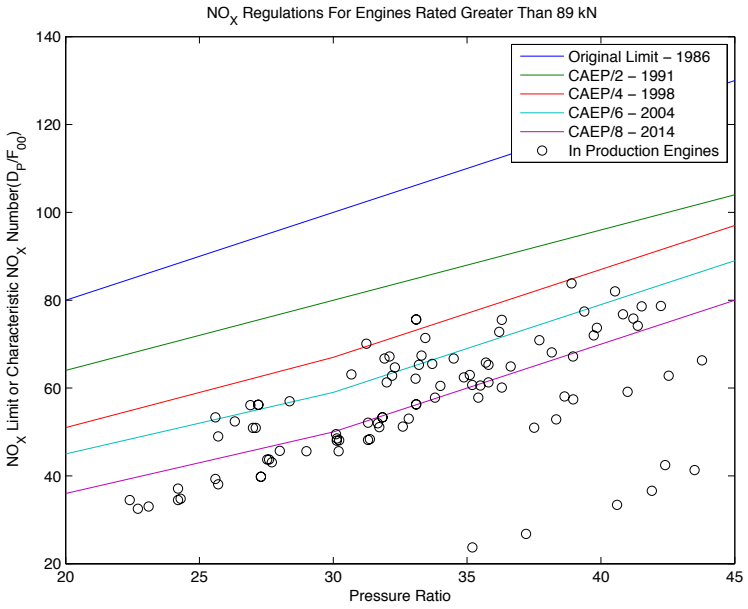

Figure 2.1: Various limits of characteristics NO_X emissions for engines with a rated output greater than 89 kN or 20000 lbs. and in production engine data.

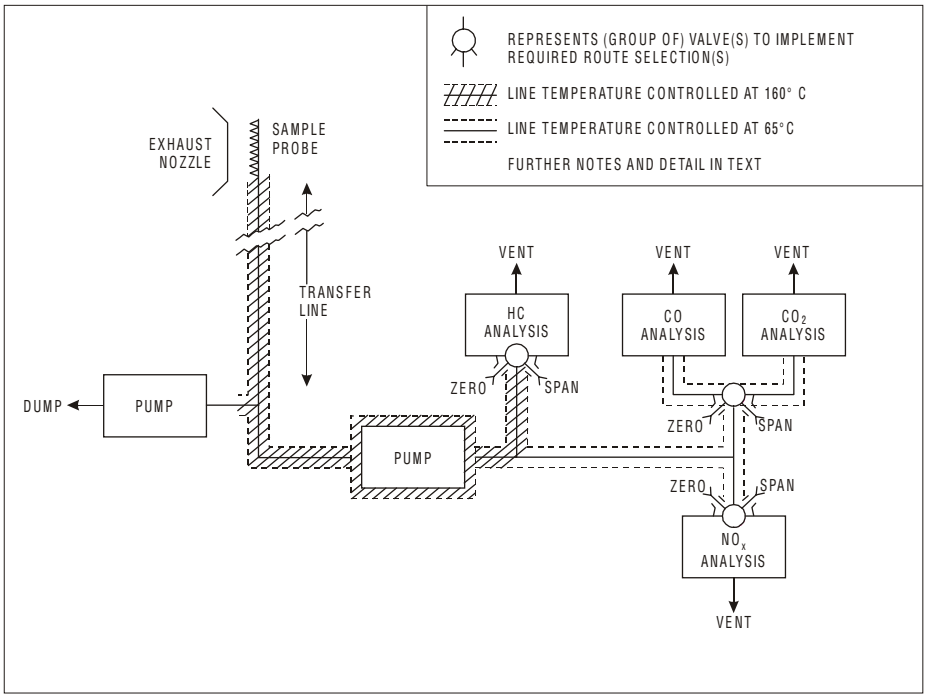

Figure 2.2: Schematic of gaseous emissions sampling and analysis system [1].

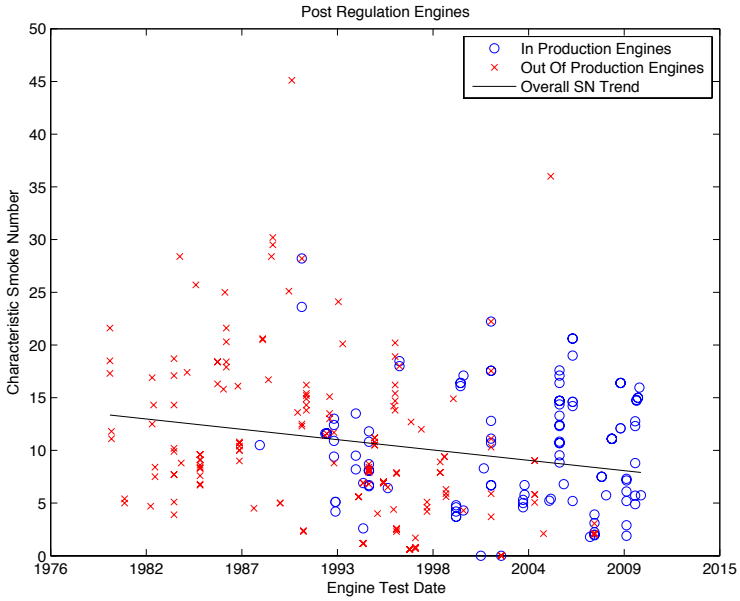

Figure 2.3: Engine characteristic smoke number by engine test date.

Smoke number is a function of the filter reflectance before and after exposure to 16.2 kg of exhaust gas per square meter of filter. A minimum of three readings are made at 16.2 kg/m^2 or a least squares straight line of at least three readings between 12 and 21 kg/m^2 evaluated at 16.2 kg/m^2 [1]. The smoke number at a single filter loading, SN', is given in Eq. 2.1,

$$SN' = 100\left[1 - \frac{R_S}{R_W}\right] \tag{2.1}$$

where R_S is the absolute reflectance of the sample spot and R_W is the absolute reflectance of the clean filter.

Once the smoke number is determined for each of the modes of operation, a characteristic smoke number is given in Eq. 2.2

$$\text{Characteristic Smoke Number} = \frac{max(SN)}{1 - \frac{0.15736}{\sqrt{i}}} \tag{2.2}$$

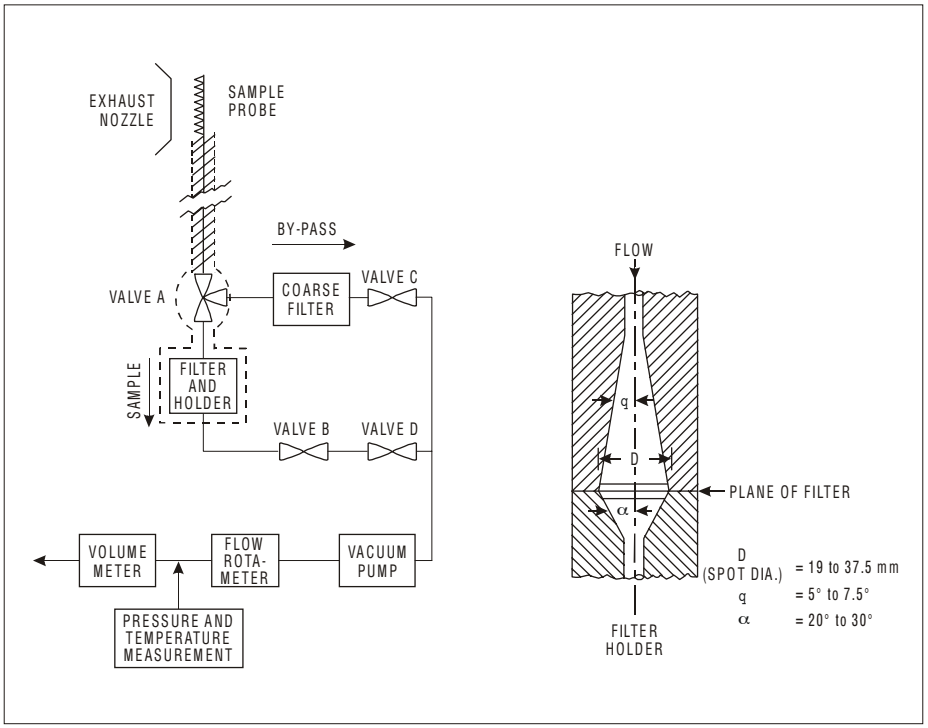

Figure 2.4: Schematic of smoke emissions sampling and analysis system [1].

where i is the number of engines tested. If the number of engines tested is less than three, the maximum smoke number is weighted more severely such that denominator equals 0.7769 for one engine or 0.8527 for two engines. This characteristic smoke number is compared to the regulatory limit for smoke number, which is defined by Eq. 2.3

$$\text{Regulatory Smoke Number} = 83.6\,(F_{00})^{-0.274} \tag{2.3}$$

or a value of 50, whichever is lower. The smoke emissions measurement system, shown in Figure 2.4, utilizes the same sample probe and sample line specifications with an added caveat that any bends need to be at least 10 times the internal diameter of the line in order to reduce particle loss. This allows for simultaneous gas and smoke measurements.

2.2. IMPACT OF PARTICULATE MATTER

Several studies have examined aircraft emissions impact on local communities downwind of airports. A study at Los Angeles International Airport (LAX) [4] found substantially higher average counts of ultra fine particles (UFP) of approximately 50,000 particles/cm^3, 500 m downwind of the airport compared to the upwind side ranging from 580 to 3800 particles/cm^3. Peaks in ultra fine particle counts were observed, corresponding to aircraft take-offs and landings, reaching a maximum of 4.8×10^6 particles/cm^3 downwind of aircraft take-offs. This study also found that black carbon (BC), NO_X, and particle-bound polycyclic aromatic hydrocarbon (PB-PAH) were slightly elevated at the same site. Upwind of LAX, the particle size distribution had a mode around 90 nm, while downwind the primary mode was around 10-15 nm. Another study [5], also at LAX, found rapid fluctuations in particle counts ranging from 18,000 to 600,000 particles/cm^3 at sites a half mile from the runway corresponding with aircraft landings. This study also examined particle counts adjacent to the I-710 freeway with counts ranging from 5,000 to 100,000 particles/cm^3. Aircraft number emissions have a greater impact downwind than highway traffic. A study at a general aviation airport [6] found 60 second average concentrations from jet departures resulted in UFP of 2.2×10^6 particles/cm^3, PB-PAH of 440 ng/m^3, and BC of 30 μg/m^3 at 100 m downwind of the runway and up from background readings by a factor of 440, 90, and 100 respectively. The primary mode for the size distribution was around 11 nm, half of the 22 nm from heavy diesel plumes. Aircraft PM emissions typically produce sizes smaller than 400 nm [7].

2.2.1. Health Impact. Several epidemiological and toxicological studies have shown links between health effects and airborne PM. Short-term exposure to airborne PM can aggravate existing pulmonary and cardiovascular conditions, while long-term exposure can lead to cardiovascular disease and death [8]. Significant levels of

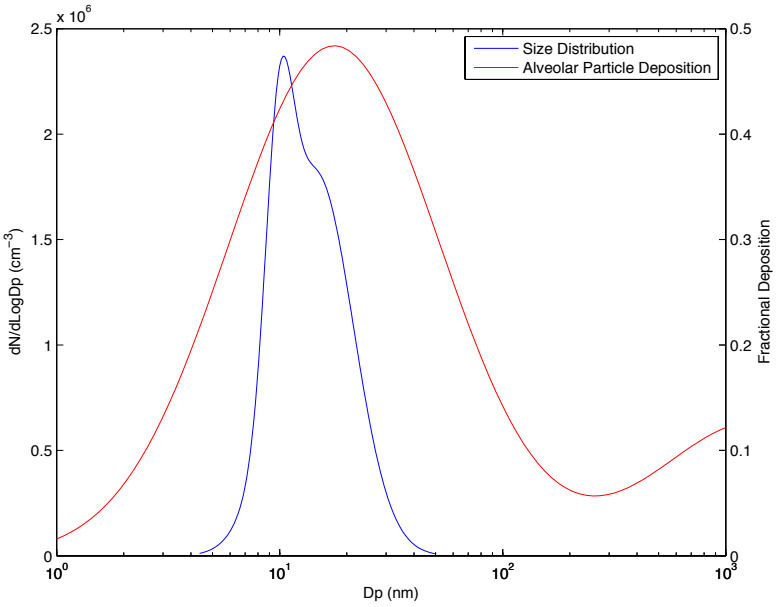

Figure 2.5: ICRP lung deposition model for the alveolar region along with a typical downstream aircraft exhaust plume.

toxins are brought into the body by ultrafine particles and promote inflammatory responses [9]. The International Commission on Radiological Protection (ICRP) developed a model for determining particle deposition in the human respiratory tract commonly referred as ICRP 66 [10]. Many ultrafine particles deposit deep in the respiratory tract, as shown in Figure 2.5. The figure shows an averaged version [11] of the ICRP 66 lung deposition model of aerosols in specifically the alveolar region, where oxygen enters the blood. Also shown is a bimodal fit to a representative size distribution [6] downstream of the Santa Monica Airport in dense residentially neighborhoods. A majority of the particles show a greater than 30% deposition rate in the alveolar region. Ultrafine particles can rapidly pass into the blood and tend to collect in the liver and bladder after leaving the lungs [12]. Particle number concentrations, especially in the ultrafine range, appear to be a main index of toxicity [13]. These

ultrafine particles become increasing reactive and toxic due to their large surface area to volume ratio when compared to more coarse particles.

2.2.2. Environmental Impact. Particulate matter emissions impact the environment on two levels. The first is the local impact on visibility by build-up of suspended particles [14]. In Austria, particles were determined to be the cause of 90% of light scattering in rural areas and 99% in urban areas [15]. Gaseous pollutants account for a relatively small amount of light scattering [16]. Most of the research into particle impact on visibility has been in correlating mass concentrations to reduction in visibility [13]. The second is on the global environment impact. Soot particles have a radiative forcing of +0.34 W/m^2, putting them as a major contributor to global warming [17]. If soot particles are covered in sulphate or organic compounds, which is common, their radiative forcing increases to +0.6 W/m^2 [18].

2.2.3. Inadequacies of Smoke Number. Smoke number provides only a relative measure of smoke intensity and does not have a basis in fundamental particle characteristics. It was developed to provide a measure and regulatory means for reducing exhaust plume visibility, essentially making them invisible [2]. With increased concern of health and environmental effects, particle mass, number, size, and composition become more relevant. Smoke number is unable to differentiate technology improvements as shown in Figure 2.6, while other techniques have been shown to differentiate between different engine types of the same family of engines [19].

While steps are taken to ensure constant filter loading, the smoke number can be inherently lowered by playing with the filter diameter. Annex 16 calls for 14 $\pm$ 0.5 lpm of exhaust gas through the filter and when the filter diameter is changed, the speed at which the gas flows through the filter is also changed. The speed of the gas has a large effect on the filter efficiency, as shown in Figure 2.7. These calculations were made with Aerosol Calculator [20] at conditions that would be present when performing simultaneous gas and PM measurements.

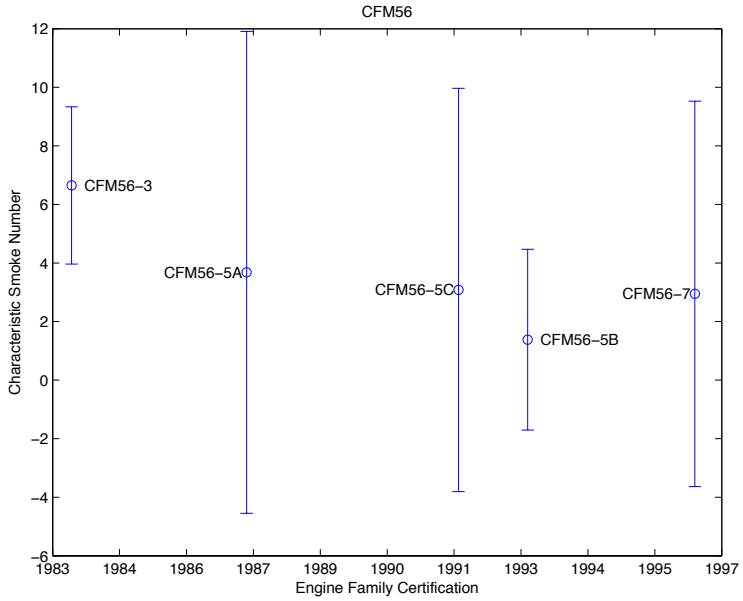

Figure 2.6: CFM56 engine families by engine family certification date.

2.3. RELEVANT PARAMETERS

From the previous section, particle mass, number, size, and composition are the most relevant parameters for defining regulatory limits. Chemical composition has significant effect on both health and environmental effects. In order to make an assessment of aircraft emissions impact at an airport without performing additional measurements, the First Order Approximation (FOA) was developed to correlate mass emissions with smoke number [21] from several tests [22, 23, 24] and ICAO data and shown in Eq. 2.4,

$$CI = 0.1573 \cdot SN^{1.8004} \tag{2.4}$$

where CI is the concentration index (mg/m^3). The FOA has been improved, resulting in FOA3.0a [25]. The portions of FOA3.0a relevant to non-volatile PM are shown in

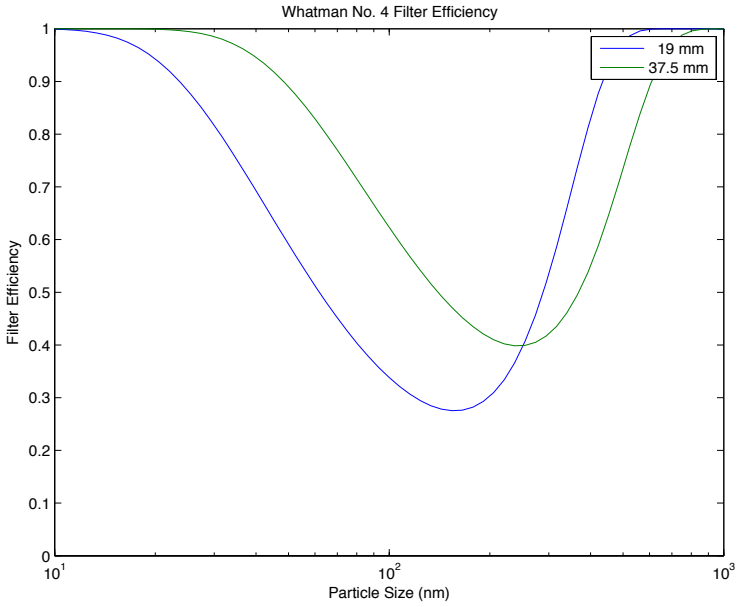

Figure 2.7: Aerosol Calculator [20] analysis of the filter efficiency of the Whatman No. 4 filter under typical conditions for an ICAO smoke measurement system for the minimum and maximum filter diameters.

Eqs. 2.5 - 2.8.

$$CI = 0.0694 \cdot SN^{1.23357} \text{ (for } SN \leq 30) \tag{2.5}$$

$$CI = 0.0297 \cdot SN^2 - 1.802 \cdot SN + 31.94 \text{ (for } SN > 30) \tag{2.6}$$

$$Q = [0.776 \cdot AFR + 0.733]\,(1 + \beta) \tag{2.7}$$

$$EI_{non-vol} = Q \cdot CI \tag{2.8}$$

Where Q is the core exhaust volume (m^{-3}), AFR is the model air-to-fuel ratio, β is the bypass ratio, and $EI_{non-vol}$ is the Emission Index of non-volatile PM (mg/kg_{fuel}). The FOA3.0a is designed to determine local air quality and the impact that aircraft have on it and includes EI calculations for volatile components as well. While the FOA allows aircraft emissions impact modeling, it does this only on a mass basis. Composition of PM emissions is partially captured with FOA3.0a but still does not

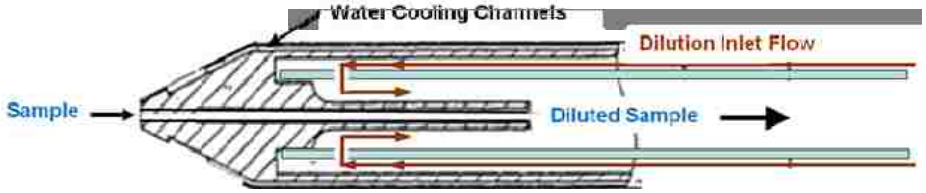

Figure 2.8: Current PM probe concept [26].

provide insight to particle number and size, which is important for assessing health and environmental impacts.

2.4. PARTICULATE MATTER SAMPLING METHODOLOGY

The SAE E-31 committee has developed sampling and measurement techniques for non-volatile PM emission in the Aerospace Information Report (AIR6037) [26], which provides descriptions of techniques for determining mass, particle size, and number measurements. There are two groups in which PM emitted from gas turbine engines are classified, non-volatile and volatile. Non-volatile PM is primarily carbonaceous matter from the combustion process, while other non-volatile particles including atmospheric particles ingested by the engine and metals may also be present. Volatile PM is composed of organics and sulfur compounds that forms as the exhaust cools [27]. The temperature threshold for volatile PM is defined as 350°C, that being, all PM present above this temperature is by definition non-volatile. The preferred method of sample collection is via probe extraction with probe-tip dilution, schematic shown in Figure 2.8. Sample dilution lowers the particle concentration to a level at which the instruments can operate while also preventing gas-to-particle conversion (formation of volatile PM or water condensation), reducing particle-to-particle interactions, and reducing particle diffusion losses. An undiluted probe could be used for PM sampling if dilution is added within a few meters. The dilution ratio can be determined two ways, (1) from the sample and dilution flow

rates, or (2) from comparing the undiluted and diluted CO_2 values, both are shown in Eq. 2.9.

$$DR = \frac{Q_S}{Q_S + Q_D} = \frac{Q_S}{Q_T} = \frac{CO_{2_{UNDIL}}}{CO_{2_{DIL}}} \tag{2.9}$$

Here Q_S, Q_D, and Q_T are the sample, dilution, and total volumetric flow rates, and $CO_{2_{UNDIL}}$ and $CO_{2_{DIL}}$ are the undiluted and diluted measure of CO_2 concentration. The sample line is at ambient temperature and has a large diameter in order to reduce particle diffusion loss.

2.4.1. Particulate Matter Mass Detection. Several instrument technologies have been developed for real-time mass measurement. Non-volatile PM emissions is made up of elemental carbon and organic carbon. At take-off conditions the non-volatile PM is nearly 100% elemental carbon, while at idle conditions the PM is approximately 10% elemental carbon and 90% organic carbon [28]. Traditionally PM has been measured on a mass basis by performing gravimetric analysis, weighing a filter before and after PM deposited on the filter. The gravimetric process requires careful filter handling and the measurement of measure total (volatile and non-volatile) PM mass with a repeatability of $\leq$0.25 μg [26]. By baking the filter and measuring carbon-dioxide outgassing, the total mass can be broken down into constituent parts. Multi-Angle Absorption Photometry (MAAP) [29] measures elemental carbon mass concentration based on light absorption and scattering. Elemental carbon primarily absorbs light, while organic carbon and volatile components typically scatter light. Laser-Induced Incandescence (LII) [30] measures black carbon mass concentration based on emitted light of particles after heating them between 2500 to 4500 K. This technique evaporates volatile matter that has formed on the outside of the non-volatile PM. PhotoAcoustic Soot Sensing (PASS) [31] periodically heats black carbon with a laser. This heating and cooling of soot produces pressure fluctuations, which are picked up by a microphone.

2.4.2. Particulate Matter Number Detection. Particle number counts are usually done with a Condensation Nucleus Counter (CNC) [32] measuring number of particles per volume. These devises are often referred to as Condensation Particle Counters (CPC). CPCs count particle by coating the outside of the particle with the working fluid, typically butanol, and increase the size of the particle to a sufficient size for optical detection. Different model CPCs have different size cut-offs, minimum size particle capable of detection. This detection limit allows counter to exclude particles in the nucleation mode. To count non-volatile PM below the limit for the accumulation mode, a Volatile Particle Remover (VPR) needs to be used if volatile PM condensation occurs.

2.4.3. Particulate Matter Size Detection. Knowledge of the PM size distribution, concentrations at various sizes, is necessary for assessing health impacts. Several types of instrumentation have been developed for determining the PM size distribution. A Scanning Mobility Particle Sizer (SMPS) [33] is comprised of two main components, (1) a Differential Mobility Analyzer (DMA) and (2) a particle counter. The DMA subjects particles to electrostatic forces, sorting particles out by size so that the particle counter gets one size to determine for a given electrostatic force. The size distribution is determined by varying the electrostatic force and counting the number of particle at each force value. Another devise is often added in front of the DMA in order to cause the particle to have a known charge distribution, resulting in a more accurate sample. A Rapid Mobility Particle Sizer (RMPS) [34] functions similar to the SMPS but uses a constant electrical field and cascaded electrometers to simultaneously count the particles at a variety of sizes. Both the SMPS and RMPS measure mobility diameter, D_m, which is equal to the geometric diameter, D_g, because non-volatile aircraft engine PM is essentially spherical [35].

2.4.4. Particulate Matter Light Impairment Detection. Local environmental impact by PM emissions generally focuses on visibility impairment.

Several instruments have been developed for measuring an aerosols impact on visibility. Particle Soot Absorption Photometer (PSAP) [36] measures a change in optical transmittance of a filter as PM is deposited. Cavity Attenuated Phase Shift (CAPS) [37] measures light extinction (light scattering and absorption) as a sample passes through an optical cavity.

2.4.5. Particulate Matter Chemical Composition Detection. Chemical composition plays an important roll in both health and environmental impact and knowing the chemical composition would allow for increased ability to assess PM potential detrimental impact. The Aerosol Mass Spectrometer (AMS) [38] was developed for this purpose. It detects aerodynamic particle size by measuring the time-of-flight of a particle in a vacuum. Chemical composition is determined by performing mass spectrometry on ionized vapors of the volatile and semi-volatile particles.

2.5. DIESEL PARTICULATE EMISSIONS MEASUREMENT

Diesel engines currently have a standard in place for both mass and number measurement of PM emissions and this standard can assist in developing aircraft PM emissions standard, as aircraft engine PM have similar characteristics to diesel engines [26]. European PM measurement and regulation began under the Particle Measurement Programme (PMP) [39]. European emission limits for gas and particles along with measurement standards are contained in Regulation No.83 of the United Nations Economic Commission for Europe [40]. Part 1065 of Title 40 of the United States Code of Federal Regulations [41] contains corresponding emission limits and measurement standards. Both U.S. and European regulations have similar measurement standards.

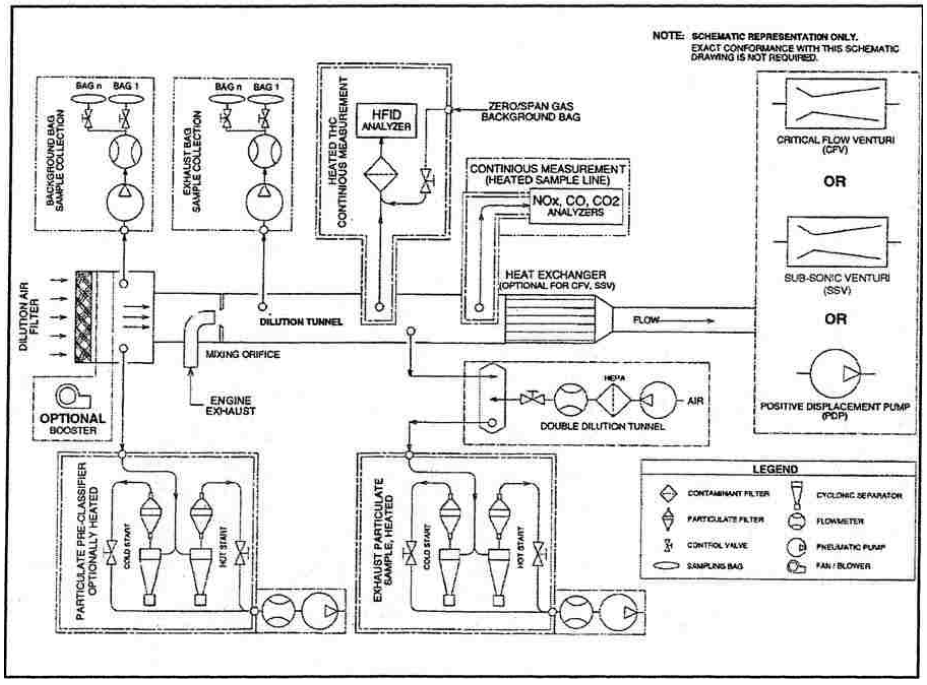

Figure 2.9: Internal combustion engines exhaust measurement system schematic from U.S. Code of Regulations [41].

The measurement system, shown in Figure 2.9 as depicted in the U.S. Code of Regulations, vents the exhaust gas into a Constant Volume Sampler (CVS) tunnel. The CVS tunnel dilutes the exhaust gas with a known dilution ratio of clean air. After the exhaust gas is well mixed with the dilution air, sample is taken off for gaseous and PM measurement. Typically, the PM sample is diluted a second time before analysis where it can be measured by gravimetric analysis or in-situ analyzers. Particle number counts are performed with mass analysis, although a size cut-off at 23 nm is required to exclude volatile PM in the nucleation mode [42]. This nucleation mode prevents accurate measurements of particle number and size with dilution tunnel measurements while tailpipe measurements do not exhibit these issues [43].

3. CONCEPT PARTICULATE MATTER MEASUREMENT SYSTEM

The concept system is designed for simulations gaseous and PM sampling and measurement. The design should meet the required design considerations as discussed in the Section 3.1. The concept system is described in detail in Section 3.2.

3.1. DESIGN CONSIDERATIONS

In the development of a PM measurement system, many considerations need to be taken into account. The most important is the accurate measurement of PM mass and number without jeopardizing gaseous emissions measurement. For accurate measurement of PM, sample dilution and line loss considerations need to be taken into account. The system should not alter the sample between probe tip and instruments.

3.1.1. Sample Dilution. There are several reasons for dilution of the PM sample, including instrumentation range, volatile PM formation, and others. Number instruments have a fairly limited range which raw engine exhaust greatly surpasses. CPCs typically have two ranges for particle counting, single particle counting up to 10^5 #/cc and a photometric mode up to 10^7, while raw engine exhaust can get up to concentration of 10^8. Typical CPCs have an accuracy of $\pm 10\%$ for single particle counting and $\pm 20\%$ for photometric mode. The method of diluting the sample for PM measurements should be prevented from back purging the sample line and introducing diluent into the gaseous measurement lines.

3.1.2. Particle Line Loss Considerations. The primary means of particle loss in the sample transfer line is due to diffusion loss [26], which is initially caused by particle impaction and adhesion to the transfer line wall. This causes a concentration gradient with low concentration near the wall, resulting in particles to diffuse to the wall. Another important means of particle loss is thermophoresis, where any

temperature gradient tends to cause particles to move to a region of lower temperature. Inertial impaction is the result of a particles inertia causing it to not follow gas streamlines in a bend. A charged particle can be attracted to the wall through electrostatic deposition. Particle coagulation occurs when multiple particles collide and adhere to each other, reducing the number concentration and altering the size distribution. Gravitational settling can effect particles but this, at the sizes present in gas turbine engine exhaust, is negligible.

Most of the means of particle loss can be significantly reduced. Diffusion loss mostly affects small particles, causing number concentration to drop significantly, and can be reduced by minimizing the sample residence time by using short transfer line and high flow rates. Thermophoresis can be reduced by lowering the sample temperature quickly through dilution and then maintaining a constant transfer line temperature. Inertial impaction affects large particles and can be reduced by using mostly straight sections and large radius bends (at least greater than 10 times the tubing diameter). The use of non-isolated electrically conductive lines can almost completely mitigate electrostatic deposition. The use of sample dilution lowers particle concentration and greatly reduces the chances of particle coagulation[11]. All of these methods of particle loss can be modeled using Aerosol Calculator[20]. Theoretical model calculations have been shown to produce similar results to line loss measurements using either diesel exhaust or NaCl particles [26].

3.1.3. Engine Manufacturer's Requirements. Annex 16 currently requires gaseous sampling and thus the engine manufactures have sampling systems set up for gaseous measurements. It is preferred by engine manufactures to avoid costly retooling of their test facilities by introducing probe tip dilution PM sampling to their set up. Probe tip dilution can also prevent simultaneous gaseous and PM measurement and could double the amount of time needed for engine testing. In order to allow for simultaneous sampling and avoid building a new sample probe assembly,

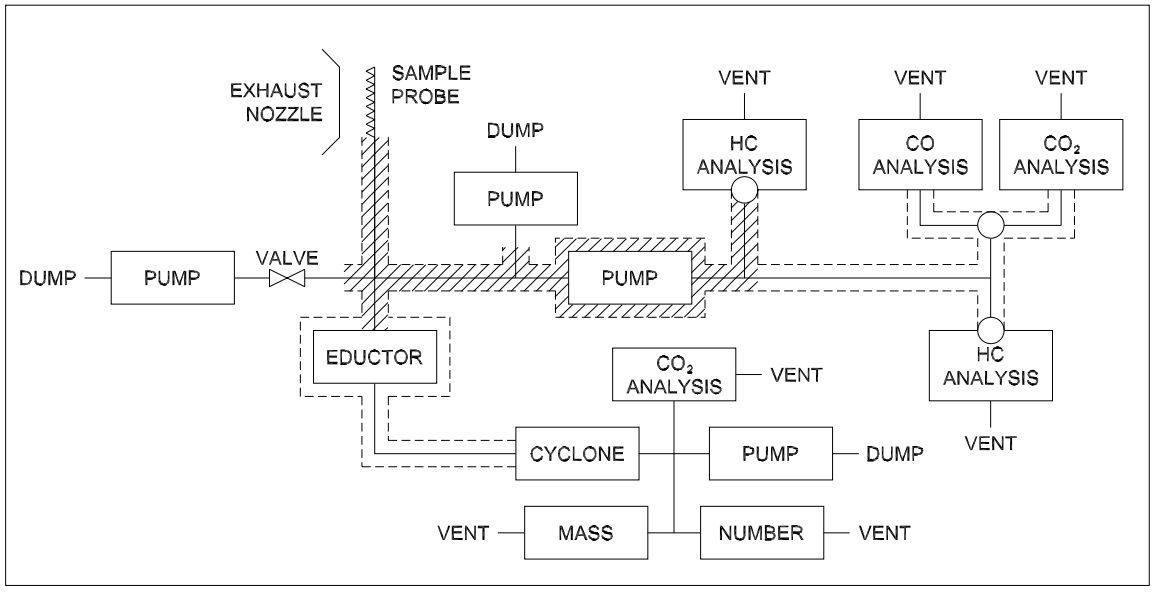

Figure 3.1: Concept system for simultaneous measurement of particulate matter and gaseous emissions.

downstream dilution is a requirement. The diluter should extract about 2 lpm of sample flow from the gaseous line as well as pose minimal risk of introducing diluent into the gaseous sample line.

3.2. CONCEPT SYSTEM

The concept system shown in Figure 3.1. The first section, from the probe tip to the main splitter (shown just above the eductor), is a portion of the Annex 16 line, where the main splitter is essentially a drop in component in the gaseous transfer line. The second section, from the main splitter to the eductor, carries just the PM sample the short distance to the eductor. The third section, from the eductor to the cyclone, is the main PM transfer line and brings the sample into the instrumentation

room. The forth section, from the cyclone to the instruments, splits the PM sample and brings it to each instrument.

3.2.1. Probe Tip To Main Splitter. The concept system is designed to be identical to an Annex 16 system up through the main splitter. This is to minimize the retooling costs by the engine manufacturers. The transfer line between the probe assembly and the main splitter should be as short as possible. The main splitter divides the sample into three segments. The first segment goes to a pressure regulating valve, such that when the engine is at idle (lowest exhaust pressure) the valve is fully closed. When the exhaust pressure goes up with higher power settings, the valve opens in order to maintain the same pressure that was at idle. Another segment goes to the gaseous analysis systems as required by Annex 16. The last segment is a straight through leading to the PM sample system. The main splitter is just a drop in on the Annex 16 gaseous transfer line, such that the gaseous analysis system from probe tip to analyzers should still meet all requirements of Annex 16. As required by Annex 16, the sample in this section should be maintained at 160°C except for the distance required for the sample to cool from exit plane temperatures. As portions of this section will be at exhaust plane temperatures, the line should be constructed of stainless steel.

3.2.2. Main Splitter To Eductor. The straight through on the main splitter is for the PM sample which leads to the eductor. The line from the main splitter to the eductor should also be as short as possible. The sample should remain at 160°C until it reaches the eductor, and the transfer line between the main splitter and the eductor should also be made of stainless steel.

3.2.3. Eductor To Cyclone. The transfer line from the eductor to the cyclone will likely be the longest and runs the sample into the instrumentation room. This transfer line should be constructed similar to the smoke analysis line in Annex

16, built of a electrically conductive material, i.e. stainless steel, copper, or carbon-loaded grounded polytetrafluoroethylene (PTFE).

3.2.4. Cyclone To Instrumentation. The primary purpose of the cyclone is to remove particles larger than $\sim$2.5 μm. As combustion PM emissions does not exist at this level or above, metal from erosion and engine wear could exist at this level and should be removed while allowing the sample to continue on to the instruments. The transfer line between the cyclone and instrumentation should be short and free of sharp bends. It should be constructed in a manner similar to other parts of the overall transfer line.

3.2.5. Instrumentation. The instrumentation suite contains a mass and a number instrument along with a volatile particle remover (VPR) in front of the number instrument and a CO_2 analyzer for determining the dilution ratio. Mass instruments should be capable of measuring a diluted sample between 0 and 50 mg/m^3. Number instruments should measure between 0 and 5x10^4 particles/cm^3, additional dilution at the device may be necessary to bring the concentration to an acceptable level. The CO_2 detecter should be have a range of 0 to 2x10^5 ppm.

4. MISSOURI S&T IN-HOUSE EXPERIMENTS

Missouri S&T Center of Excellence for Aerospace Particulate Emissions Reduction Research (COE) performed a series of in-house experiments during the development of the E-31 ARP for PM measurement. The experiments primarily used a miniCAST model 6203 Type C as a jet engine surrogate PM source. Some early experiments used COE's diesel generator as the PM source.

4.1. EXPERIMENT SUMMARY

The basic experiment setup is shown in Figure 4.1. The system begins with the PM source, miniCAST, which exhausts into the heat treatment plenum which is heated to further emphasize the jet engine exhaust simulation. The heat treatment plenum has 2 probe ports which can be filled with any combination of reference probes (probe tip dilution) and OEM probes (gaseous probes). There is also an exhaust at the far back end of the plenum pulling flow past the probes. There are 2 sample lines running from the probes into the sampling system.

At the entrance of the sampling system, there is a group of valves to select a probe to sample from and dump the other. The sampling system contains 2 Cambustion DMS 500s, one which has a thermal discriminator in front of it, a Sable Systems CA-2A, a TSI 3071 DMA, and a TSI 3775 CPC.

Sections 4.2-4.5 deal with checking the aircraft engine surrogate used over the course of the in-house experiments. The experiments started with verifying the source with the stability and reproducibility experiment. The first group of experiments after the source verification involved checking the setup from source output to sampling lines. The first experiment of the group was to verify that the source is decoupled from the sampling system such that any change in the sampling system does not alter

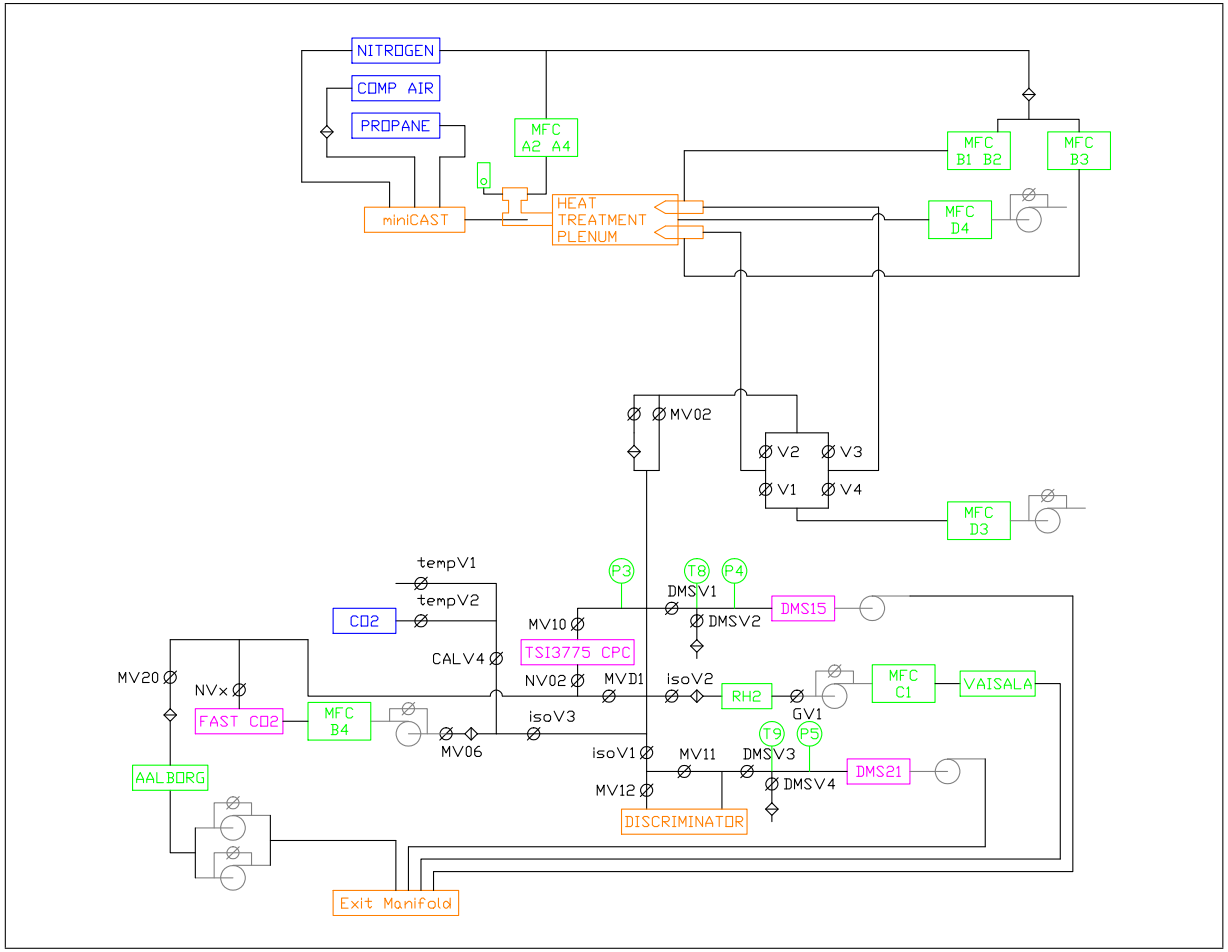

Figure 4.1: Basic setup of the Missouri S&T in-house experiments.

the behavior of the source. Next was plenum spatial uniformity experiment to check that both probes see the same sample. The next experiment was to check how the elemental and organic carbon varied with dilution and size.

The next two sections, Sections 4.6 and 4.7, look at the PM sample line. A line conditioning study was performed in order to determine a procedure for breaking in a new line. After the line conditioning was performed, measurements were made with the PM line at various temperatures to determine if line temperature had a significant effect on sample integrity. Section 4.8 examines diluter placement from immediately behind the probe to 6 m down the sample line. The last two sections examine various components in the sample line beginning with investigating the performance of several commercially available eductors and finally checking the performance of a catalytic stripper for removing volatile PM from the sample.

4.2. MINICAST STABILITY AND REPRODUCIBILITY EXPERIMENT

The reliability of the source, both in terms of sample stability and reproducibility, was determined to ensure confidence for all experiments to follow. The miniCAST was used to produce two different PM size distributions with geometric mean diameters (GMD) of approximately 15 and 30 nm. For each miniCAST setting, three series were conducted, alternating between the 15 and 30 nm setting, with data acquisition periods lasting between 9 and 17 minutes. Size distributions were measured with a Cambustion DMS 500 while PM number concentration was measured with a TSI 3775. The miniCAST was shutdown several times throughout the tests.

The system configuration for this experiment, shown in Figure 4.2, is different than the standard one shown in Figure 4.1. The miniCAST exhausted into a short transfer line where a small amount ($\sim$2 L/min) was extracted for undiluted CO_2 measurement and excess exhaust gases were expelled from the system or filtered

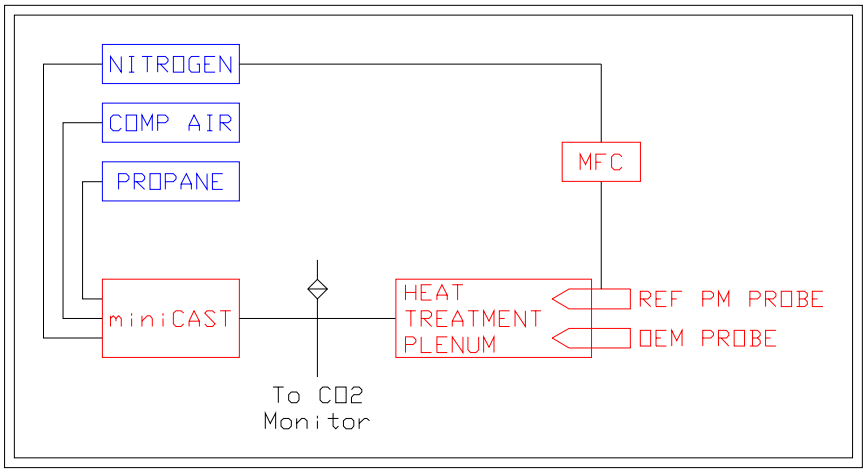

Figure 4.2: Setup of miniCAST stability and reproducibility experiment.

room air was sucked in if not enough sample flow was present. The transfer line brought the sample to the heat treatment plenum (operating at room temperature) before being sucked into PM probe operating at 10:1 dilution ratio. The second probe in the plenum was blocked off. A second transfer line brought the diluted sample to the instrumentation suite, consisting of a Cambustion DMS 500 and a TSI 3775.

The average PM distributions measured and shown in Figure 4.3 are fairly stable over the sizes shown with a maximum standard deviation of 0.044 and 1.140 nm for the 15 and 30 nm size distributions, respectively. The sizes not shown were down in the noise of the DMS and had standard deviations greatly exceeding their average values. For each of the series, the GMD was recorded on a second by second basis with the average value and standard deviation presented in Table 4.1. The overall average and standard deviation are also shown. The miniCAST consistently produced the same size particles with little variance, especially at the 15 nm GMD size. The overall geometric standard deviation (GSD), width of the log-normal distribution fit, was 1.57 and 1.61 for the 15 and 30 nm GMD size distributions.

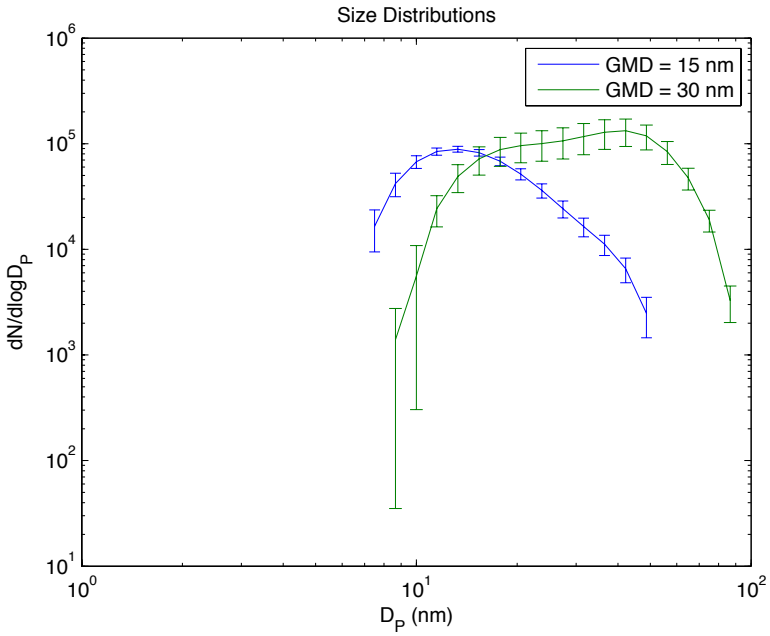

Figure 4.3: Size distributions of miniCAST at geometric mean diameters of 15 and 30 nm.

Table 4.1: miniCAST size reproducibility. Values reported are the GMD and standard deviation of the GMD.

Series	15 nm	30 nm
1	14.92±0.044	29.85±0.150
2	14.61±0.035	30.30±0.215
3	15.37±0.039	30.77±1.140
Overall	14.97±0.040	30.31±0.502

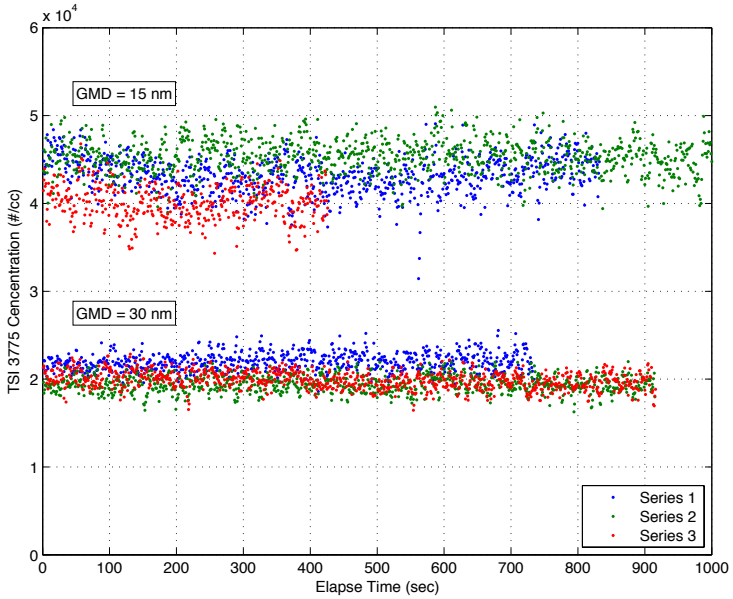

Figure 4.4: miniCAST stability as a function of elapse time.

The total particle counts (TCN) by the TSI 3775 for the 15 and 30 nm GMD as a function of series elapse time is shown in Figure 4.4 and Table 4.2. The 30 nm GMD TCN data fit in a much narrower band than the 15 nm. The overall uncertainty in the TCN produced by the miniCAST was ~7%, with GMD uncertainty less than 2%.

Table 4.2: Total particle count stability.

Series	15 nm		30 nm	
	avg	stdev	avg	stdev
1	4.319E+04	2.089E+03	2.195E+04	1.034E+03
2	4.536E+04	1.892E+03	1.943E+04	9.668E+02
3	4.006E+04	1.970E+03	1.988E+04	1.013E+03
Overall	4.357E+04	2.777E+03	2.031E+04	1.458E+03

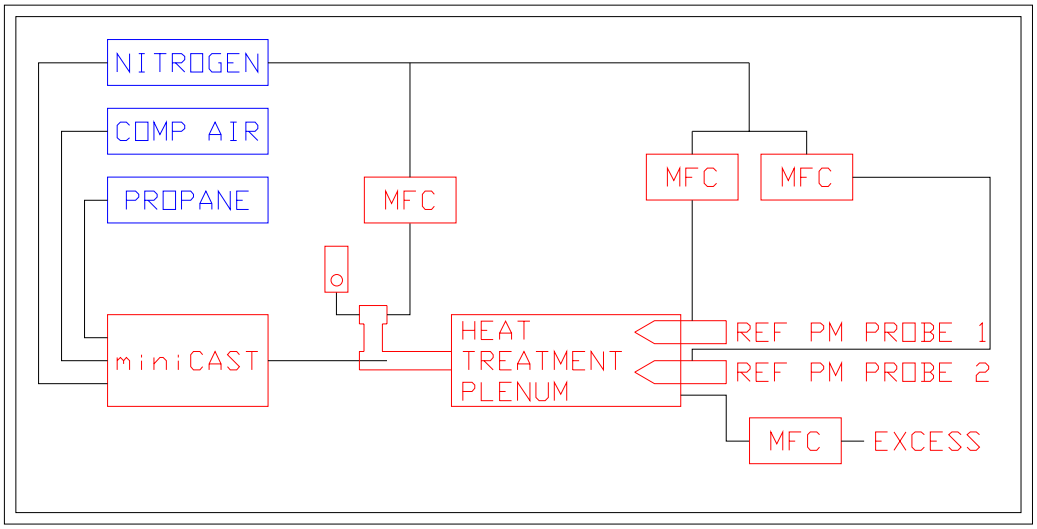

Figure 4.5: New setup to decouple the source from sampling system.

4.3. DECOUPLING VERIFICATION EXPERIMENT

During the initial experiments, it was noticed that source varied slightly with sampling volume. This was primarily due to allowing the system to intake room air through a filter and varying reference probe dilution, causing the miniCAST output to be at different pressures depending on the sampling volume. The new setup, shown in Figure 4.5, used a mass flow controller to dilute the raw miniCAST output. Additionally, some the the pre-diluted sample was bled off and monitored with flowmeter.

To verify the source was decoupled, the miniCAST was set to produce a size distribution with a GMD of 40 nm. The flow rates through reference probe 1, reference probe 2, and the excess flow rate were varied, and neither reference probe used probe tip dilution. Size distributions were measured using a TSI 3071 DMA, number concentrations with a TSI 3775 CPC, and CO_2 concentration with a Sable Systems CA-2A with data being acquired over a 5 minute time span. Settings and results are presented in Table 4.3. Series 1-3 showed 0.29% variation in CO_2 concentration

Table 4.3: Decoupling verification summary.

Series	Sample Probe	Q_{ref1} (lpm)	Q_{ref2} (lpm)	Q_{excess} (lpm)	CO_2 (ppm)		TCN (#/cc)	
					avg	stdev	avg	stdev
1	1	4.5	1	7	4650	9.1	5.58E+06	5.50E+05
2	1	4.5	3	5	4677	9.9	5.28E+06	4.18E+05
3	1	4.5	5	3	4664	8.4	5.30E+06	4.33E+05
4	2	1	4.5	12.5	4543	8.0	6.65E+06	4.98E+05
5	2	3	4.5	10.5	4649	9.9	6.78E+06	3.95E+05
6	2	5	4.5	8.5	4754	9.5	6.85E+06	4.86E+05

and 3.10% variation in TCN, while series 4-6 had 2.27% and 1.49% variation in CO_2 concentration and TCN. Series 4-6 were measured several days after series 1-3, so the difference in TCN from one group to the next was small. The overall average TCN of 6.07x10^6 particles/cm^3 encompasses all data points when the instruments ±20% accuracy is taken into account. The size distributions, shown in Figure 4.6, show little variation within each group. Series 1-3 had an average GMD of 39.6 ±0.6 nm with a GSD of 1.68 while series 4-6 had an average GMD of 38.8 ±0.5 nm with a GSD of 1.69. The reconfigured system successfully decoupled the source from the sampling system, such that varying the flow rate through a reference probe had negligible impact on the performance of the miniCAST.

4.4. SPATIAL UNIFORMITY VERIFICATION EXPERIMENT

The spatial uniformity of the heat treat plenum was to be verified next. For probe tip dilution and down stream dilution to be accurately compared, both probe had to be seeing the same sample. The same setup as the decoupling verification was used for the spatial uniformity check with both reference probes sampling 5 lpm at 3 different source settings. Test settings along with CO_2 and TCN values are shown in Table 4.4. Overall CO_2 variation from one probe to the next was less than ±20 ppm or 1% across all source settings. Likewise, TCN variation was at worst 10% from one

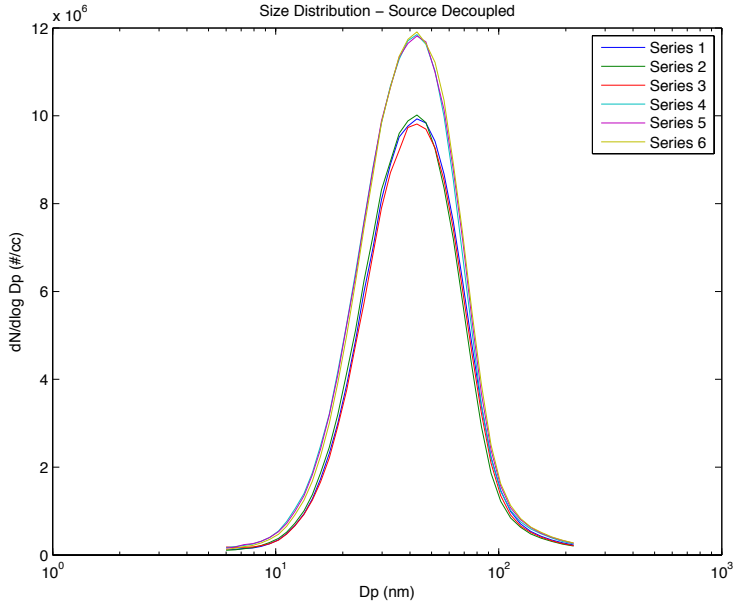

Figure 4.6: Size distributions from miniCAST decoupling verification.

Table 4.4: Spatial uniformity verification summary.

Series	Sample Probe	miniCAST Set Point	CO_2 (ppm)		TCN (particles/cm^3)	
			avg	stdev	avg	stdev
1	1	40 nm	4029	8.7	7.38E+04	5.77E+04
2	2	40 nm	4023	8.0	7.95E+06	6.09E+04
3	1	30 nm	3045	10.5	9.08E+05	6.30E+03
4	2	30 nm	3009	11.3	8.25E+05	5.09E+03
5	1	25 nm	2037	5.0	4.13E+06	2.14E+04
6	2	25 nm	2045	4.7	4.05E+06	2.54E+04

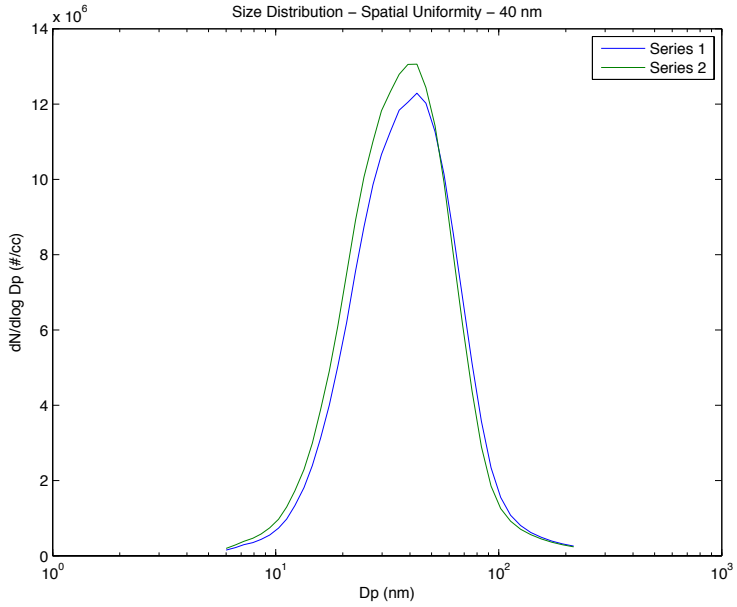

Figure 4.7: Size distributions from miniCAST spatial uniformity verification. - 40 nm.

probe to the next, well within the instruments accuracy. The size distributions for the 40 nm source setting are shown in Figure 4.7 contained the greatest variance in terms of GMD of the 3 source settings from one probe to the next. The average GMD was 36.1 ±1.1 with a GSD of 1.71 ±0.01. The 30 nm source setting had average GMD of 33.7 ±0.7 with a GSD of 1.90 ±0.03, while the 25 nm setting had a GMD of 22.7 ±0.4 with a GSD of 1.71 ±0.01. All variations were within instrument uncertainty, due to the heat treat plenum being spatially uniform.

4.5. EC-OC FILTER ANALYSIS

It was also desired to know how elemental carbon (EC) to organic carbon (OC) ratio varied with GMD and dilution. Three filters were used for each test point, an undiluted just behind an OEM probe and 2 downstream of a reference probe with 1 of them behind a thermal discriminator. The filters were inserted for a sufficient amount

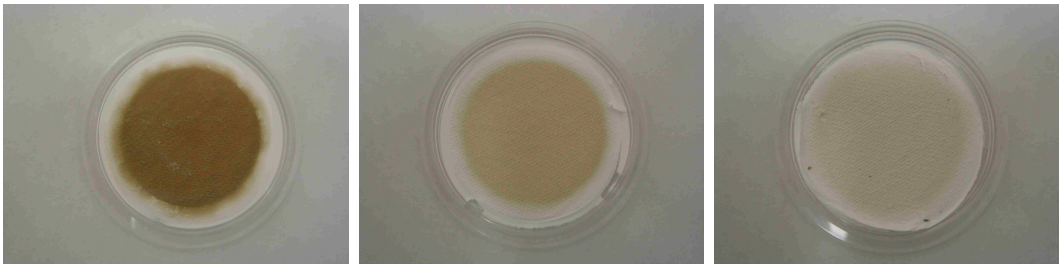

(a) (b) (c)

Figure 4.8: Filter images from GMD 20 nm source with a dilution ratio of 10:1. Images are typical for other test points. (a) Undiluted filter sample. (b) Diluted filter sample. (c) Diluted and discriminated sample.

of time in order to ensure adequate deposition, as seen in Figure 4.8. Typically, the undiluted filter was in the system for less than 10 minutes while to other 2 filters could be in for several hours. This prevents EC and OC masses from being used in the condition comparison.

First, the EC-OC ratio was checked to dilution at a source GMD of 20 nm. Three dilution ratios were used (5, 10, and 20) with the results shown in Figure 4.9. At 20 nm, the EC-OC ratio is insensitive to dilution. Second, the EC-OC ratio was checked to GMD dependence, with results shown in Figure 4.10. Three different sizes were used (20, 28, and 80 nm), with both the 20 and 28 nm sizes being checked at a dilution ratio of 5 and the 80 nm being checked at a dilution ratio of 10. The EC fraction increased with GMD from ∼10% at 20 nm to ∼50% at 80 nm. All data points showed about the same EC fraction for the undiluted, the diluted, and the diluted and discriminated at a given data point except for the GMD 28 nm test point. The higher discriminated EC fraction for this test condition may indicate some evolution of the exhaust taking place or a bad filter.

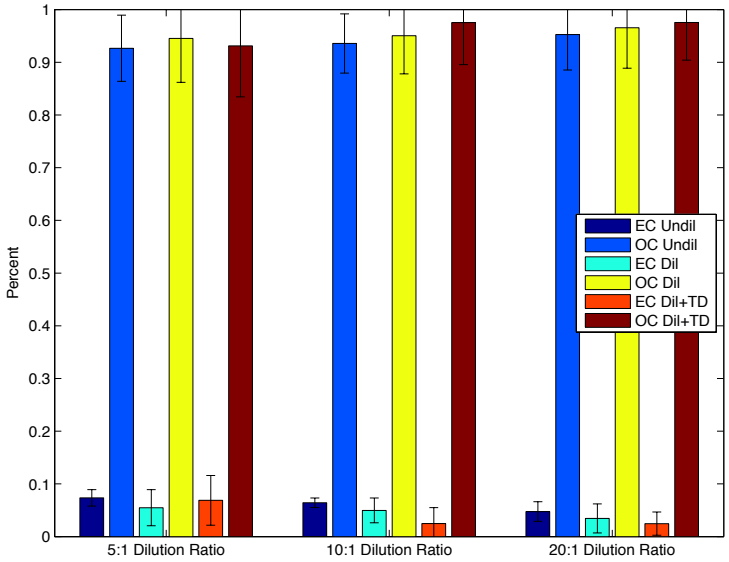

Figure 4.9: EC-OC ratios with source at 20 nm and various dilution ratios.

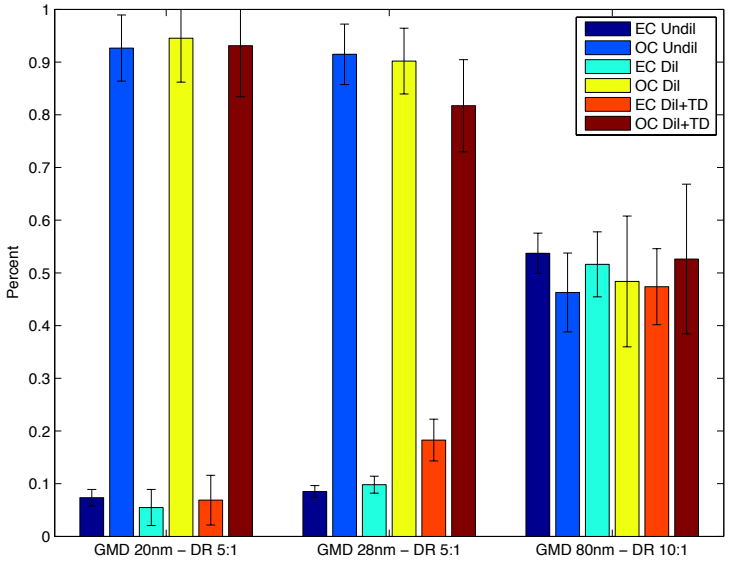

Figure 4.10: EC-OC ratios with source at 28 nm and 80 nm.

4.6. LINE CONDITIONING EXPERIMENT

The primary objective of the line conditioning experiment was to determine the amount of time necessary for a 25 m line to reach a particle loss steady state. A clean, electro-polished line was used behind an OEM probe with a tap at the beginning and end of the line to measure the PM entering and exiting the line being conditioned. The line penetration, percentage of particles of a given size passing through the length of line, was measured throughout the experiment. The instrumentation used included a Cambustion DMS 500, TSI 3775 CPC, and a Thermo Scientific 5012 MAAP. The miniCAST was set to produce a sample with a GMD of ∼40 nm and concentration of $\sim 10^6$ #/cc. The line conditioning experiment proceeded over 3 days.

The first day of conditioning began with heating the line to 160°C and running nitrogen through it to purge any residuals. A total of 90 minutes of line conditioning took place on the first day, split into 6 cycles of inlet and outlet measurements. As seen in Figure 4.11, the TCN was stable for the duration of the run while the black carbon (BC) mass ratio began increasing around 1 hour 15 minutes into the test. The penetration efficiency remained roughly stable, see Figure 4.12, but was greater than unity for particles larger than 70 nm, suggesting particles shedding from the line. The line was purged with nitrogen for 15 minutes to end the day.

Day 2 began with 15 minutes of nitrogen purging with line at 160°C and then proceeded with 45 minutes of line conditioning. As shown in Figure 4.13, the initial penetration (15 minutes) was similar to those seen on day 1 with large particle shedding from the line. At the end of the line conditioning for the day (45 minutes), the penetration was less than unity for all sizes. Due to concerns for the potential to cause large particle shedding because the line penetration efficiency was greater than 100% for some sizes initially during the day, the line was not purged.

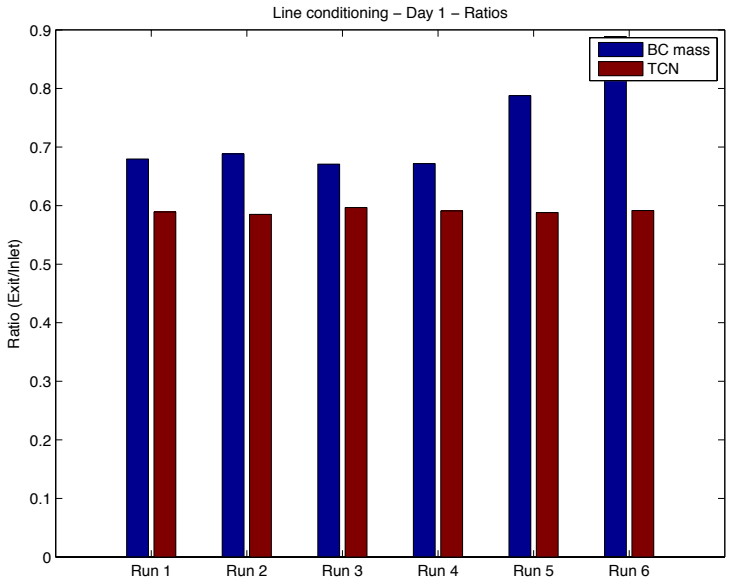

Figure 4.11: Day 1 of line conditioning TCN and BC mass ratios as a function of elapse time.

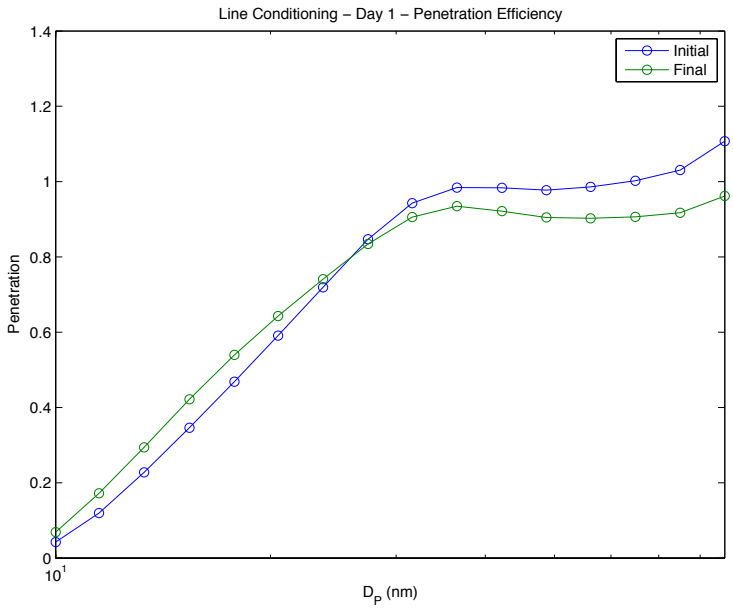

Figure 4.12: Day 1 of line conditioning size penetration effectiveness.

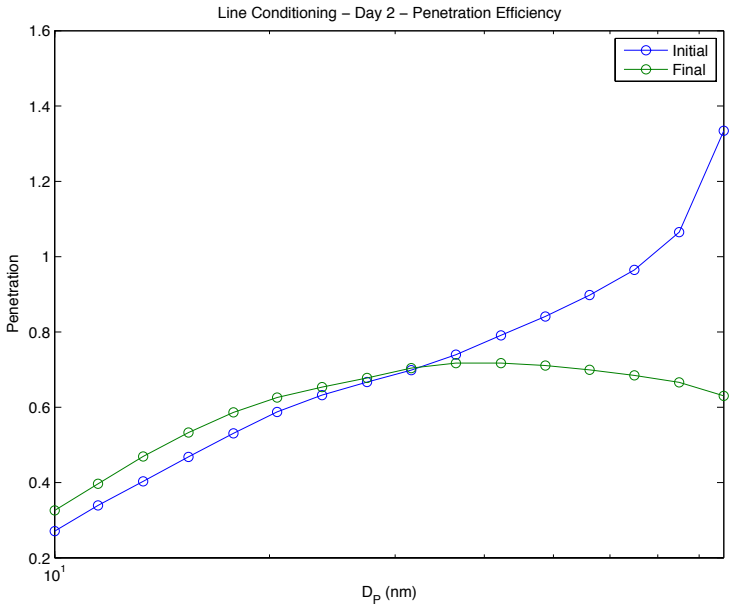

Figure 4.13: Day 2 of line conditioning size penetration effectiveness.

Day 3 consisted of 30 minutes of line conditioning with no nitrogen purging and consisted of 4 cycles. By all measures, the line was stable for the duration of the day 3 line conditioning. Shown in Figure 4.14, the average penetration did not very much, with a maximum uncertainty of 31.7% at the 5.62 nm size and average uncertainty of 8.8%. Likewise, all of the ratios, shown in Figure 4.15, show relatively constant values across all 4 runs.

The total line conditioning time was about 3 hours with stable penetration occurring around the 2 hour mark. The initial large particle shedding from the line diminished with time and maybe worsened by nitrogen purging. A sample line should be conditioned, as a new line will have a different penetration than a used line. A clean new sample line should be exposed to exhaust emissions for 2-3 hours prior to collecting data. Purging the line should be minimized or eliminated if possible, with a re-conditioning period of 30 minutes in the event of purging.

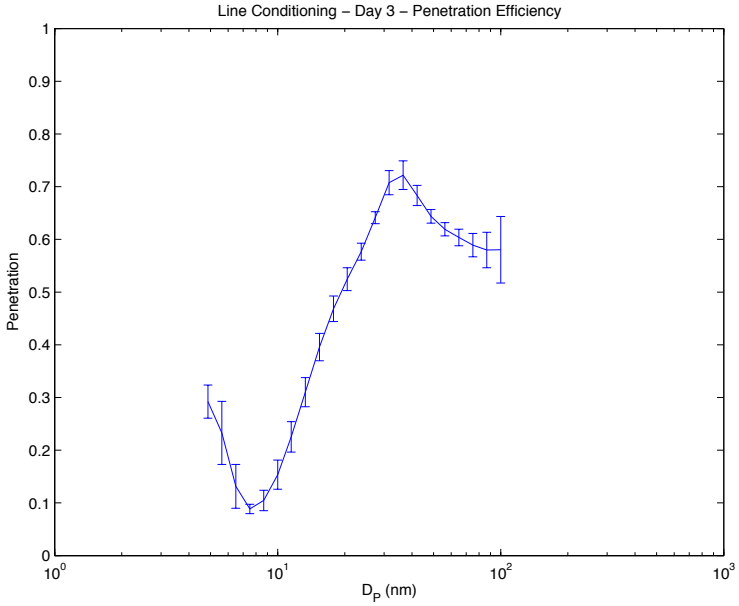

Figure 4.14: Day 3 average line penetration efficiency.

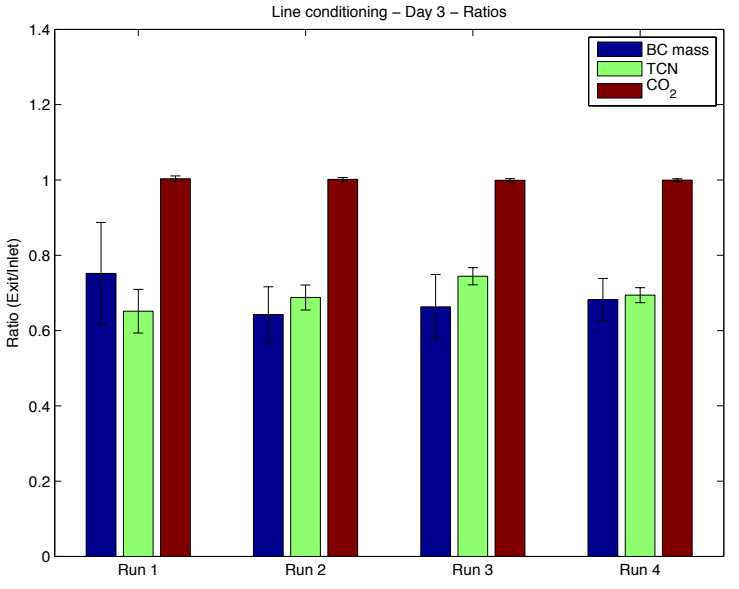

Figure 4.15: Day 3 ratios of BC mass, TCN, and CO_2.

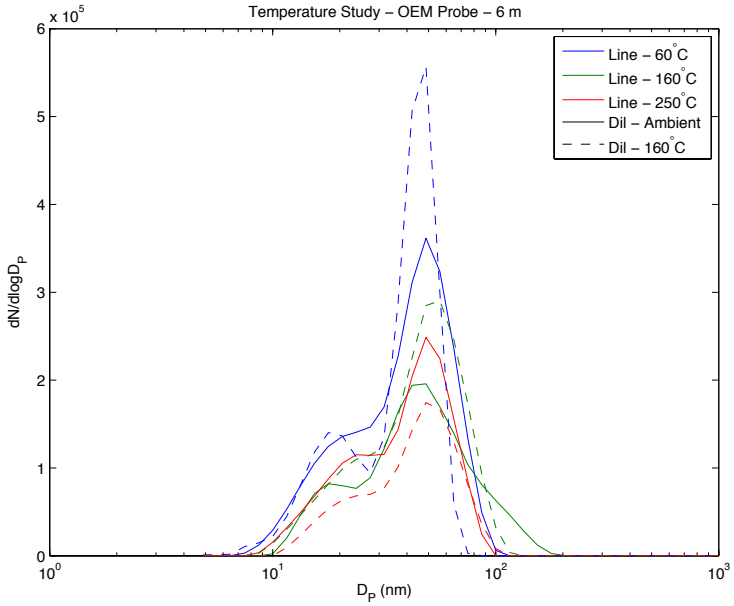

Figure 4.16: OEM sample line size distributions with dilution at 0 m and 6 m from probe exit with a dilution factor of 20.

4.7. LINE TEMPERATURE STUDY

The line temperature study used the exact same setup as the dilution study. The study comprised of 3 different line temperatures (60, 160, and 250°C), each with dilution temperature at both ambient and 160°C. All test points used a furnace temperature of 320°C except for the line temperatures of 250°C, which had a furnace temperature of 350°C.

The size distributions from the OEM probe at 6 m dilution distance with a dilution factor of 20 are shown in Figure 4.16. For both the 60 and 160°C line temperatures, the size distribution increased in concentration with heating the dilution gas while the GMD stayed roughly the same. At a line temperature of 250°C the increase in dilution temperature decreased the concentration. The concentration also decreased when the line temperature went from 60 to 160°C but increased when it went to 250°C, possibly due to particle burning off of the line.

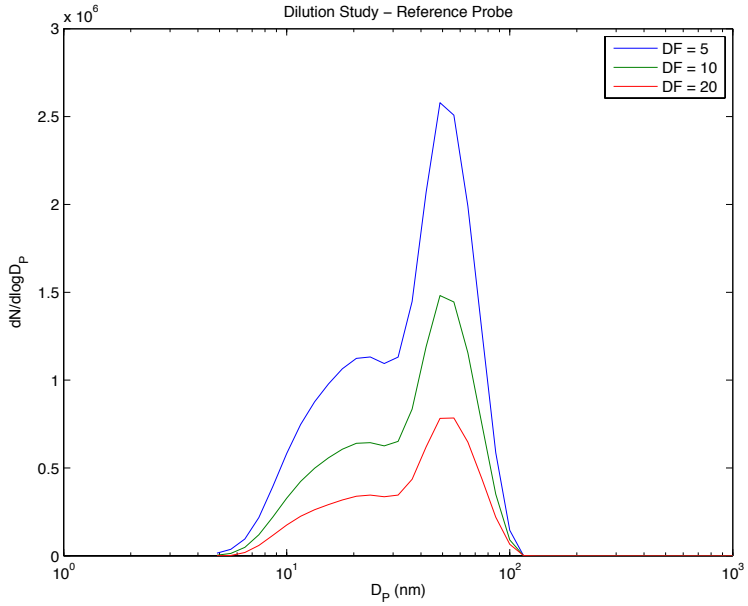

Figure 4.17: Probe tip dilution size distributions. Values were as measured and not corrected for dilution factor or particle line loss.

4.8. PROBE TIP vs. DOWNSTREAM DILUTION

One of the primary goals of the in-house set of experiments was to compare probe tip to downstream dilution. To accomplish this, the standard set up had 2 simple concentric tube diluters inserted at the OEM probe exit and 6 m down the sample line, while a reference probe occupied the other slot in the plenum. The sample line coming off of the reference probe, shown in Figure 4.17, was only a few meters while the OEM sample line was 25 m long. None of the data was corrected for line loss so direct comparison of the OEM line and reference line was not possible. For the results presented in this section, the furnace was at 320°C and both the sample line and dilution temperatures were at 160°C. The next section will examine temperature variance.

The comparison of the OEM line when diluted at various distances is shown in Figure 4.18. The reference probe averaged 33.76 ±0.53 nm on the GMD and 1.90

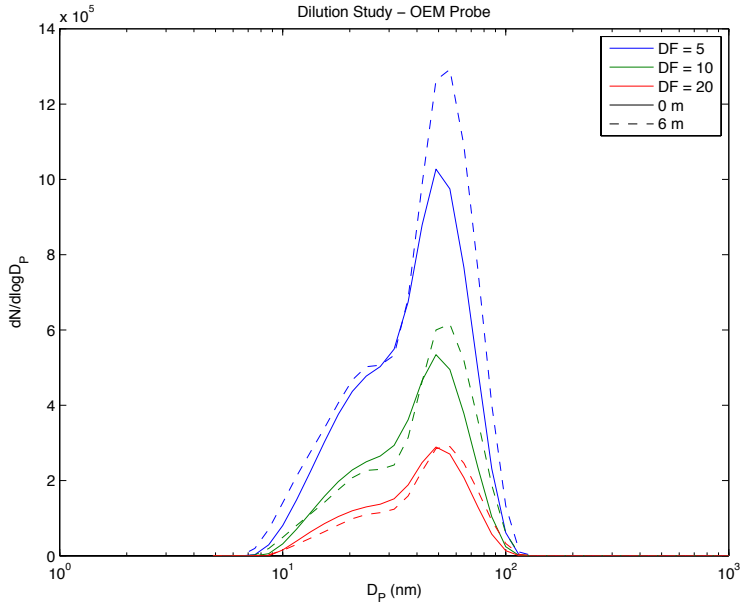

Figure 4.18: OEM Sample line size distributions at both 0 m and 6 m from probe exit. Values were as measured and not corrected for dilution factor or particle line loss.

±0.00 on the GSD. The size distributions between the 0 and 6 m downstream dilution were more closely aligned at the large dilution factors. For both the dilution factors of 5 and 10, the 6 m size distribution was higher in concentration than the 0 m dilution location, while at a dilution factor of 20 both locations were about the same. The 0 m dilution location averaged 37.13 ±0.16 nm for the GMD and 1.70 ±0.01 for the GSD, while the 6 m location averaged 39.90 ±1.09 nm and 1.74 ±0.04 for the GMD and GSD, respectively. The 6 m location shifted the size distributions over to increased sizes slightly when compared to the 0 m dilution location with no difference in GSD. The BC mass emission factors were at 0.0216 ±0.0063 and 0.0385 ±0.0054 for the 0 and 6 m dilution locations while the PM number emission factors were 1.62E+03 ±7.22E+01 and 1.30E+03 ±5.08E+01 for the same. The mass increased by about 40% while the number decreased by about 20% with dilution distance. The 0 and 6 m dilution locations would likely agree more, had extra sample been pulled through the

pre-diluted section for a gas bench as would happen in a full system due to increased line loss from slower sample velocity.

4.9. EDUCTOR STUDY

The eductor study evaluated the performance of 3 different commercially produced eductors from Fox Valve, Air-Vac, and Dekati. The first check done on the eductors was to determine driver flow rate as a function of driver pressure. A similar check was done to determine sample flow rate as a function of sample pressure for various driver pressures. These results were then evaluated to determine which eductors satisfy the following desired characteristics for simultaneous gaseous and PM measurement: a diluted flow rate greater than 14 lpm, a sample flow rate of $\sim$2 lpm, and a dilution factor from 2 to 20, for a sample with pressure varying between 0.8 and 1.2 atm. The last performance criteria checked was the penetration efficiency for the same sample pressure range.

The driver flow rate was measured at pressures ranging from 1 to 70 psi_g, although the range for a particular eductor varied as shown in Figure 4.19. The Fox Valve eductor was by far the smallest one tested and required a much higher pressure to generate a comparable amount of flow rate to the other eductors tested. Both the Air-Vac and Dekati eductor produced a linear relation between driver pressure and driver flow rate above about 10 psi_g. Below this pressure, the flow rates quickly tappered off to zero.

The sample flow rate was also measured at pressure ranging from 10 to 14 psi_a at various driver pressures. Figure 4.20 shows the sample flow rate map for the Dekati eductor. The sample flow rate graphs for the other eductors studied are presented in Appendix C. All of the eductors tested were at the sample flow rate limit at the minimum driver pressure approximately of atmospheric sample pressure, meaning

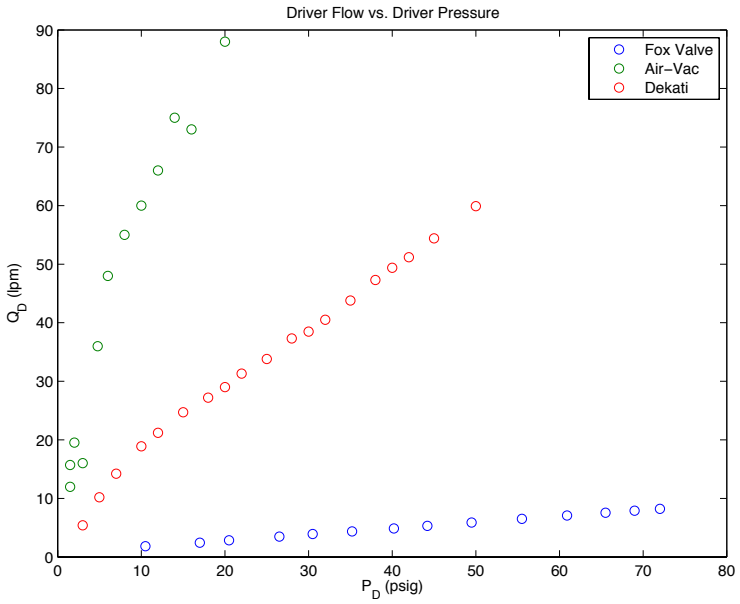

Figure 4.19: Eductor diver flow rate as a function of driver pressure.

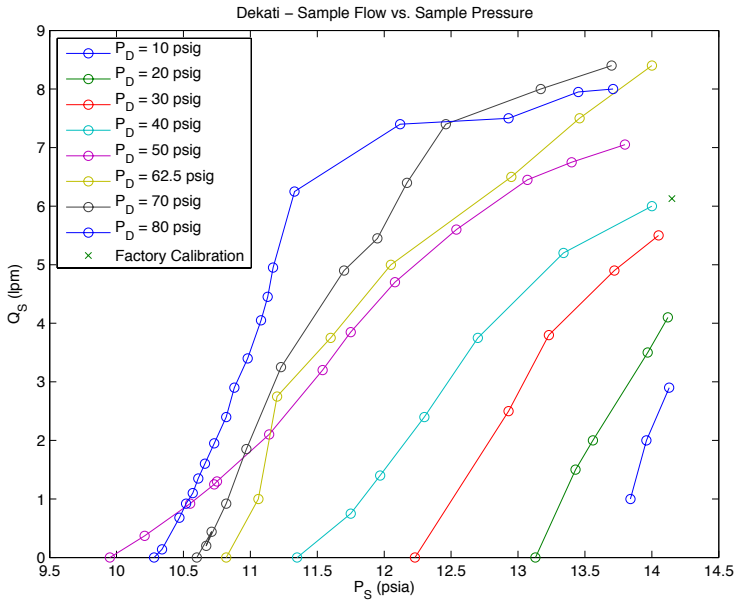

Figure 4.20: Dekati eductor sample flow rate as a function of sample pressure at various diver pressures.

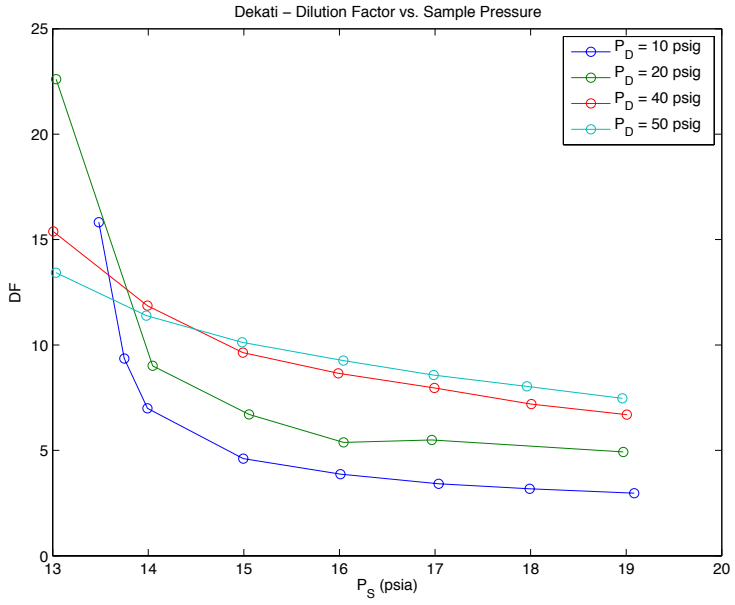

Figure 4.21: Dekati eductor dilution factor versus sample pressure at various diver pressures.

that a sample pressure above 1 atm will result in too much sample flow. This implies that a sampling system needs pressure regulating valve to drop the sample pressure to approximately 1 atm near the PM/gaseous sample splitter. The dilution factors for the Dekati eductor are shown in Figure 4.21. The dilution factor was fairly linear for sample pressures above 1 atm and inversely proportional below 1 atm. Higher driver pressures increased the dilution factor above atmospheric pressure for the sample but lowered the inverse portion of the curve significantly. A higher driver pressure would allow the instruments to see similar diluted sample as the sample pressure varies slightly.

The penetration efficiency was also studied for the 3 eductors using a mono-dispersed salt ($(NH_4)_2SO_4$), with results shown in Figure 4.22. The Air-Vac eductor performed the best in this check, allowing nearly 100% of all particle sizes through. The Dekati eductor also performed well, allowing a constant 50 to 60% of particles

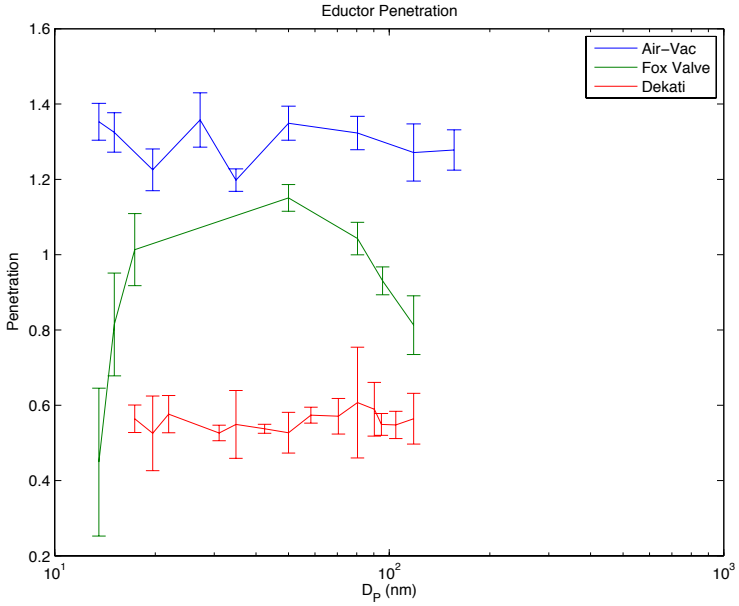

Figure 4.22: Penetration efficiency for the 3 eductors studied.

through for the size range checked. Although for the same model eductor, Giechaskiel, et al. [44] found that particle losses in the 15-300 nm range were between 0-5%. The Fox Valve, however, had a penetration efficiency peak of ∼100% at 50 nm and dropping significantly below 20 nm and tailing off to about 50% above 50 nm.

While none of the eductor satisfied all of the desired characteristics, especially above 1 atm as shown in Table 4.5, both the Air-Vac and Dekati eductors featured a relatively flat particle penetration efficiency, at ∼1.0 and ∼0.65 respectively, making both of these eductor desirable in that criteria. The Fox Valve eductor had a penetration efficiency that decreased substantially below 20 nm and above 80 nm from its maximum. Both the Fox Valve and the Dekati eductors had a relatively flat sample flow rate versus sample pressure, making both of these eductor desirable. This is because small fluctuation in sample line pressure have a minimal effect on sample flow rate and dilution factor. When looking at the criteria of a dilution factor between 2 and 20, sample flow less than 2 lpm, and a total diluted sample flow greater than 14

Table 4.5: Eductor study summary.

Eductor	P sample (atm)	P driver (psig)	DF (2 to 20)	Q sample (<2 lpm)	Q total (>14 lpm)
Fox Valve	1.15	-	-	12.8	-
	1.10	-	-	10.3	-
	1.05	-	-	6.62	-
	1.00	20	15.3	1.94	29.7
	0.90	56	36.3	1.87	67.8
	0.85	67	42.0	1.91	79.7
Air-Vac	1.05	-	-	15.7	-
	0.99	3.5	17.8	2	35.6
	0.94	10	35.3	2	70.6
	0.89	16	44.7	2	89.4
	0.84	22	55.3	2	110.6
	0.79	28	66.2	2	132.4
Dekati	1.15	-	-	11.85	-
	1.10	-	-	7.81	-
	1.05	-	-	2.08	-
	1.00	6	7.7	1.93	17
	0.90	33	21.4	2.03	45.8
	0.80	63	39.9	1.89	77.3

lpm, all 3 eductors performed well at or below 1 atm. If the sample pressure were to drop to 0.80 atm, the Air-Vac eductor would have a dilution factor of nearly 70 while the Fox Valve and the Dekati would be around 40. Overall the Dekati eductor performed the best.

4.10. CATALYTIC STRIPPER

The proposed ARP is for the measurement of non-volatile PM. Any volatile PM that forms in the sample line needs to be removed prior to the instruments. To accomplish this, a catalytic stripper was examined for its ability to remove volatile material and penetration efficiency. This study used a similar setup to the eductor study and was comprised of 3 parts. First, the penetration efficiency was examined

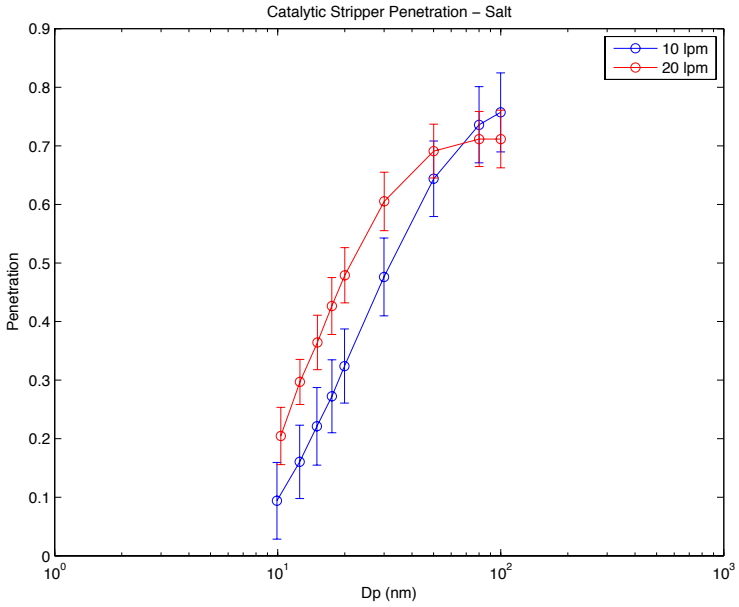

Figure 4.23: Penetration efficiency of the catalytic stripper using mono-dispersed NaCL aerosol with flow rates of 10 and 20 lpm.

using a mono-dispersed salt (NaCl) aerosol ranging from 10 to 150 nm. Second, the penetration was measured using a mono-dispersed carbonaceous aerosol over the same size range. Last, the volatile material removal efficiency was determined using a poly-dispersed aerosols with variable EC-OC ratios. The first portion used a nebulizer and furnace to generate a NaCl aerosol while the second and third portions used the miniCAST as the PM source. All portions of the study were done at two flow rates, 10 and 20 lpm, with the catalytic stripper at 300°C.

The penetration efficiency using mono-dispersed salt aerosol is shown in Figure 4.23. The penetration was slightly higher at 20 lpm than at 10 lpm below 35 nm, while above the 2 flow rates had statistically the same penetration. The results from using a mono-dispersed carbonaceous aerosol are shown in Figure 4.24. Similar to the salt aerosol, the higher flow rate showed greater penetration, although the point at which the become statistically the same increased to 60 nm. Figure 4.25 shows the

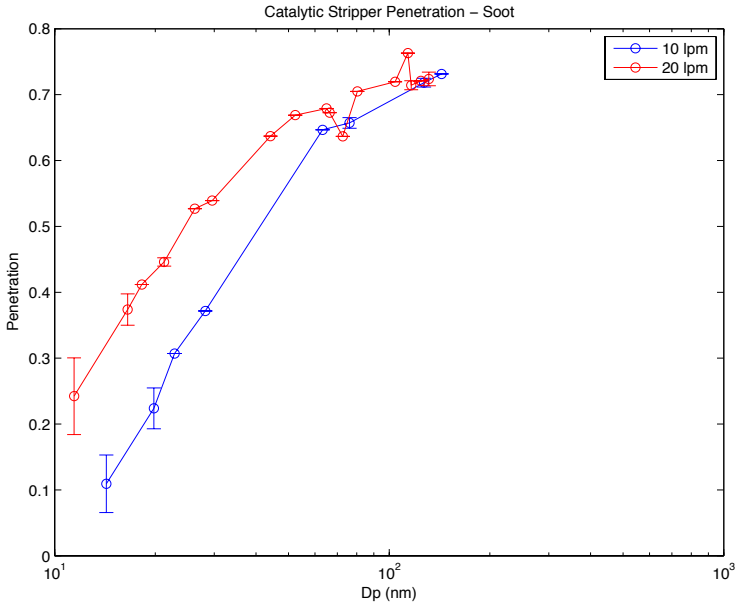

Figure 4.24: Penetration efficiency of the catalytic stripper using mono-dispersed carbonaceous aerosol with flow rates of 10 and 20 lpm.

penetration efficiency for both the salt and carbonaceous aerosols at the 10 lpm flow rate. Both aerosol types displayed statistically similar penetration efficiency over the size range examined.

When examining the volatile removal efficiency, the miniCAST was set to produce a series of PM samples with mean sizes ranging from 10 to 110 nm. For each size segment, the upstream and downstream size distributions were recorded and from each the associated mean diameters were calculated. Mean masses were also calculated by assuming a spherical particle with a given density. A volatile mass fraction was calculated for each size segment using the upstream and downstream mean masses using Eq. 4.1,

$$\epsilon = \frac{V_U - V_D}{V_U} = 1 - \left(\frac{x_D}{x_U}\right)^3 \tag{4.1}$$

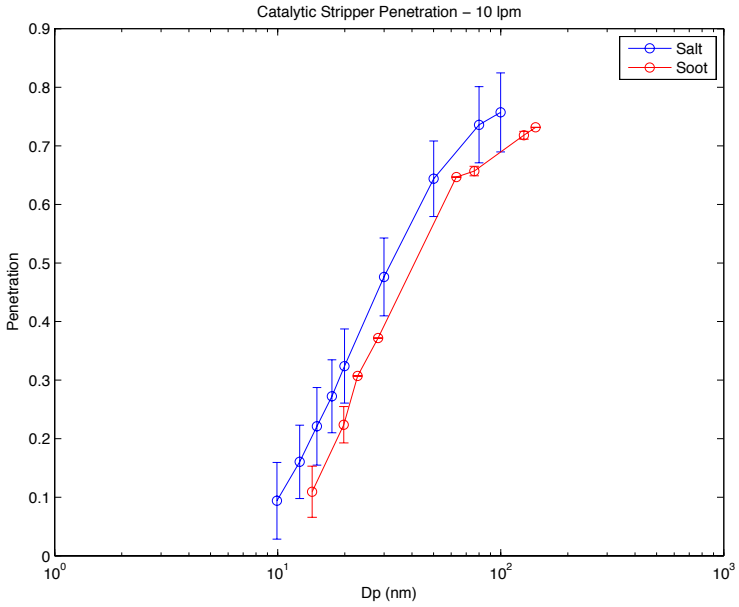

Figure 4.25: Penetration efficiency of the catalytic stripper at a flow rate of 10 lpm using both mono-dispersed salt and carbonaceous aerosols.

where ϵ is the volatile mass fraction, V is the particle volume, and x is the particle diameter. Both the particle diameter and volume have upstream and downstream conditions denoted by the subscripts D and U.

The results from the volatile mass fraction examination are shown in Figure 4.26. The miniCAST PM contained volatile material with a mass fraction ranging from 0.1 to 0.8. The volatile mass fraction was greatest (0.7 to 0.8) for downstream sizes below 40 nm and droped below 0.2 above the 65 nm size. The volatile mass fraction distribution was well fit with a Fermi-Dirac distribution function, with an uncertainty of 3%.

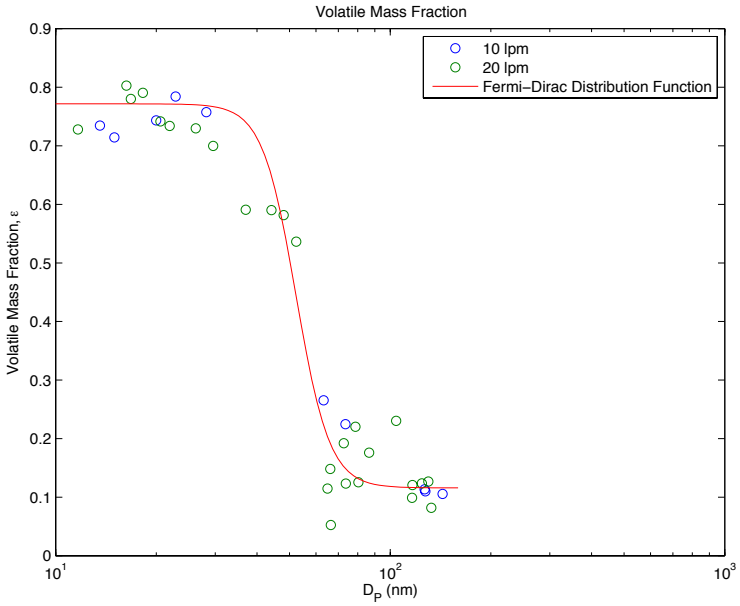

Figure 4.26: The volatile mass fraction as a function of downstream particle size at both 10 and 20 lpm flow rate through the catalytic stripper.

5. AAFEX II FIELD STUDY

The Alternative Aviation Fuel EXperiment (AAFEX) is a series of field studies designed to assess the changes in engine performance and emissions characteristics of alternative fuels when compared to standard JP-8. The field studies were performed on the Dryden Flight Research Center DC-8 aircraft equipped with CFM-56-2C engines. The first field study (AAFEX) was conducted from 19 January through 3 February in 2009. The second field study (AAFEX II) was conducted from 21 March through 3 April in 2011. The AAFEX II Field study was the first trial of a concept E-31 ARP system with jet engines as the combustion source. The primary objectives were to produce a matrix of fuel effects on engine and exhaust gas temperatures and compressor speeds, engine and auxiliary power unit (APU) gas phase and particle emissions and characteristics and, volatile aerosol formation in aging exhaust plumes. While secondary objectives included examining ambient temperature effects on volatile aerosol formation and AAFEX II included trial of the concept E-31 ARP system. The AAFEX II field campaign also included an in depth investigation of measured line loss and theoretical line loss. The discussion in this section will focus on the concept E-31 ARP system and its comparison to probe tip dilution as used in current research studies.

5.1. EXPERIMENTAL SETUP

The E-31 portion of the AAFEX field study, basic setup shown in Figure 5.1, involved 2 probes, a gaseous probe supplying an Annex 16 line and an Dekati Eductor, and a reference particle probe. The Annex 16 line lead to gas bench which contained only a CO_2 analyzer. There was a suite of particle devices which were able to pull from either the E-31 line or the reference PM probe, along with another CO_2 analyzer

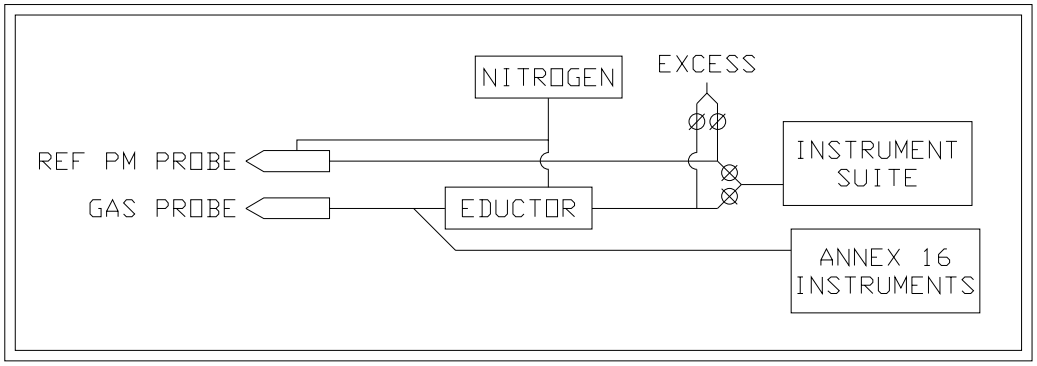

Figure 5.1: Basic setup of the E-31 portion of the AAFEX field study.

to measure the diluted CO_2 amount. The suite of particle devices contained two PM mass measurement devices; an Artium Technologies LII 300, and a Thermo Scientific 5012 MAAP. The suite also contained six PM number measurement devices; an AVL Particle Counter (APC), three TSI CPC's models 3772, 3775, and 3776, as well as a FMPS, and a SMPS.

5.2. LINE LOSS STUDY

During the AAFEX II field campaign several line loss measurements were made of the of the E-31 sample line to be compared to the theoretical calculations from Aerosol Calculator [20]. The purpose of this experiment was to determine both the random error and the systematic error present in line loss measurements. The measured and calculated line loss are presented in Figure 5.2 as penetration efficiency, the percentage of particles passing through the line. The calculated results show a very strong correlation with the measured values, with a maximum error of 4.5% at the 29 nm and the greatest standard deviation of 13.6% at the smallest particle size of 10 nm. The random error was determined from the standard deviation present in the line loss measurements and is presented in Figure 5.3 with a rms error of 7.0%.

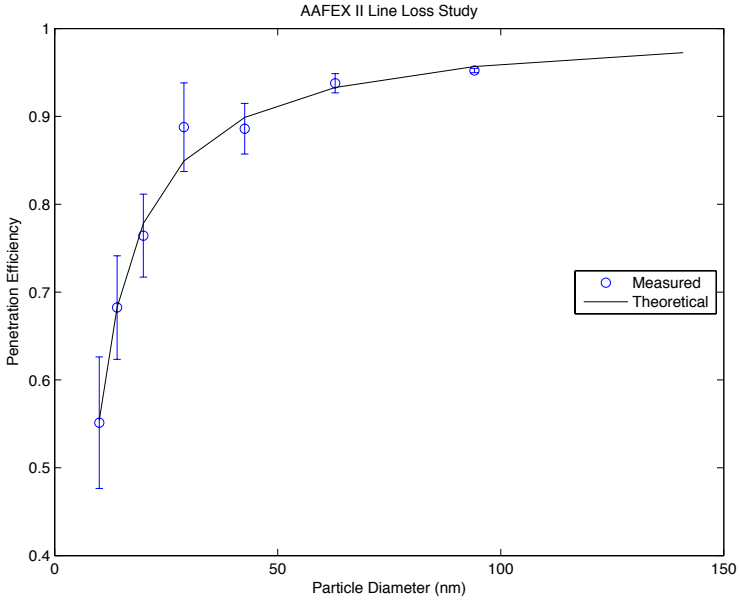

Figure 5.2: Results of the AAFEX II line loss study.

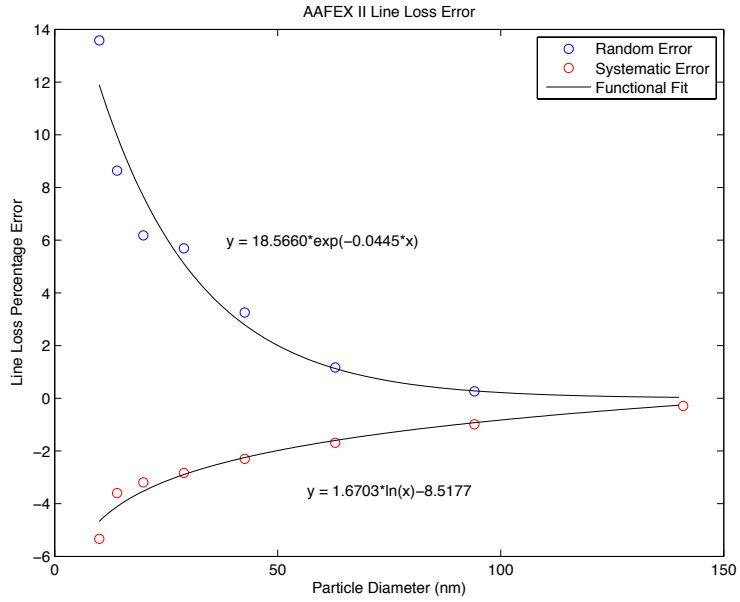

Figure 5.3: Random and systematic error of line loss measurements.

Also shown is the systematic error calculated from the difference in the measured values and the theoretical values and had an rms error of 2.9%.

5.3. PROBE TIP vs. DOWNSTREAM DILUTION

For the purpose of examining probe tip vs. downstream dilution only results from the LII and APC will be examined; an unpublished study by David Liscinsky considered an instrument comparison from the same data collected during this field study. Both the LII and the APC represent likely instruments utilized in a full E-31 system deployment. For this comparison, test points pairs were selected using same run conditions, i.e. engine power, fuel type, etc., pairs occurring near in time with one test point sampling from the E-31 line and the other from the reference probe. The plot shown in Figure 5.4 fit a black line to the data points constrained to pass through point (0,0), with a purple line representing unity, and the test point represented by blue circles with the uncertainties shown for each line.

The results from the LII, shown in Figure 5.4, show the reference line measuring overall 3% higher overall than the E-31 line in terms of EIm. Although many points overlapped unity and the linear fit accuracy mean this is not statistically different from unity. The number based emissions index as determined by the APC, shown in Figure 5.5, show the reference line measuring 26% higher than the E-31 line on average. The sample line penetrations as determined experimentally, shown in Figure 5.6, suggest that the reference line should produce higher EIs, particularly higher EIn due the the difference in line penetration for the smaller particles, when compared to the E-31 line. By combining some size distributions from the main AAFEX II experiment with the line penetration data and an integration to calculate the theoretical mass and number of the sample entering the instrument suite, a 36% higher EIn and 27% higher EIm is obtained for the reference line when compared

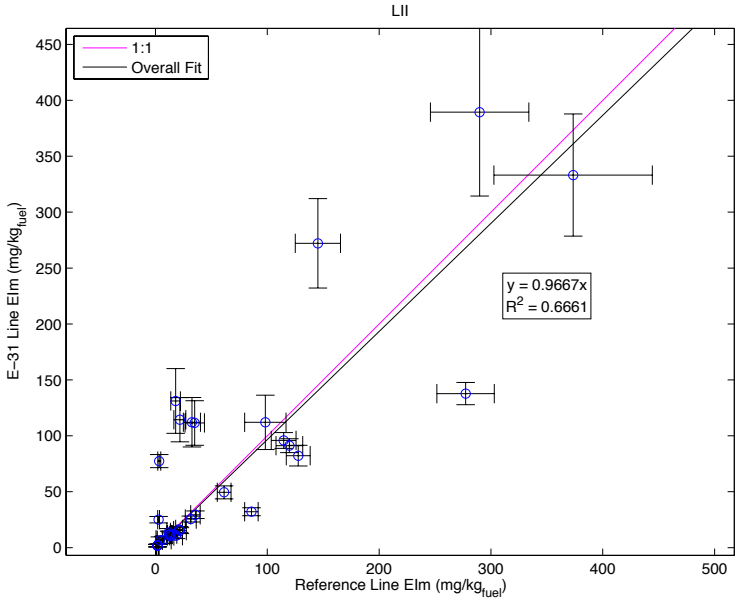

Figure 5.4: EIm comparison of the reference PM sample line to the E-31 sample line at AAFEX.

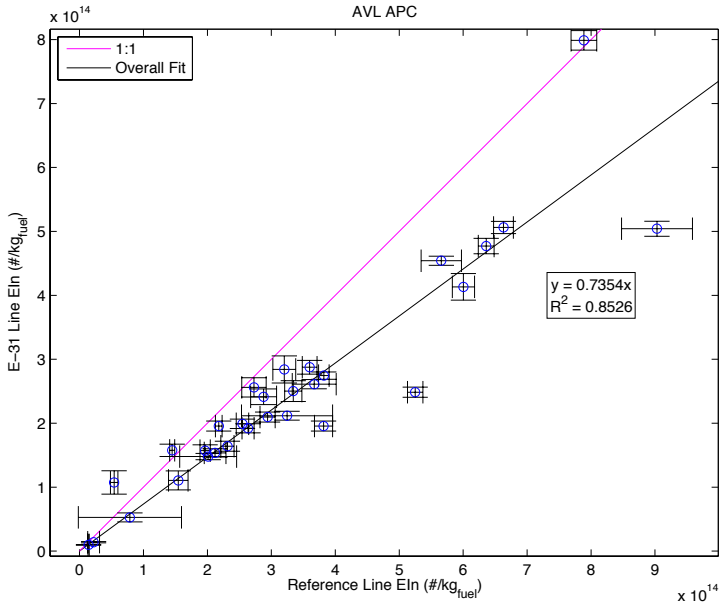

Figure 5.5: EIn comparison of the reference PM sample line to the E-31 sample line at AAFEX.

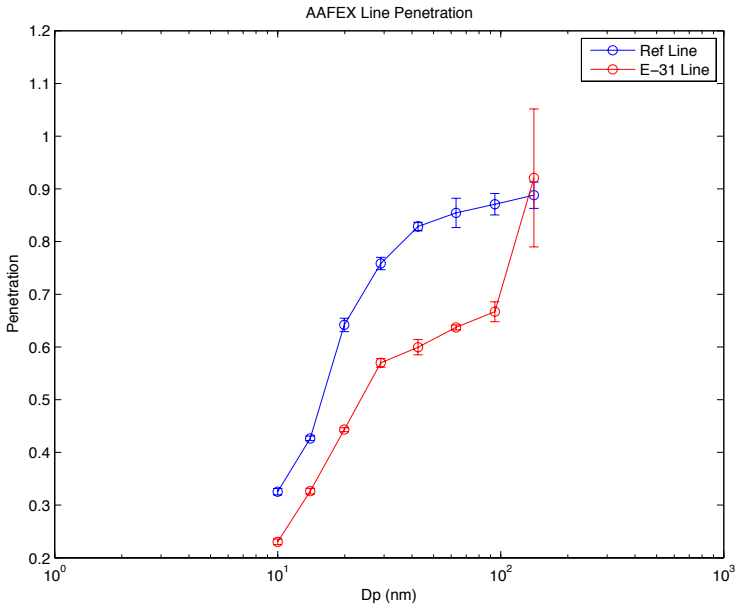

Figure 5.6: Sample line penetration from AAFEX.

to the E-31 line. Although penetration was only measured to 140 nm hindering a theoretical determination of the line penetration effect on the mass measurement.

5.4. GENERAL FINDINGS

Using downstream dilution as is currently proposed, had a negligible effect on the mass measurement and decreased the number measurement by 26% when compared to using probe tip dilution. Similar results were obtained by inserting AAFEX II size distributions in to the line loss data and calculating the resulting EIm and EIn ratios for the two lines of 27% and 36%, respectively. The size penetration data was only measured up to a particle diameter of 140 nm, preventing a complete analysis on the effect that penetration has on mass measurement. Using a theoretical model to calculate the penetration of a sample line provides a good alternative to measuring penetration experimentally. Experimental penetration measurements had

size dependent random and systematic uncertainties that increased as the particle size decreased. The current proposed ARP calls for line loss data to be given which could be used to make an estimation of actual values in the exhaust stream.

6. SAE E-31 ARP DEMONSTRATION

The SAE E-31 ARP demonstration took place from 30 November through 16 December 2011 at SR Technics facility in Zurich, Switzerland. This demonstration included participants from Federal Office for Civil Aviation of Switzerland (FOCA), Missouri University of Science and Technology, Aerodyne Research, Swiss Federal Institute of Technology Zurich (ETH), Canada's National Research Council (NRC), Anstalt für Verbrennungskraftmaschinen List (AVL), Cambridge University, Dekati, and TSI. The primary test objectives were to compare the performance of the FOCA and Missouri S&T versions of the ARP sample train systems in terms of PM number, mass, size, and composition. Additional primary objectives included inter-comparison of similar instrument pairs and evaluation of CPC size cutoff (i.e. 10 vs. 23 nm). The secondary objective was to investigate the impact on number measurement of volatile PM removal using a catalytic stripper.

6.1. EXPERIMENTAL SETUP

The E-31 ARP demonstration, schematically shown in Figure 6.1, consisted of a gas sampling system, and two PM sampling systems. The sampling probe consisted of a 10 mm stainless steel tube uninsulated with a length of approximately 1 m in order to bring the sample up out of the engine exhaust. Another 10 mm stainless steel tube 6 m in length and heated to 160°C brought the sample to the first splitter. The straight through on the splitter was for the PM sample consisting of approximately 10 lpm of raw exhaust at this point. One of the branches on the first splitter was a pressure regulation valve designed to keep the splitter at 10 mbar above atmospheric pressure; this ensures an approximately constant splitter pressure and eductor inlet pressures. The other branch was an Annex 16 gas line of 6 mm carbon loaded PTFE

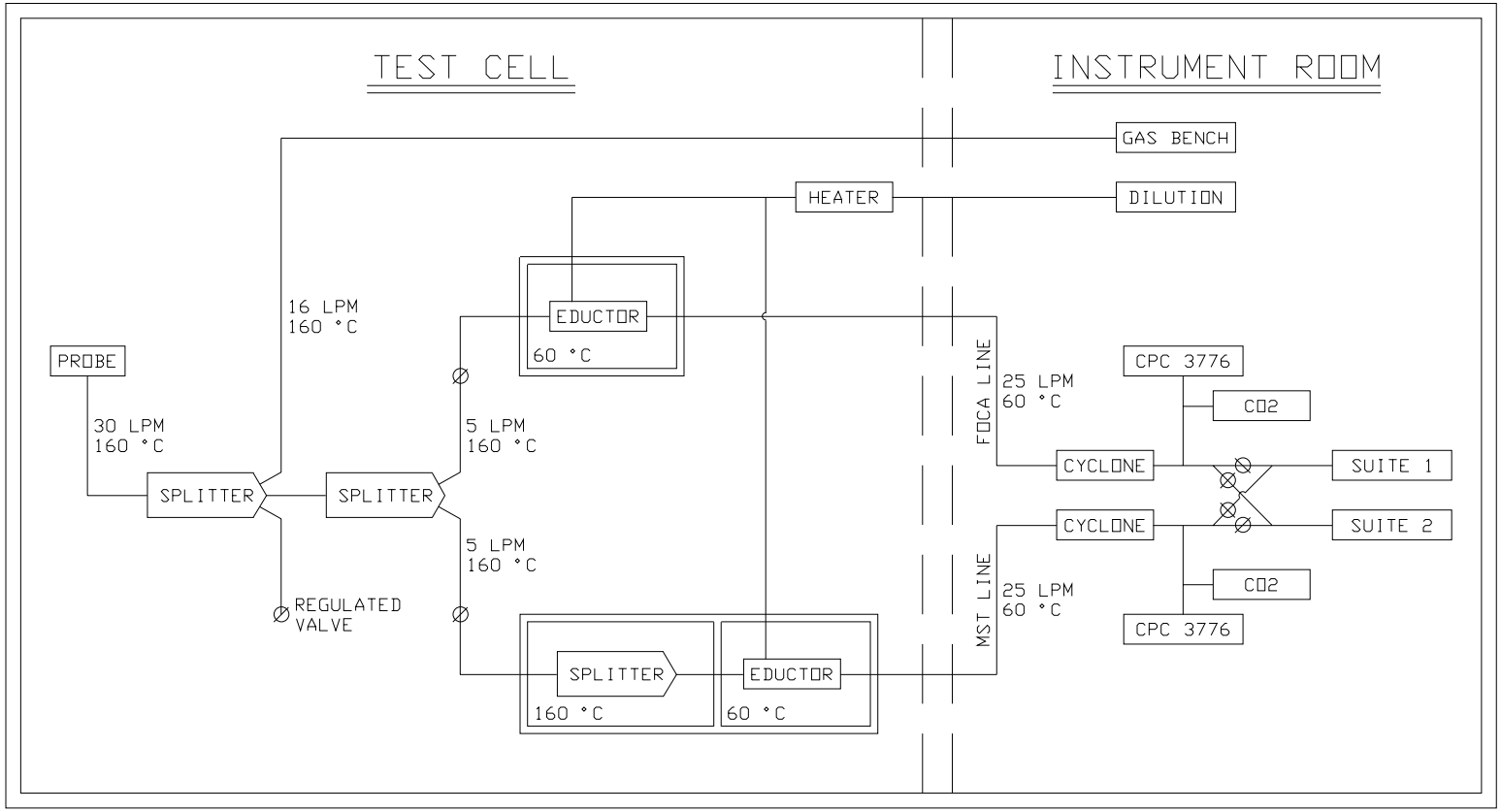

Figure 6.1: Basic setup of the E-31 ARP demonstration.

tubing and 27 m in length heated to 160°C with approximately 16 lpm of raw exhaust. A Horiba PG-250 was used to provide measurements of NO_X, SO_2, CO, CO_2, and O_2 and a Horiba MEXA-1170HFID for UHC measurements, both provided by FOCA.

The PM sample train begins with a 5 ft (1.5 m) 3/8 inch (0.95 cm) diameter carbon loaded PTFE line. A splitter box heated to 160°C separated the FOCA and Missouri S&T PM sample with each line containing an isolation valve that is capable to shutting off the sample in order to allow an instrumentation zero with only dilution gas and to isolate the two lines. Two 3/8 inch carbon loaded PTFE tubes of 10 ft (3.0 m) in length connected the splitter box to the eductors. The 10 ft line brought the PM sample straight into the FOCA eductor while the other brought the PM sample to the dilutor box for the Missouri S&T line. The Missouri S&T dilutor box contained two chambers, one heated to 160°C for a splitter and another heated to 60°C for the eductor. The splitter had both branches caped due to only one gas analysis system being present. Both eductors used a common dilution supply which was heated to 60°C. All PM sample lines prior to the eductors were heated to 160°C while the transfer lines after the eductors and before the cyclones were heated to 60°C. The main transfer lines consisted of a 12 m long, 10 mm tube for the FOCA line while the Missouri S&T line was 50 ft (15.2 m) of 3/8 inch carbon loaded PTFE line. The total sample line length was approximately 26.5 m for the Missouri S&T line and 23.5 m for the FOCA line with 11.5 m of length prior to dilution being added for both lines. Each transfer line had a flow rate of approximately 25 lpm.

At the end of each transfer line was a cyclone designed to remove particle greater than 2.5 μm at a flow rate of 10 lpm, which both protects the instruments and reduces erroneous data from metal particles from engine wear. With 25 lpm going through the cyclone, the cut size was reduced to about 1 μm. After the cyclone, there was a branch in each line leading to a LI-COR LI-840A provided by Missouri S&T and a TSI 3776 provided by the EPA with a filter capillary dilutor (in order to bring

Table 6.1: Instruments included on each suite (similar instruments paired).

Suite 1	Suite 2
APC (1 CPC)	DEED (3 CPCs)
LII (NRC)	LII (Honeywell)
MSS 1	MSS 2
DMS500/MAAP	DMS500
SP-AMS	AMS

the particle count down so it does not max out) for the purpose of monitoring line stability. A series of valves and wyes was inserted to allow the sample to be quickly transferred from one instrument suite to the other. Three valve configurations were used. The first, called "Default," had instrument suite 1 sampling from the FOCA line while suite 2 was sampling from the Missouri S&T line. The second configuration, called "Switch," was the opposite valve configuration as the default. The third configuration, called "Both," had all four valves open such that each instrument suite was sampling the same sample; this was used for instrument comparison while the other valve configurations provided the means for line comparison.

The PM sample was then split several times through a series of wyes to bring it to each instrument. Each instrument suite consisted of mass, number, size, and chemical composition instruments; a break down is shown in Table 6.1. The mass instruments included two AVL Micro Soot Sensors (MSS) provided by AVL and two Artium Technologies LII 300s, one provided by NRC and the other by Honeywell. An additional mass instrument, a Thermo Model 5012 MAAP, provided by Aerodyne, was switched in and out in place of the DMS on suite 1. Two additional diluters were used for the number instruments. Suite 1 contained an AVL Particle Counter (APC), provided by AVL, which contains a catalytic stripper and a TSI 3790 which has a cutoff of 10 nm. Suite 2 had a Dekati Engine Exhaust Diluter (DEED), provided by Dekati, containing two Dekati eductors in front of three TSI CPCs provided by TSI

Table 6.2: Engine test details.

Test	Date	Engine Model	Test Cycle	Notes
1	5 Dec 2011	CFM56-7B27/3	Warm Up	Shakedown Test
2	6 Dec 2011	CFM56-5C4/P	Seal Test	
3	7 Dec 2011	CFM56-5C4	Seal Test	
4	9 Dec 2011	CFM56-7B24/3	Seal Test	
5	9 Dec 2011	CFM56-7B24/3	Seal Test	
6	12 Dec 2011	PW4060	Seal Test	
7	12 Dec 2011	CFM56-5C4	Seal Test	
8	13 Dec 2011	PW4060	Vibration Test	"Both"
9	15 Dec 2011	CFM56-7B27	Seal Test	Catalytic Stripper
10	15 Dec 2011	CFM56-7B27	Vibration Test	Catalytic Stripper
11	15 Dec 2011	CFM56-7B27	Trim Balance Test	Catalytic Stripper

downstream; a 3790 with a 23 nm cutoff, a 3772 with a 10 nm cutoff, and a 3788 with a 2.5 nm cutoff. Additional non-ARP instruments used for system verification included two Cambustion DMS500s provided by Missouri S&T that provided PM size distributions. Chemical composition was measured by two AMSs, one a SP-AMS provided by ETH in suite 1 and the other AMS provided by Aerodyne in suite 2. The last day of testing included two catalytic strippers, provided by Cambridge University, operating in parallel inserted before the instruments in suite 2.

6.2. TEST DETAILS

The experiment consisted of 11 engine runs as shown in Table 6.2 with all emissions measurements piggybacked on post maintenance engine test cycles. The first test, taking place on 5 December, was a "Shakedown" which has the primary purpose of checking the experiment setup integrity and test procedures. While data was recorded, it was never analyzed, and not all necessary instruments were setup at that point. The test on 6 December did not have the Dekati DEED up and running along with the 3 downstream CPCs. Temperature and pressure monitoring

programs were not up for this run either. The test on 13 December used the valve configuration "Both" as discussed earlier for the purpose of performing instrument comparison. Two catalytic strippers were inserted in parallel before suite 2 for the tests on 15 December and had operating temperatures of 250°C, 350°C, and 400°C at different points throughout the 3 tests. All tests were conducted with engines that were undergoing initial tests after maintenance.

6.3. LINE COMPARISON

The first primary objective of the test was to compare the two PM sample lines. While both the FOCA and Missouri S&T lines were constructed similarly with the exception of the main transfer lines, which varied in length by 3 m. While the inner diameters of the two lines were roughly equivalent, the FOCA transfer line was 12 m long while the Missouri S&T transfer line was 15 m long. Additionally the two eductors were operating at different dilution factors due to the Missouri S&T eductor having its spill tube reduced to 3/8 inch from 12 mm while the FOCA spill tube remained at 12 mm. By performing a both a "Default" and "Switch" valve configuration during a single stable engine operating condition, a single point can be determined for comparing the FOCA and Missouri S&T transfer lines for each instrument.

There were 28 corresponding test points used for line comparison, 12 for CFM56-5Cs, 14 for CFM56-7Bs, and 2 for PW4060s. Figure 6.2 depicts the the overall line comparison for the mass instruments, while Figure 6.3 does the same for the number instruments. The graphs for individual instruments are located in Appendix C. The figures all present the FOCA line on the x-axis and the Missouri S&T line on the y-axis with a line representing unity in purple. The data points for each engine type is represented by a separate color with a linear fit made to all data points.

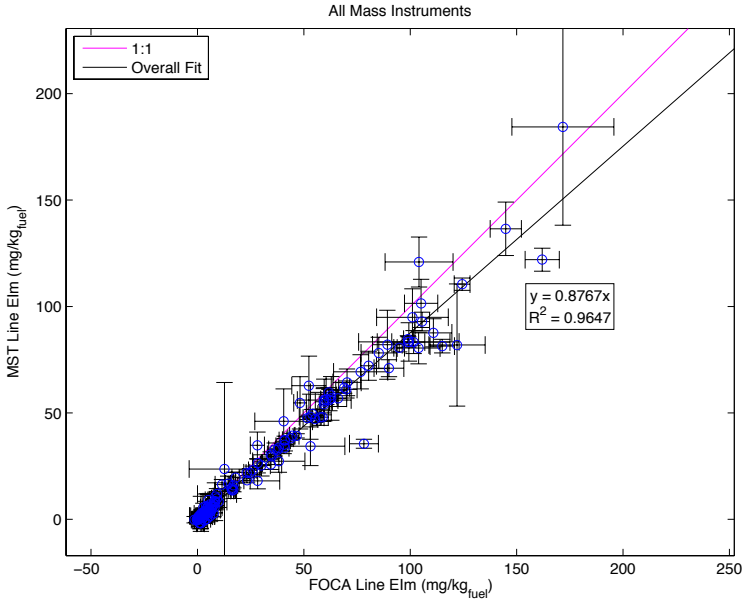

Figure 6.2: Overall line comparison for mass instruments.

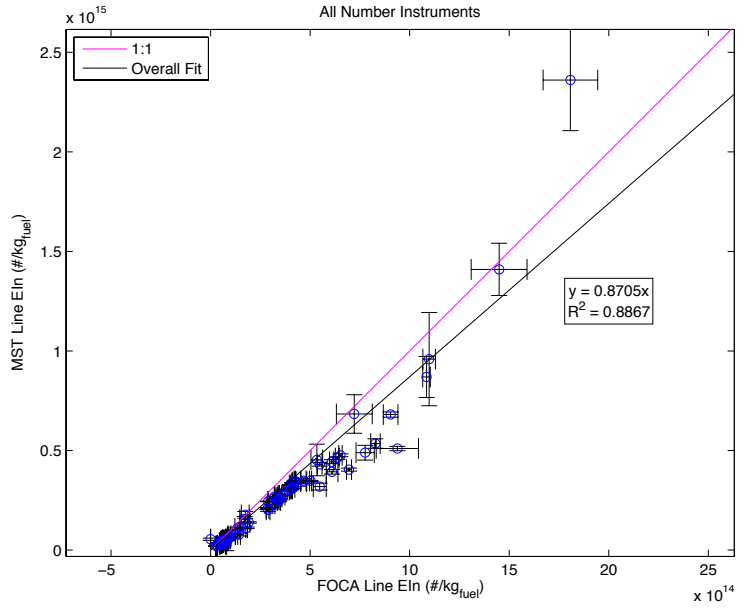

Figure 6.3: Overall line comparison for number instruments.

The linear fit was constrained to pass through the point (0,0) with the slope and R^2 value from the fit shown for each instrument. Overall the two lines compared rather well, with the FOCA line reading higher on average by 12.3% ,for the mass instruments and 13.0% for the number instruments. All percentage differences are given with respect to the FOCA line having the higher EI value, such that a negative percentage would indicate the Missouri S&T line containing the greater EI value. Suite 2, overall, was closer to unity than suite 1 with a 9.6% and 3.7% difference compared to a 16.2% and 27.5% difference for mass and number instruments, respectively.

6.4. INSTRUMENT COMPARISON

The second primary objective was to compare instruments. This was done in two aspects, the first was to compare similar instrument in each suite to each other, and the second was to compare identical instruments to each other. In terms of mass instruments, each suite had two dedicated instruments, a LII and MSS, as well as a DMS from which the mass can be calculated. Each suite had one dedicated number instrument (only looking at the TSI 3790 in suite 2 for this section) along with a DMS. On 13 December, the test featured the valve configuration "Both" to allow for similar instruments on each suite to be compared using an assumed common source. All instrument comparison data points in this section are valid when both instruments are on similar conditions (i.e. same engine setting and line configuration) from 5-13 December 2011.

Both instrument suites contained a DMS 500 for measuring the size distribution, from which a number and mass value could be calculated. This allowed a common instrument of comparison for both number and mass devices. Figure 6.4 shows the mass result comparison for DMS devices. The DMS on suite 2 read on average 23% higher than the suite 1 DMS. The R^2 value was 47% primarily due to a

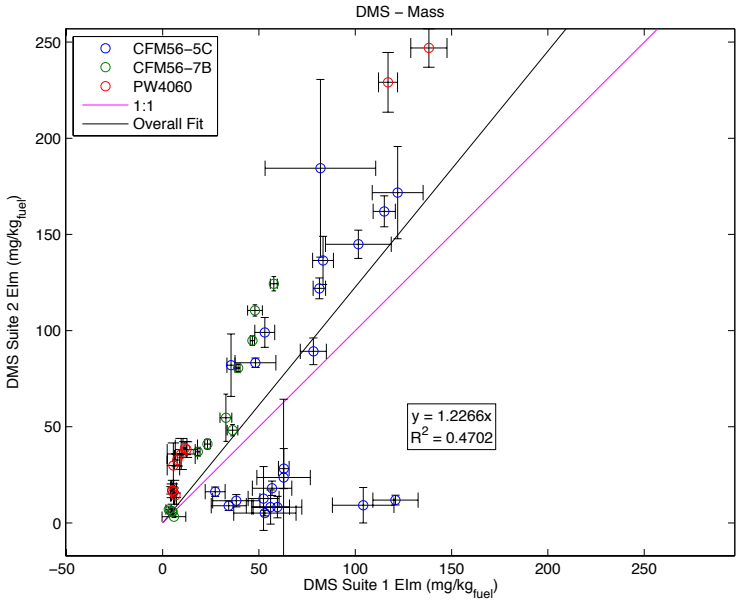

Figure 6.4: DMS mass result instrument comparison.

group of data points where the suite 2 DMS, showed a mass result near 0 while the suite 1 DMS was much higher. If the data points in which the suite 1 DMS was three times the value of the suite 2 DMS the overall results show that the suite 2 DMS was 60% higher in mass measurements with a R^2 value of 83%. Figure 6.5 shows the number result comparison for DMS devices. For number measurements, the suite 2 DMS was 55% higher with a R^2 value of 73%. This is much closer to the filtered mass overall result.

Both of the dedicated mass instruments agreed well with the similar instrument in the opposite suite. The LII in suite 2 was on average 15% higher than the LII in suite 1 as shown in Figure 6.6. The MSS in suite 1 was 2% higher on average than the MSS in suite 2 as shown in Figure 6.7. Both of the dedicated mass instruments had a high correlation, with a R^2 value of 99% for the LII and 99% for the MSS. The comparison of the suite 1 LII and MSS is shown if Figure 6.8 with the LII reading on average 37% higher than the MSS with a R^2 value of 99%. The suite 2 LII was

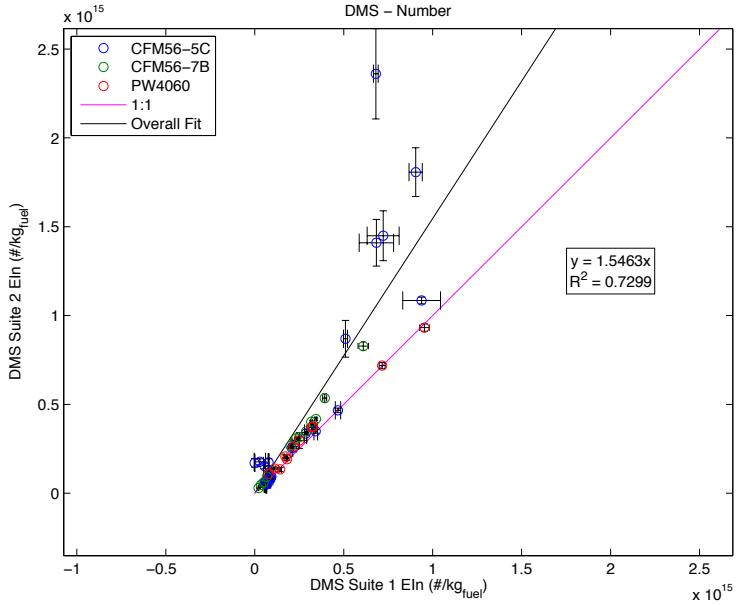

Figure 6.5: DMS number result instrument comparison.

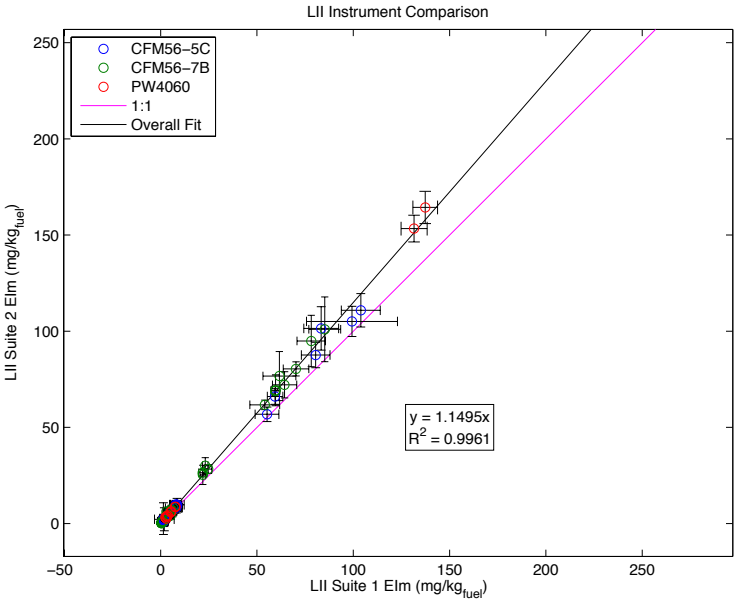

Figure 6.6: LII instrument comparison.

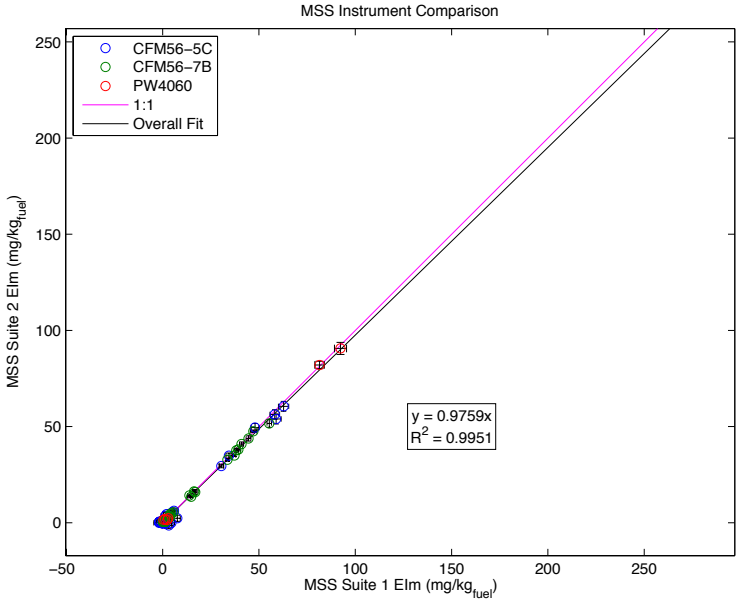

Figure 6.7: MSS instrument comparison.

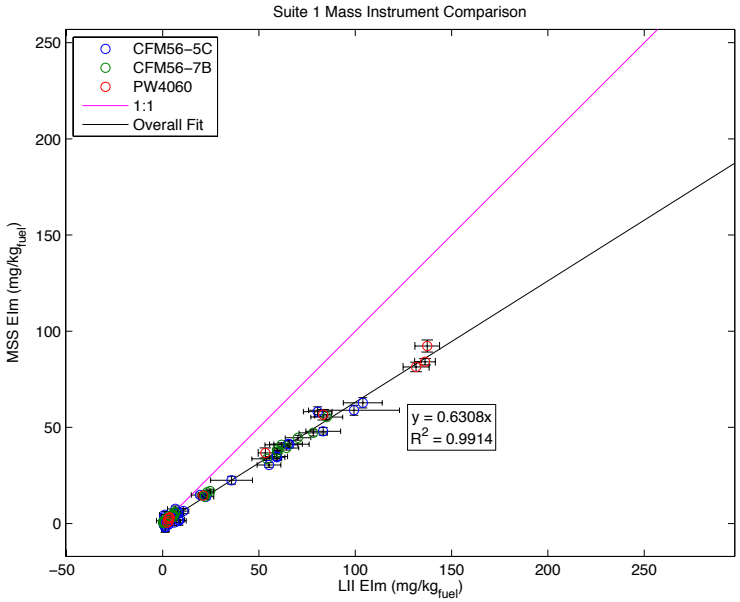

Figure 6.8: Suite 1. LII and MSS instrument comparison.

Table 6.3: Mass instrument summary. Mass instrument summary. Values are A(R^2), where y=Ax.

Suite 1		
	LII	MSS
DMS	0.5979(0.3701)	0.3786(0.3537)
LII	-	0.6308(0.9914)
Suite 2		
	LII	MSS
DMS	0.5502(0.7158)	0.2981(0.7163)
LII	-	0.5374(0.9950)

46.3% higher on average than the MSS with a R^2 value of 99%. Table 6.3 shows a summary of the mass instrument comparison. Overall, the DMS's measured EIm 40-45% higher than the LIIs, and the LIIs were 37-46% higher than the MSSs. For both suites the LII-MSS had a high rate of correlation, greater than 99%, while the suite 1 DMS-LII and DMS-MSS were around 36% and suite 2 around 72%. Although there was about a 40% difference in the measurements, both the LII and MSS had very linear EIm ratio over the entire range of engine conditions, while the DMS's integrated calculation did not.

In terms of number instruments, this section will only look at the DMS's, APC, and the TSI 3790 (23 nm cutoff). The other TSI CPC's will be looked at in the next section. For the number instruments in suite 1, there was a 91% agreement with a R^2 value of 86.4%, as shown in Figure 6.9 between the DMS and APC. The number instruments in suite 2, shown in Figure 6.10, show an agreement of 16% between the DMS and TSI 3790. Both the TSI 3790 and the APC have a size cutoff of 23 nm and are further diluted when compared to the other instrument, the method of dilution vary substantially. The APC uses a chopper diluter, which chops in a known sample volume with a constant dilution flow. This produces a fairly constant dilution ratio over a range of pressures and the instrument takes into account particle loss in its sample line. The TSI 3790 was downstream of a Dekati DEED, which contained

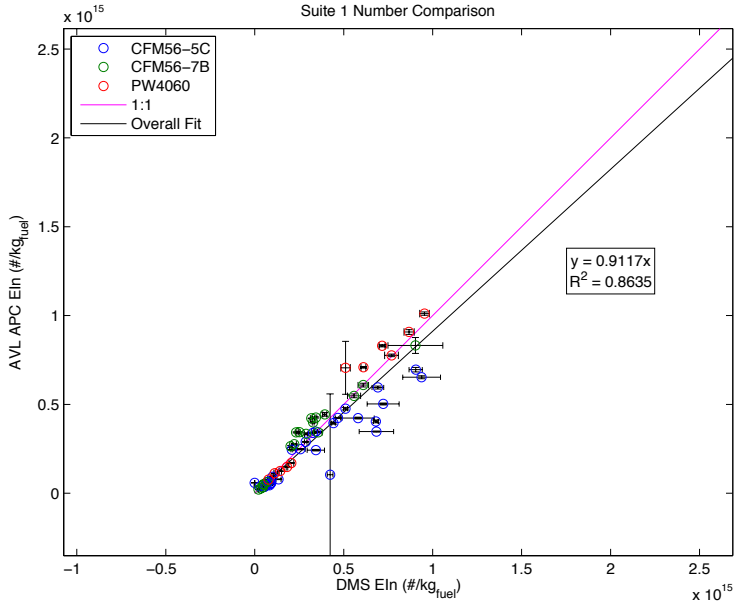

Figure 6.9: Suite 1. DMS and APC instrument comparison.

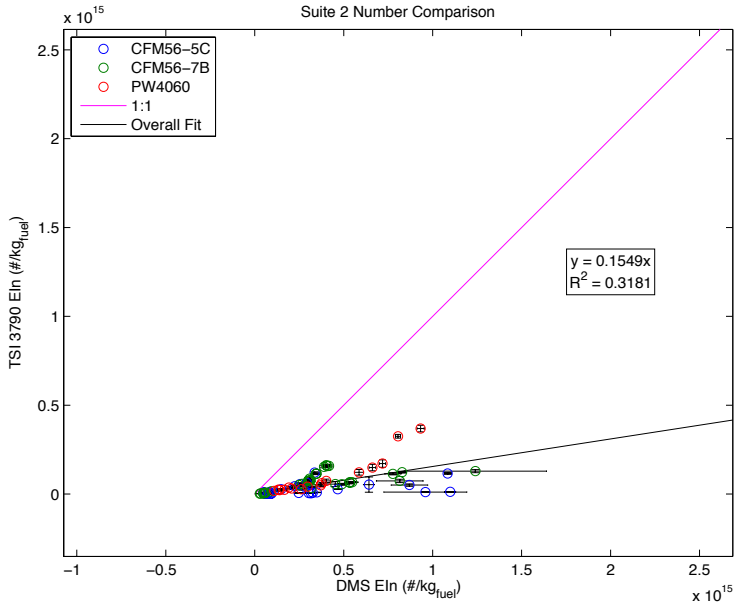

Figure 6.10: Suite 2. DMS and TSI 3790 instrument comparison.

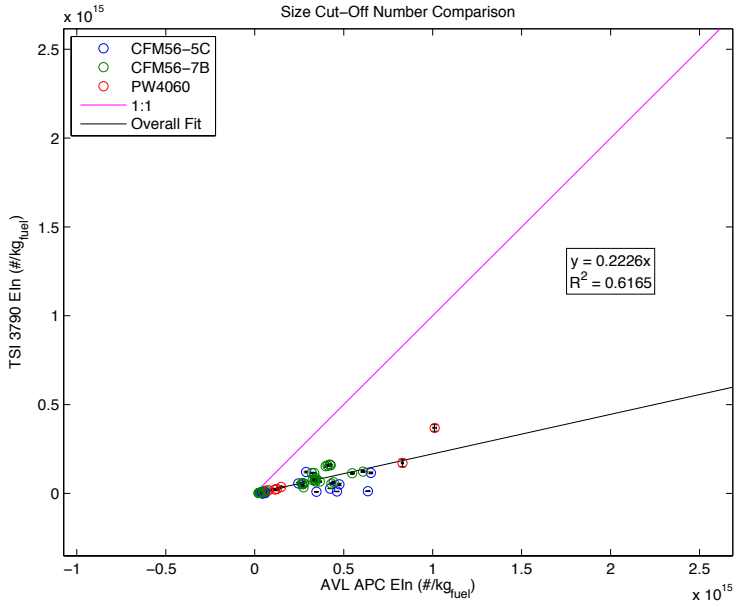

Figure 6.11: APC and TSI 3790 instrument comparison.

two eductors. The eductor's dilution ratio vary depending on sample and dilution pressure, both of which were measured. The dilution ratio used for calculating EIn for the CPC's were based on experimental data provided by Dekati for the DEED used in this experiment. This method was less certain and could be a reason for the substantial difference in number EI for the CPCs compared to the other instruments. The comparison between the APC and the TSI 3790, shown if Figure 6.11, show a similar result to the DMS and TSI 3790 with an agreement of 22% and R^2 of 62%.

6.5. CPC CUTOFF SIZE

The third primary objective was to investigate the impact of CPC cutoff size. Downstream of the Dekati DEED were 3 CPCs, a TSI 3790, 3772, and a 3788 with cutoff sizes of 23, 10 and 2.5 nm respectively. Figure 6.12 shows the TSI 3790 CPCs compared to the suite 2 DMS. The TSI 3790 with a 23 nm cutoff when compared with the DMS (15% agreement) or APC (22% agreement) showed very similar rela-

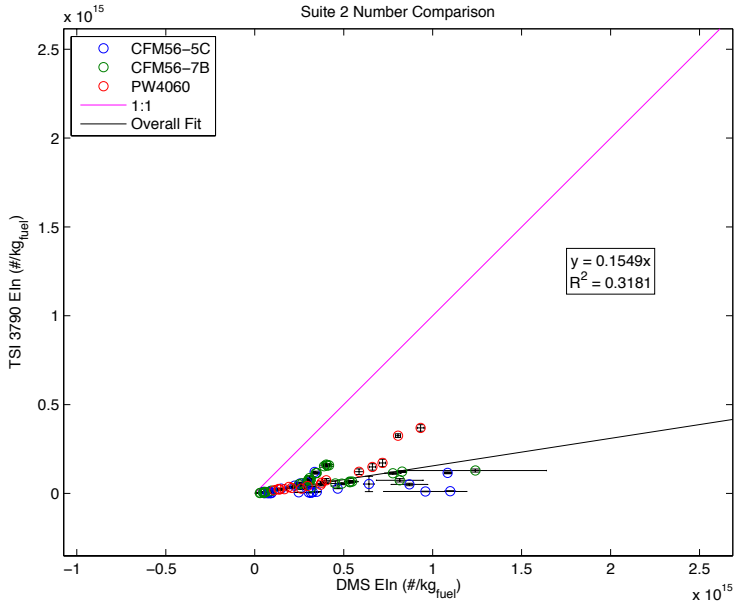

Figure 6.12: CPC Cutoff Size 23 nm vs. DMS 500.

tionships. Both the 10 and 2.5 nm cutoff, shown in Appendix C, presented similar relationships when compared to the DMS with an agreement of 36% and 34% respectively. When the CPCs are compared to one another, the 2.5 and 10 nm cutoff presented in Figure 6.13 showed a 95% agreement with uncertainty for each test point overlapping unity. This is primarily due to the size distributions dropping off around 10 nm. Although when the 10 and 23 nm cutoff are compared, shown in Figure 6.14, there was a 34% departure in agreement. This large increase in measured particles occurs in an area where volatile PM came form, making it likely that if a CPC were used with a low cutoff size, that a catalytic stripper would also need to be deployed. The dilution ratio for the DEED was calculated using recorded pressures and experimental results provided by Dekati and not CO_2 measurements as used in most other calculations. It is possible that this multistep estimation of the dilution ratio may be greatly under estimated. In any future deployment of a system with this type of

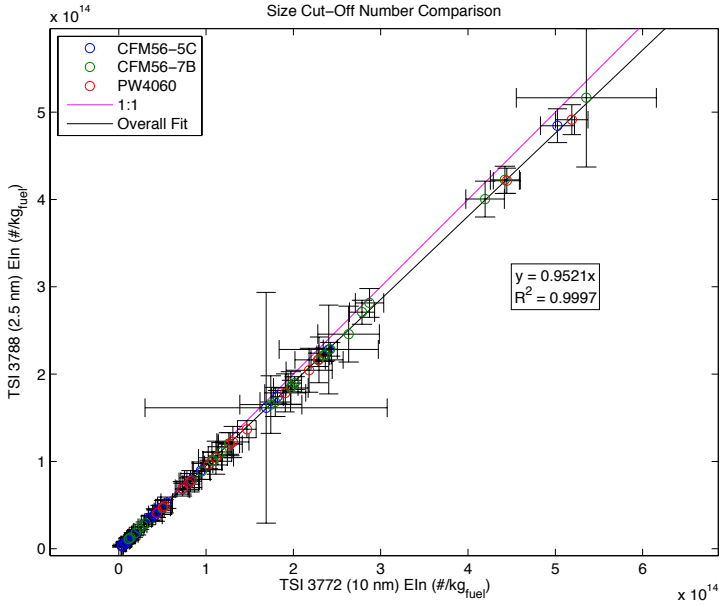

Figure 6.13: CPC Cutoff Size 10 nm vs 2.5 nm.

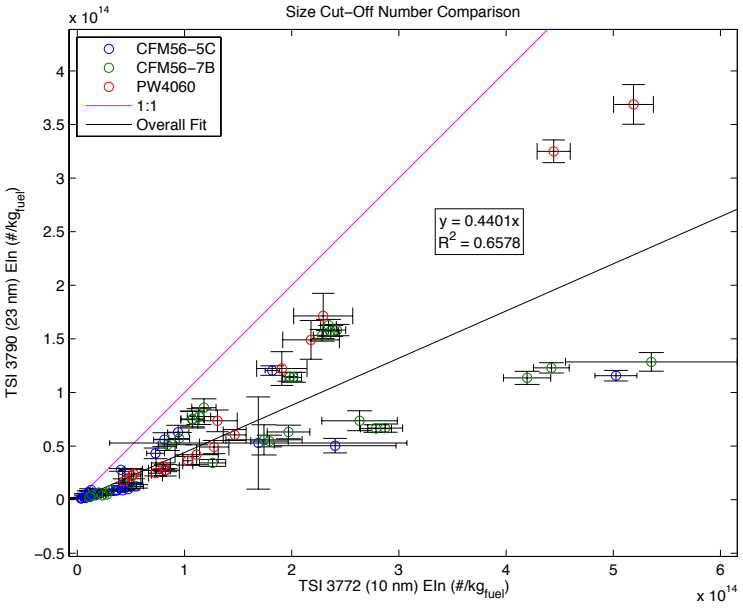

Figure 6.14: CPC Cutoff Size 10 nm vs 23 nm.

additional dilution, a second CO_2 monitor should be included to accurately measure the additional dilution ratio.

6.6. CATALYTIC STRIPPER PERFORMANCE

Another objective was to assess catalytic stripper performance; runs for this purpose were conducted on 15 December. The catalytic stripper was included as volatile PM could form in the system due to using downstream dilution and the objective was to measure only non-volatile PM. The catalytic stripper was operated at 3 different temperatures over the course of the tests, 250, 350, 400°C, with a majority of the test point occurring at the 250°C operating condition. From an ARP standpoint, the only instrument that would be impacted is the number instrument as the mass instruments considered measure non-volayile elemental carbon only. As typical volatile PM have diameters less than 23 nm, the use of a catalytic stripper would allow CPCs to be used with a lower size cutoff, producing a less truncated number measurement.

The catalytic stripper had little effect on the mass instruments, as shown in Figure 6.15 as well as Appendix C. At the 250°C setting on the catalytic stripper, all of the uncertainty bars overlapped with the overall averages without the catalytic stripper inserted. This indicated that the mass instruments were measuring non-volatile PM only.

The number instruments, however, displayed significant reduction in measured EIn values, shown in Figures 6.16 and 6.17 with additional graphs shown in Appendix C. The DMS on Suite 2 went from reading 55% on average greater than Suite 1 DMS to 41% and 60% below the Suite 1 DMS for the 250°C and 400°C conditions. When the CPCs were compared to the APC, the measured EIn value dropped to 93% less than the APC reading for the both TSI 3772 and 3788 and 96% less than

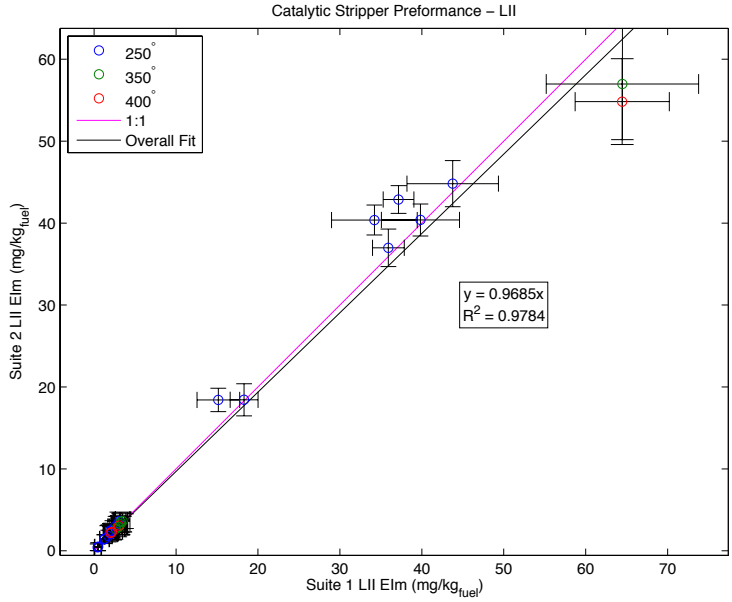

Figure 6.15: LII comparison with catalytic stripper inserted before instruments on Suite 2.

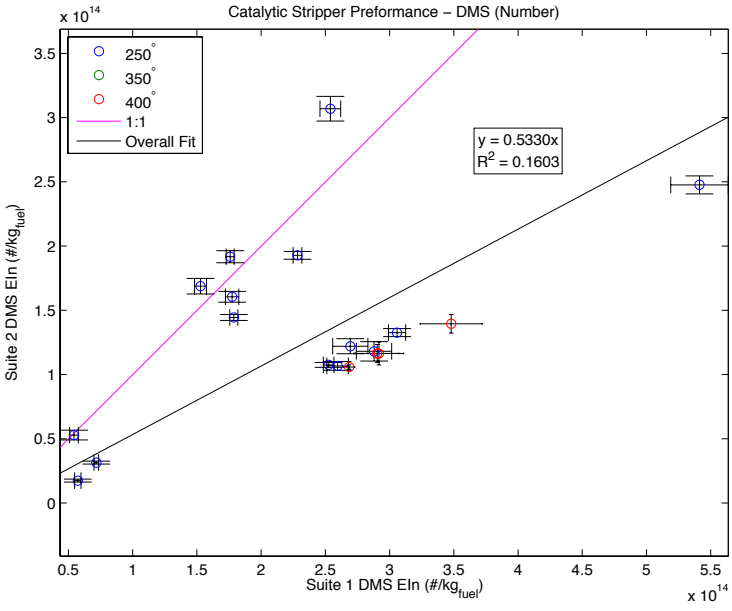

Figure 6.16: DMS number comparison with catalytic stripper inserted before instruments on Suite 2.

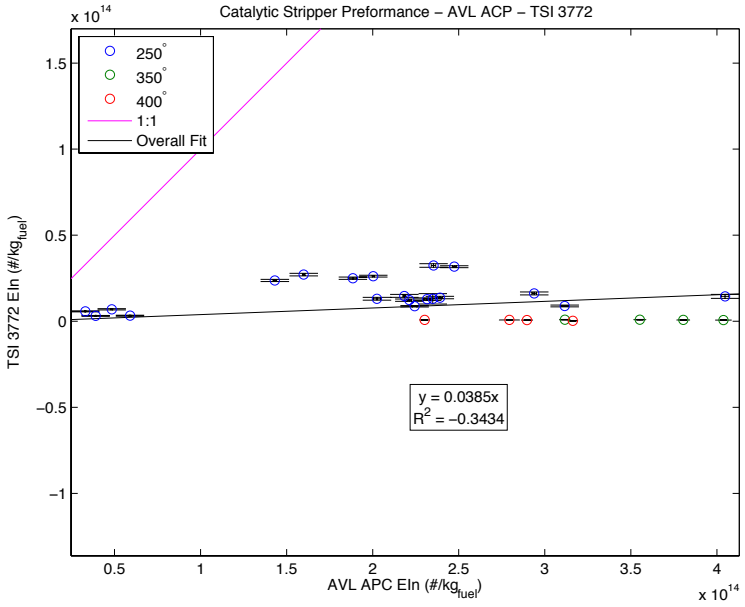

Figure 6.17: APC to TSI 3772 number comparison with catalytic stripper inserted before instruments on Suite 2.

for the TSI 3790. Without the catalytic stripper inserted, the 3772 and 3788 were at 55% less while the 3790 was 78% less then the APC. When the catalytic stripper was at 350°C and 400°C, the 3 CPC's reported an EIn 99% less than the APC. It is likely that there was some volatile material forming in the system with diameters greater than 23 nm. The catalytic stripper had little effect of CPC cutoff size results, as shown in Figures 6.18 and 6.19. The results from the 10 to 23 nm cutoff check were vertically unchanged compared to without the catalytic stripper, indicating that the volatile PM was present mostly in sizes greater than 23 nm.

6.7. CONCLUSIONS

The primary objective of the Zurich tests was to compare if 2 different sample line could provide the same results. Both line had results within 13% of each other for both mass and number measurements, with most of the uncertainty on the data points

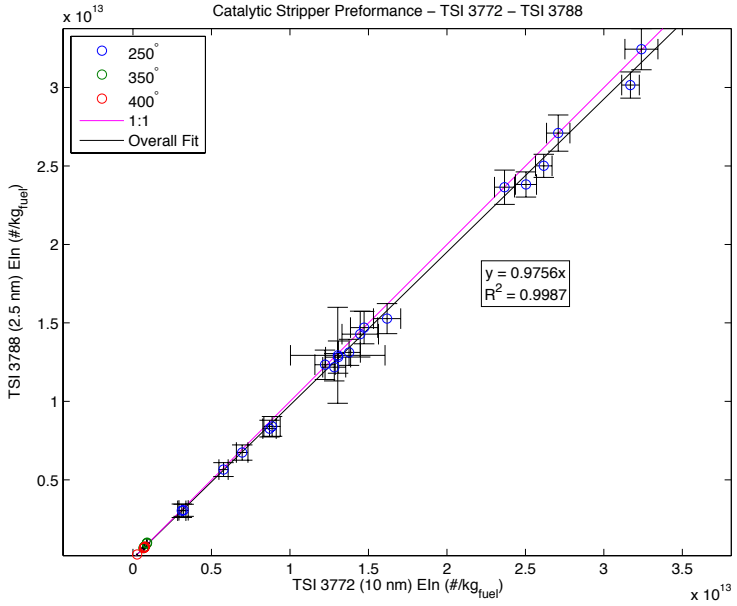

Figure 6.18: TSI 3772 to TSI 3788 size cut-off check with catalytic stripper.

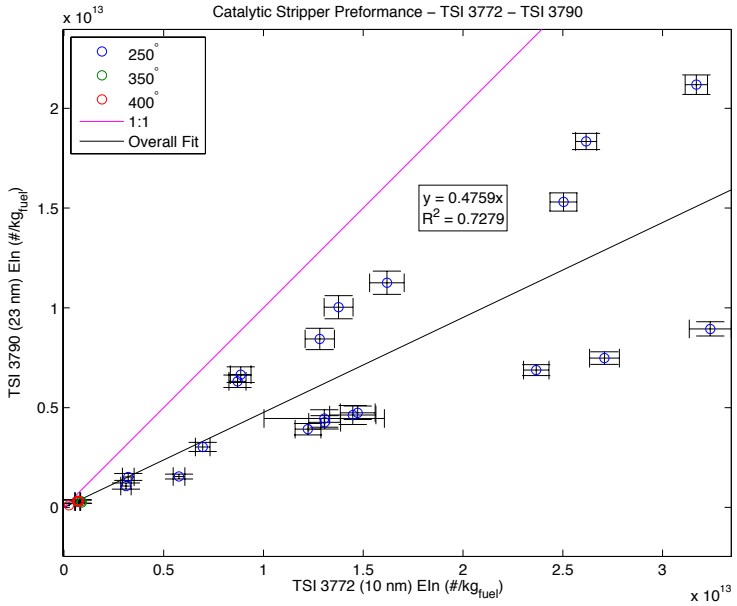

Figure 6.19: TSI 3772 to TSI 3790 size cut-off check with catalytic stripper.

overlapping the unity line. Another main objective of these tests was to compare similar instruments. Both of the mass instruments tested, LII and MSS, agreed well with the same instrument in the opposite suite. The LII on average measured higher than the MSS by 37% with a high correlation between the 2 instruments. For number instruments, the APC agreed within 9% of the DMS's integrated calculation, while the CPCss measured between 50 and 80% less than the APC on average. The final main object was to investigate CPC cutoff size. There was little difference between the CPC's with a cutoff size of 10 and 2.5 nm with both measuring 55% less than the APC, while the CPC with the 23 nm cutoff measured 78% than the APC. By dropping the cutoff size from 23 to 10 nm, an additional 23% of particles were measured. The secondary objective was to examine the catalytic stripper performance. The mass instruments should change little in EIm measurement, indicating that they were already measuring only non-volatile PM. The size instrument showed a dropped of 32% in terms of mass measurement of comparison, while the number measurement drop 101%. The CPCs however dropped to -93 and -96% in terms of EIn when compared to the APC, drop of 38% for the 2.5 and 10 nm cutoff and 19% for the 23 nm cutoff. It is likely that a number device with integrated diluter and catalytic stripper will function better than a CPC with external diluter and catalytic stripper.

7. CONCLUSIONS AND RECOMMENDATIONS

This thesis has discussed experiments conducted by Missouri S&T to help produce recommendations and perform background research to aid the SAE E-31 Committee in creating an Aerospace Recommended Practice (ARP) for the measurement of non-volatile particulate matter (PM) in aircraft engine exhaust for engine emissions certification. This process arose out of the concerns of the health and environmental implications the PM pose and the inadequacies of smoke number in investigating these issues. The research study began in the Missouri S&T Center of Excellence for Aerospace Particulate Emissions Reduction Research (COE) laboratory, as discussed in Section 4, with an examination of the jet engine surrogate used, the miniCAST. This determined stability and reproducibility of the device as well as finding operating conditions that provided similar PM size distributions to aircraft previously measured by COE. The miniCAST was also integrated into the COE's PM measurement system so that the source PM size and concentration was independent of changes in the PM measurement system.

Most of the experiments conducted at Missouri S&T involved investigating component performance. One of the most significant of these experiments was a line conditioning experiment where a PM sample line was constructed out of clean electropolished line and subjected to the miniCAST exhaust to determine the time needed for the measured signal to stabilize. This experiment produced a recommended PM sample line break-in procedure of 2-3 hours of being exposed to engine exhaust prior to data collection. Also determined was that if the PM sample line should not be purged with particle free air and in the event of a purging, the line should undergo 30 minutes of reconditioning prior to data collection. These two recommendations are to help insure that the line loss characteristics of the PM sample line are constant

with time. A volatile particle remover (VPR) was also studied as part of the in-house experiments. It was determined that salt (NaCl) particles provide similar results for penetration measurements to soot particles. The miniCAST PM was found to contain a significant amount of volatile PM below 50 nm for certain operating conditions.

Another component test was the evaluation of three different eductors to act as the primary diluter for the PM sampling system. These eductors were checked for their performance characteristics, dilution and sample flow at different pressures, allowing the dilution ratio to be calculated at a variety of different operating conditions. The three eductors were also investigated for their particle loss characteristics and two of the eductors, when heated to 60°C, had penetration efficiency greater than 100% because particles were being produced by the eductor. There were a few operating characteristics that were desirable, a sample flow rate of less than 2 lpm, a total diluted flow of greater than 14 lpm, and a dilution ratio between 2 and 20. None of the eductors satisfied all of the desired characteristics over the range of pressures studied, leading to the need for a pressure relief valve to be included in the system just prior to the eductor. This pressure relief valve would allow the eductor to operate over a narrow range of dilution ratios while preventing the eductors from extracting too much sample flow. Of the three eductors evaluated, the Dekati Diluter DI-1000 performed the best with relatively constant particle loss over a large range of sizes, meeting the other operating characteristics at atmospheric pressure and below. When combined with a pressure relief valve it would operate as desired above atmospheric pressure.

The first E-31 prototype system was set up at the second alternative aviation fuel experiment (AAFEX II), as discussed in Section 5. This experiment provided direct comparison between a system operating with probe tip dilution and one diluting the sample down stream. Probe tip dilution provided 26% higher EIn measurements than the E-31 line although these differences can be accounted for by particle line

loss. There was negligible difference between the two dilution methods in terms of EIm measurement. This allows current engine testing facilities to have the gaseous sampling system slightly modified with the inclusion of a splitter near the beginning of the sample transfer line and the addition of a PM sample line and instrument suite to allow the measurement of non-volatile PM as well. Also performed at AAFEX II was a study that compared measured sample line penetration with theoretical calculations. It was determined that the theoretical calculations provide a good quick alternative to measuring penetration with a maximum error of 5.3% and size dependent random and systematic error that increased as size decreased.

The ARP demonstration at SR Technics, discussed in Section 6, compared two different PM sampling systems, checking what will be two non-volatile PM measurement reference systems. The two PM sample lines had a 13% difference in both mass and number measurements. Two mass instruments, the Artium laser-induced incandescence (LII) and AVL Micro Soot Sensor (MSS) and, showed an 37% difference in measured soot concentration, while the LII's in opposite suites showed a 13% difference and the MSS's showed a 2% difference. The AVL Particle Counter (APC) showed a 9% difference compared to the Cambustion DMS 500. A Dekati DEED was used to further dilute the PM sample for several CPC's which resulted in measured number values appreciably below the APC, although the dilution factor through the DEED was estimated from pressure measurements. If additional dilution is needed to improve CPC accuracy, a known dilution factor needs to be determined. If a CPC with a 10 nm size cutoff is used as opposed to a CPC with a 23 nm cutoff that is common with diesel measurements, an additional 55% of particles can be counted. Reducing the size cutoff further has a negligible increase in measured particles. A volatile particle remover (VPR) was added to the system, resulting in

significant drop in measured EIn with minor impact on measured EIm. The present mass instruments measured only non-volatile PM while a number instrument will require a VPR preceding it.

APPENDIX A

DATA REDUCTION PROCESS

This section describes the general process in reducing the data measured (typically recorded at 1 Hz) to a final emissions index value for a test point.

DATA TIME SYNCING AND TEST POINT DETERMINATION

All data sets are time synced to a master data set. The master data set is typically an instrument that is recording for the duration of the experiment or if available fuel flow rates. This is necessary due to different instruments response times or even computers set to different times. Data is time synced by visually lining up peaks and valleys that usually correspond to engine power changes and valve switches, an example is shown in Figure A.1 In the example shown, the undiluted

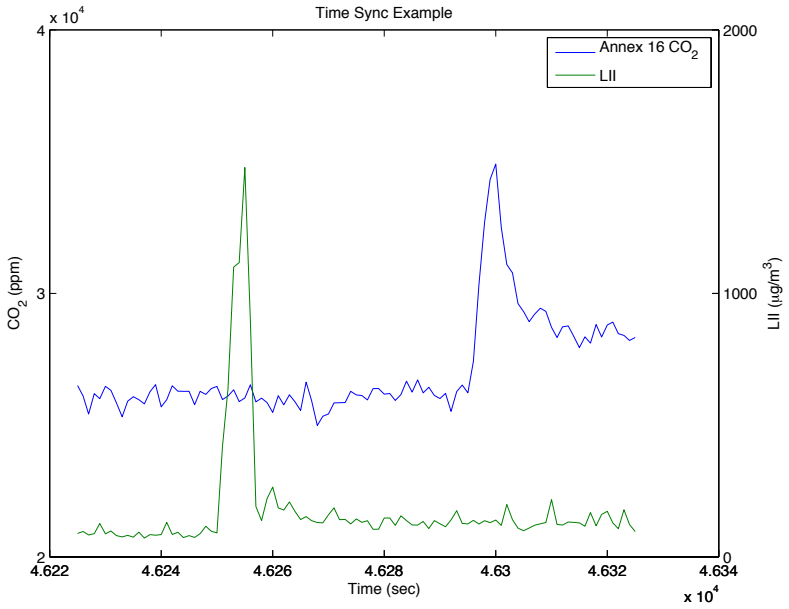

Figure A.1: Example of data time syncing.

CO_2 has a single peak at 46300 sec and the LII has one at 46255 sec, resulting in 45 sec added to all LII times. Typically the time sync value will stay constant (within a few seconds) over the duration of the run, but in some cases additional offset may be needed for short test points. After the data is time synced the test point start and end times are adjusted to encompass the duration of the stable signal.

MASS AND NUMBER EMISSION INDICES CALCULATION

The emission indices (EI) can be calculated 2 different ways, either on a second by second basis or using the average values over the test point. When calculating on a second by second basis the time sync value needs to be constant over the duration of the run group. The mass and number based EI calculations are given in Eq. A.1-A.2,

$$EI_M = PM_M \frac{0.082 T_{sample}}{[CO_2]\,(M_C + \alpha M_H)\,P_{sample}} \tag{A.1}$$

$$EI_N = PM_M \frac{0.082 T_{sample}}{[CO_2]\,(M_C + \alpha M_H)\,P_{sample}} 10^6 \tag{A.2}$$

where PM_M and PM_N are the particle mass and number concentration in the exhaust mixture, $[CO_2]$ is the CO_2 concentration in the exhaust mixture, P_{sample} and T_{sample} are the pressure and temperature of the sample at the instrument, and α is the hydrogen-carbon ratio of the fuel. These equations are the simplified particle EI equations given in AIR 6037 [26]. The CO_2 and PM concentrations are the undiluted value but due to the them being a in a ratio the only the diluted values are needed for the simplified calculation.

SIZE DISTRIBUTIONS CALCULATIONS

For instruments with that output a size distribution require additional calculations to be made to determine the emission indices. Before these calculation are made the size distributions are typically corrected for background signal and then line loss. The background signal is measured typically at the beginning and end of the run without the PM source operating. The line loss can be determined either experimentally or theoretically from Aerocalc or similar calculations. The mass and

number based EI calculation are shown in Eq. A.3-A.4,

$$EI_M = \frac{\pi\rho}{6}\sum_{i=1}^{n} {x_{cm_i}}^3 \Delta_i pm_i \frac{0.082T_{sample}}{[CO_2]\,(M_C + \alpha M_H)\,P_{sample}} \tag{A.3}$$

$$EI_N = \sum_{i=1}^{n} \Delta_i pm_i \frac{0.082T_{sample}}{[CO_2]\,(M_C + \alpha M_H)\,P_{sample}} 10^6 \tag{A.4}$$

where Δ_i is the logarithmic based width of the size bin and pm_i is the particle concentration in size bin i. Additionally the geometric mean diameter (GMD) and geometric standard deviation (GSD) can be calculated from Eq. A.5-A.9.

$$PMNC = \sum_{i=1}^{n} \Delta_i pm_i \tag{A.5}$$

$$A_M = \frac{1}{PMNC}\sum_{i=1}^{n} \Delta_i \log D_{P_i} pm_i \tag{A.6}$$

$$A_{2M} = \frac{1}{PMNC}\sum_{i=1}^{n} \Delta_i \left(\log D_{P_i}\right)^2 pm_i \tag{A.7}$$

$$GMD = 10^{A_M} \tag{A.8}$$

$$GMD = 10^{\sqrt{{A_{2M} - A_M}^2}} \tag{A.9}$$

APPENDIX B

DEVICES USED

This section lists the devices used during the course of the study along with specifications and concludes with a short discussion of instrument calibration uncertainty.

ARTIUM TECHNOLOGIES LII 300

The LII 300 was produced by Artium Technologies Inc and measured soot concentration, specific surface area, and primary particle diameter using laser-induced incandescence (LII). The LII had a minimum mass reading of 0.2 $\mu g/m^3$ with a maximum reading of 20 g/m^3 with a precision of $\pm 2\%$. For the primary particle size in had a range from 10 to 100 nm with a precision of 2 nm and a specific surface area range from 50 to 200 m^2/g [45].

AVL PARTICLE COUNTER

The AVL Particle Counter, commonly referred to in the text as the AVL APC, was produced by AVL and used a TSI CPC to measure non-volatile particle number concentrations with a range of 0 to 10,000 particles/cm^3 (calibrated) and 0 to 50,000 particles/cm^3 (single count mode) with a size cutoff of 23 nm [46]. The device used during the AAFEX and Zurich experiments was a pre-production model with a size cutoff of 10 nm.

AVL MSS

The AVL Micro Soot Sensor was produced by AVL and measures soot concentration using photoacoustic soot sensing (PASS). It had a minimum detection limit of ~ 5 $\mu g/m^3$ with a maximum reading of 50 mg/m^3 [47].

CAMBUSTION DMS 500

The DMS 500 Fast Particle Analyzer was produced by Cambustion Limited and utilizes particle electrical mobility and sensitive electrometer detectors to measure particle size distributions in size spectral density ($dN/dlogD_P/cm^3$), allowing size, number, and mass to be calculated. The DMS 500 measures particles from 5 to 1000 nm in diameter with concentrations of 10^3 $dN/dlogD_P/cm^3$ at 10 nm and 80 $dN/dlogD_P/cm^3$ at 300 nm. This results in a number and mass sensitivity of $\sim$170 particles/cm^3 and $\sim$0.5 $\mu g/m^3$ for a typical diesel accumulation mode with a GMD of 80 nm and GSD of 1.8 [48].

MINICAST

The miniCAST model 6203 Type C was produced by Jing Ltd and produced soot particles with GMDs ranging from 10 to 60 nm at concentrations up to 10^8 particles/cm^3 with a mass output of up to 30 mg/h. The miniCAST had an undiluted exhaust of 3 lpm with up to 10 lpm of internal dilution [49]. It used propane as the fuel source and was supplied with air and nitrogen for operation.

LI-COR LI-840A

The LI-840A was a CO_2 and H_2O analyzer produced by Li-Cor. It has a measurement range of 0 to 20,000 ppm of CO_2 and 0 to 60 mmol/mol of H_2O with an accuracy of 1% for CO_2 and 1.5% for H_2O [50].

SABLE SYSTEMS CA-2A

The CA-2A was produced by Sable Systems and measures CO_2 over the range of 1 ppm to 10% [51].

THERMO SCIENTIFIC MAAP

The 2012 MAAP produced by Thermo Scientific measures black carbon with a minimum detection level of 50 ng/m^3 over a 10 minute average using multi-angle absorption photometry [52].

TSI 3772

The TSI 3772 was a condensation particle counter (CPC) that used n-butyl alcohol as the working fluid and only processed a single particle count mode. It detected particles 10 nm and above at concentration up to 10^4 particles/cm^3 with an accuracy of 10% [53].

TSI 3775

The TSI 3775 was a condensation particle counter (CPC) that used n-butyl alcohol as the working fluid. It detected particles 4 nm and above at concentration up to 5x10^4 particles/cm^3 in single count mode and 10^7 in photometric mode with an accuracy of 10% for single count mode and 20% for photometric mode [54].

TSI 3788

The TSI 3788 was a condensation particle counter (CPC) that used water as the working fluid and only processed a single particle count mode and was capable of 10 Hz data output. It detected particles 2.5 nm and above at concentration up to 4x1054 particles/cm^3 with an accuracy of 10% [55].

TSI 3790

The TSI 3790 was a condensation particle counter (CPC) that used n-butyl alcohol as the working fluid and only processed a single particle count mode and was capable of 10 Hz data output. It detected particles 23 nm and above to meet European PMP requirements at concentration up to 10^4 particles/cm^3 with an accuracy of 10% and contained an internal diluter with dilution factors ranging from 1 to 11 [56].

INSTRUMENT CALIBRATION ERROR

Condensation particle counter (CPC) calibration is detailed by Liu and Pui [57] uses an aerosol generator with electrostatic classification to produce uniform NaCl particles with an size accuracy of 2% and concentration accuracy of 5%. The DMS 500 uses a similar calibration method to CPC's [58], which produces a size accuracy of 5% for the range of 5 to 300 nm and 10% above and a number accuracy of 10%. Mass instruments are calibrated using a method detailed in NIOSH 5040 method [59]. The method uses deposited elemental carbon (EC) measurements on filters as the standard and the process has an accuracy of 16.7%.

APPENDIX C

ADDITIONAL GRAPHS

This appendix shows graphs that were not presented in the main portion of the document. Most of these graphs are similar to each other and were removed from the main portion of the document to aid in readability, i.e. not have several consecutive pages only containing graphs.

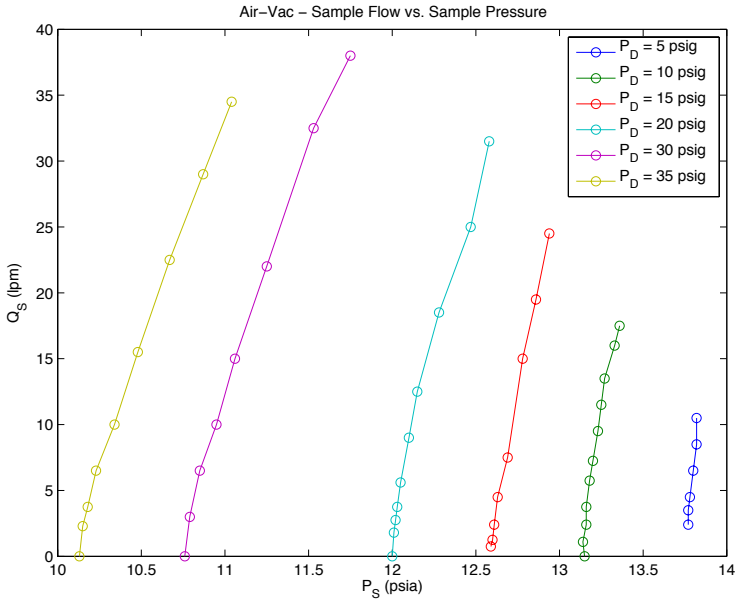

Figure C.1: Air-Vac eductor sample flow rate as a function of sample pressure at various diver pressures.

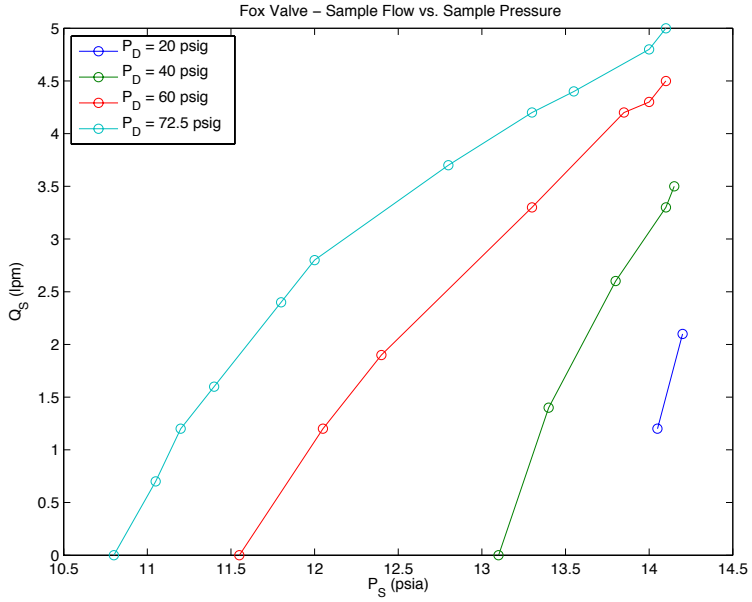

Figure C.2: Fox Valve eductor sample flow rate as a function of sample pressure at various diver pressures.

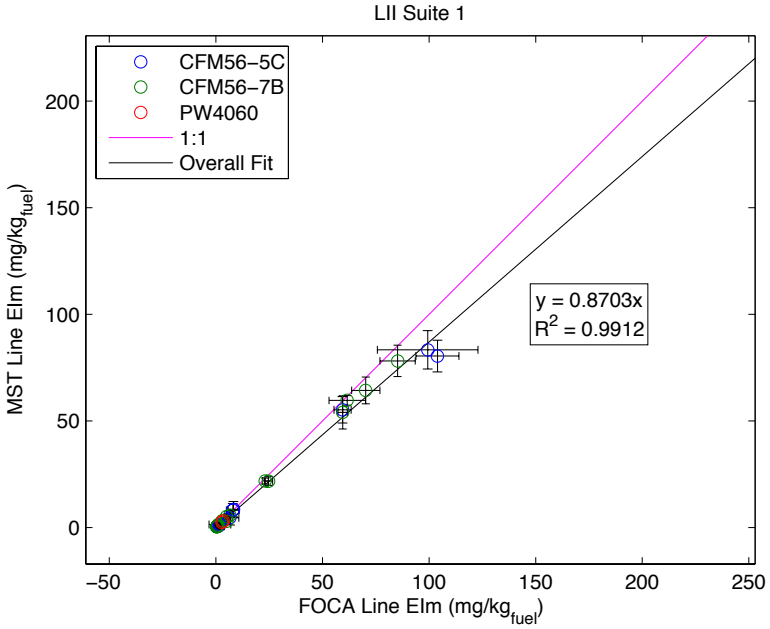

Figure C.3: Line comparison for the LII in suite 1. Overall the LII in suite 1 showed a 13.0% difference between the two lines.

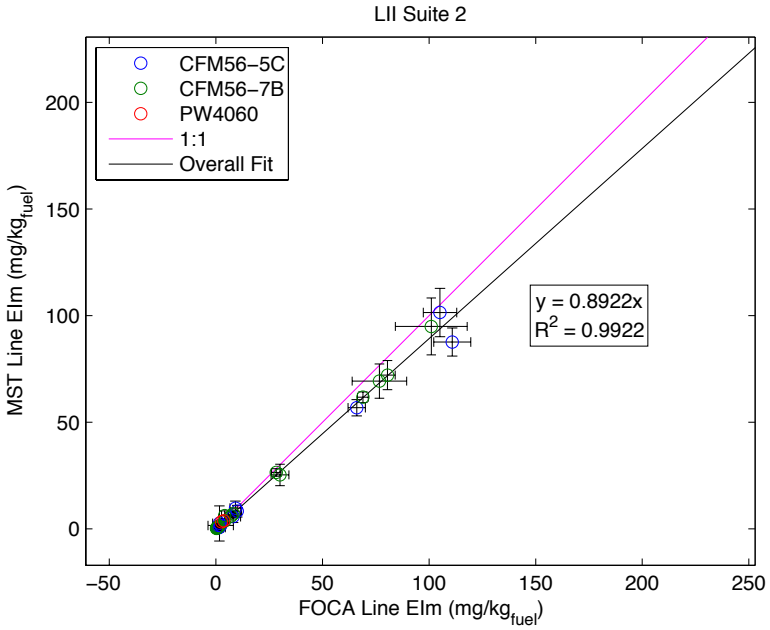

Figure C.4: Line comparison for the LII in suite 2. Overall the LII in suite 2 showed a 10.8% difference between the two lines.

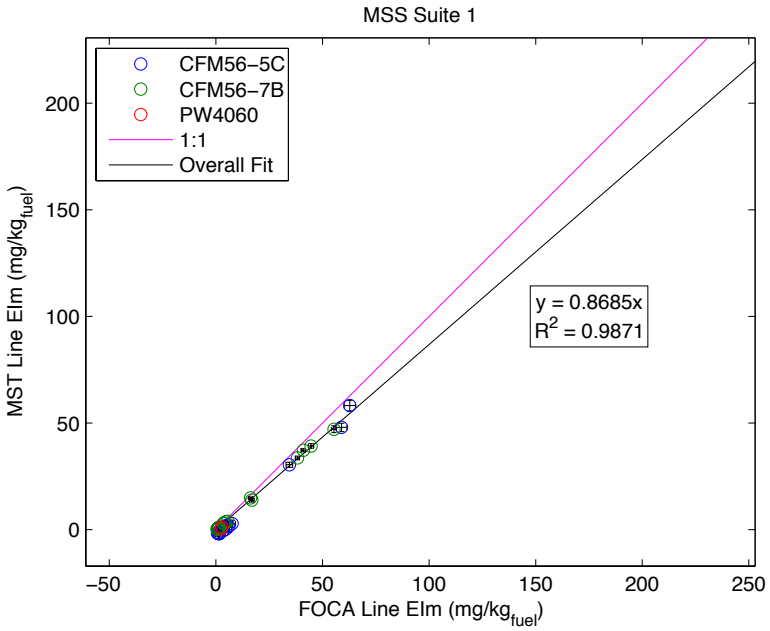

Figure C.5: Line comparison for the MSS in suite 1. Overall the MSS in suite 1 showed a 13.2% difference between the two lines.

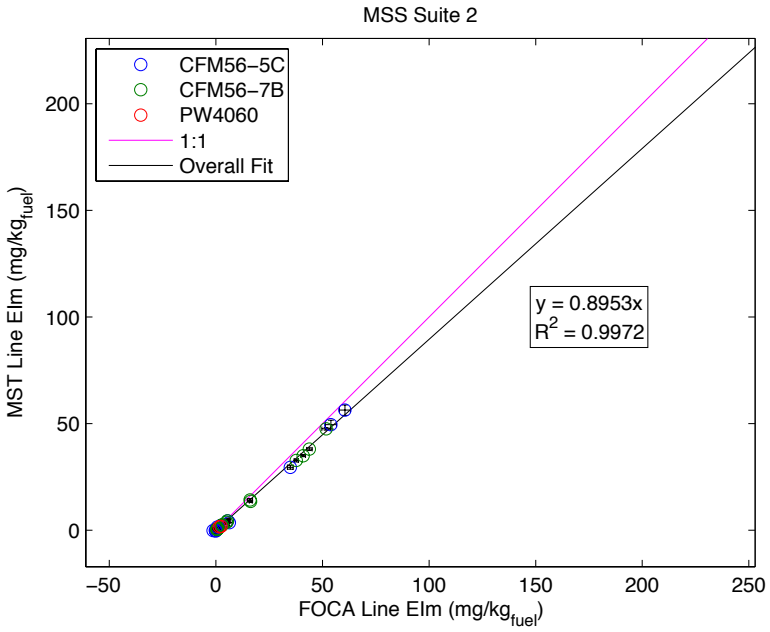

Figure C.6: Line comparison for the MSS in suite 2. Overall the MSS in suite 2 showed a 10.5% difference between the two lines.

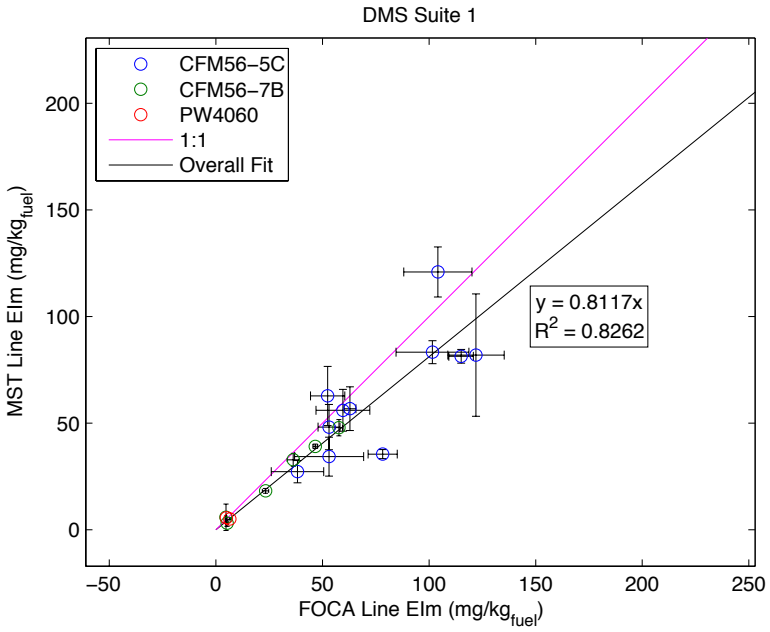

Figure C.7: Line comparison for the DMS (mass) in suite 1. The DMS was switched in and out opposite of the MAAP. Overall the DMS in suite 1 showed a 18.8% difference between the two lines.

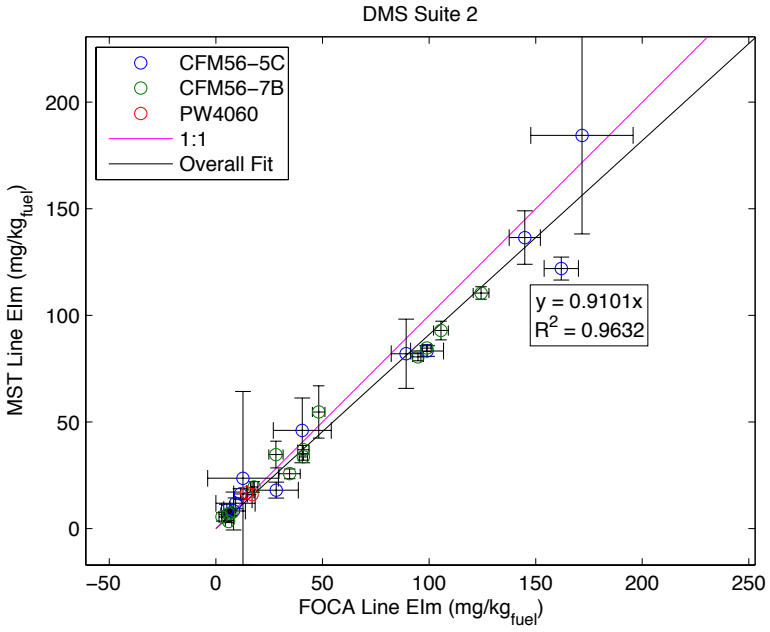

Figure C.8: Line comparison for the DMS (mass) in suite 2. Overall the DMS in suite 2 showed a 9.0% difference between the two lines.

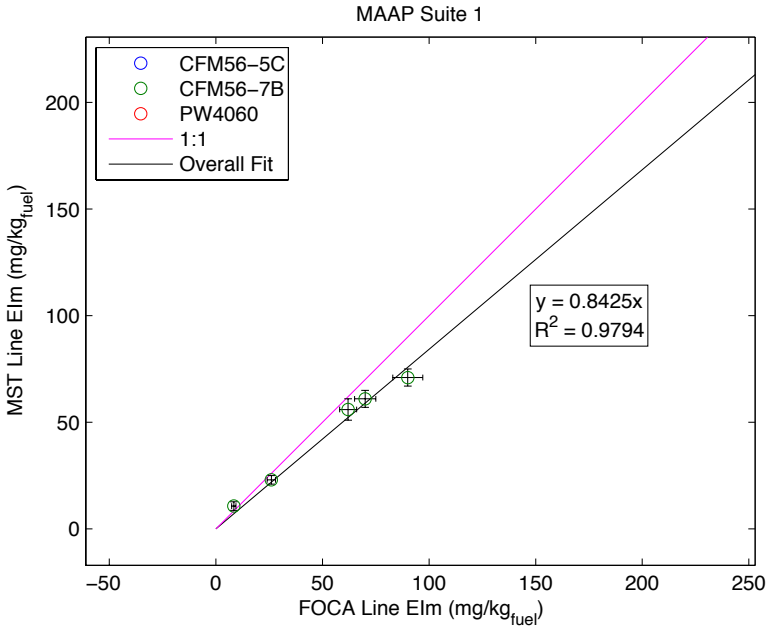

Figure C.9: Line comparison for the MAAP in suite 1. The MAAP was switched in and out opposite of the DMS in suite 1 and only had test points for the CFM56-7B. For the CFM56-7B engines it showed a 15.8% difference between the two lines.

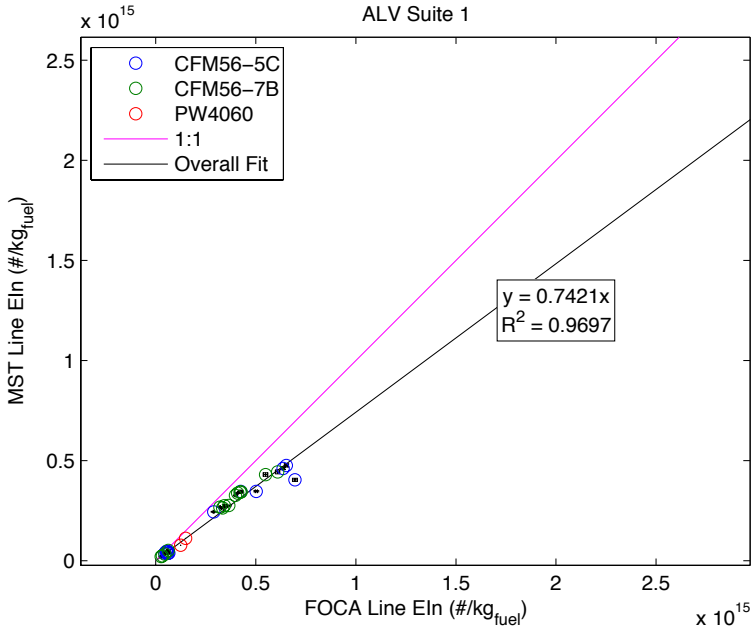

Figure C.10: Line comparison for the AVL in suite 1. Overall the AVL in suite 1 showed a 25.8% difference between the two lines.

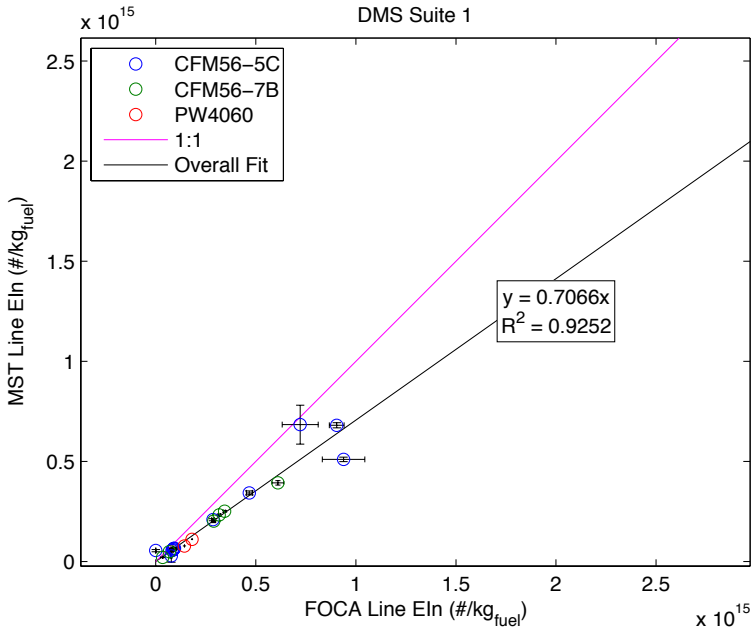

Figure C.11: Line comparison for the DMS (number) in suite 1. Overall the DMS in suite 1 showed a 29.3% difference between the two lines.

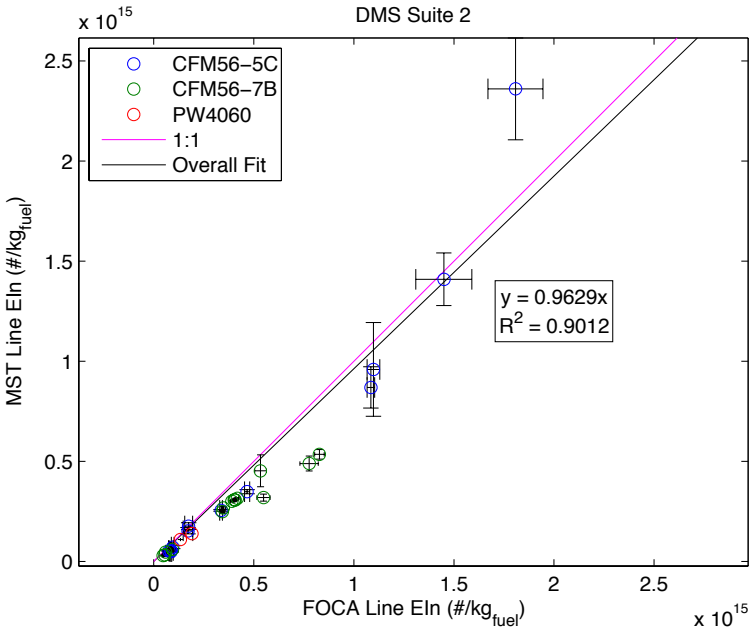

Figure C.12: Line comparison for the DMS (number) in suite 2. Overall the DMS in suite 2 showed a 3.7% difference between the two lines.

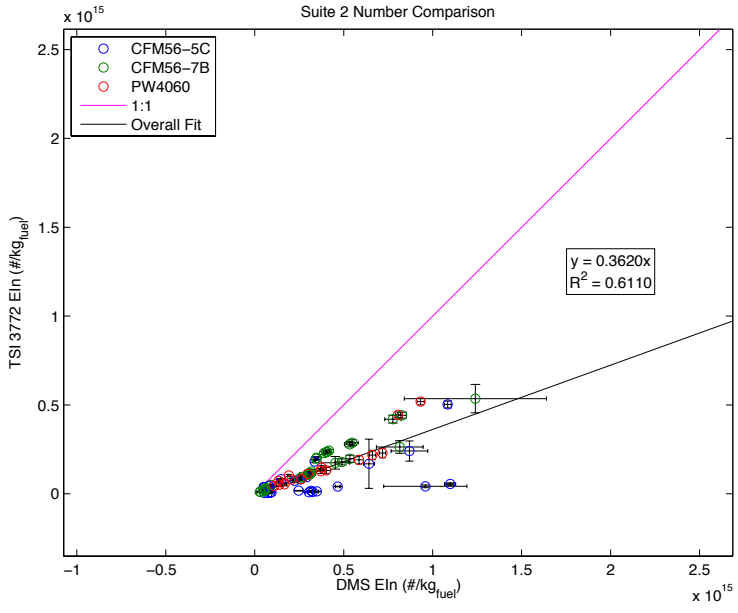

Figure C.13: CPC Cutoff Size 10 nm. TSI 3772.

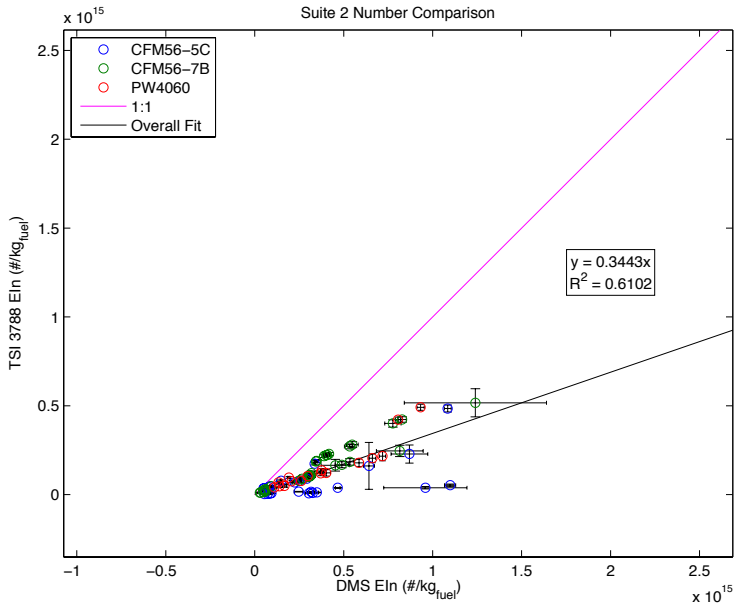

Figure C.14: CPC Cutoff Size 2.5 nm. TSI 3788.

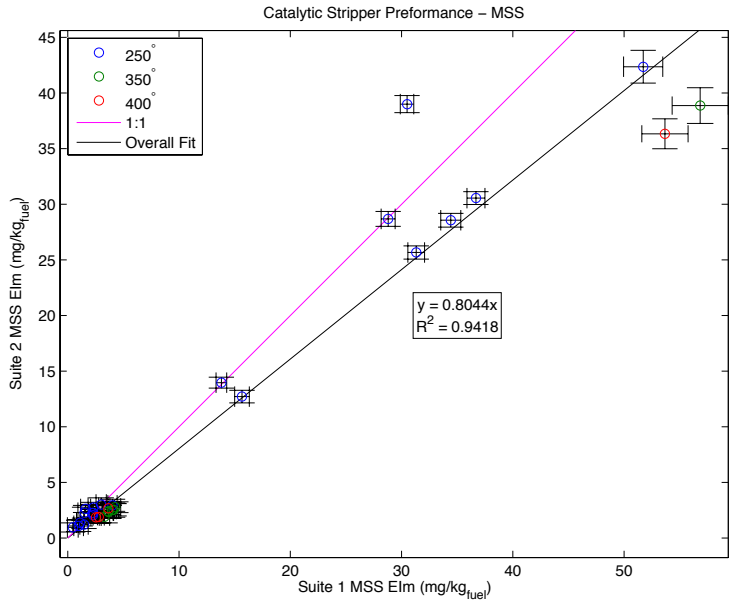

Figure C.15: MSS comparison with catalytic stripper inserted before instruments on Suite 2.

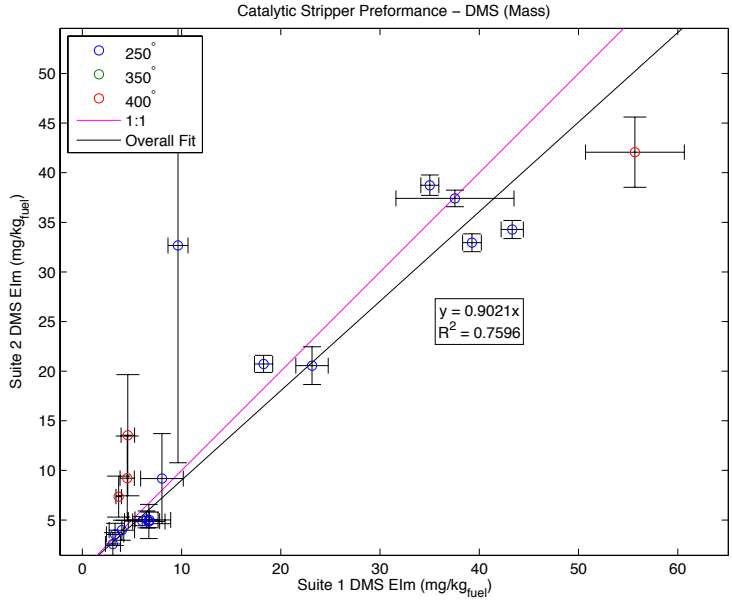

Figure C.16: DMS mass comparison with catalytic stripper inserted before instruments on Suite 2.

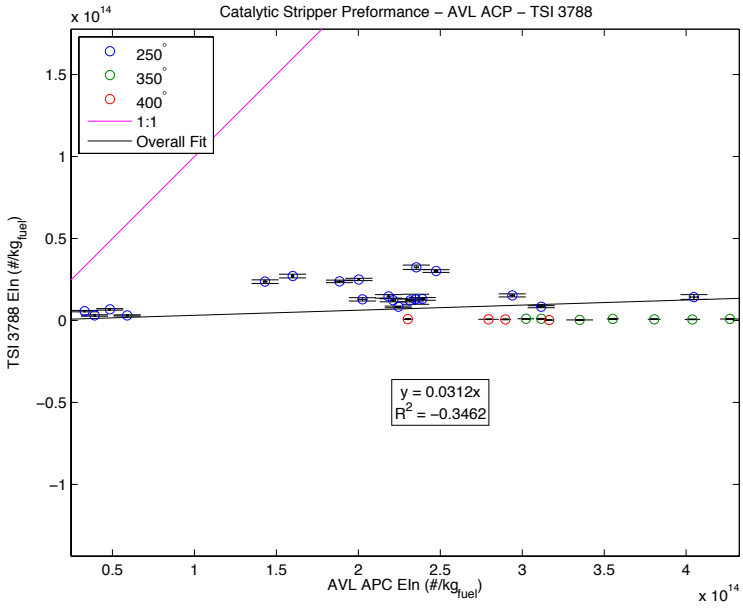

Figure C.17: AVL APC to TSI 3788 number comparison with catalytic stripper inserted before instruments on Suite 2.

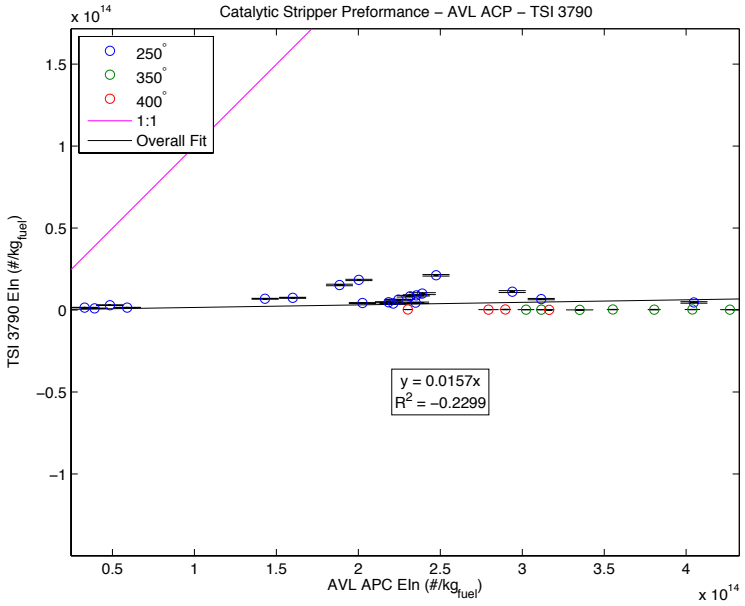

Figure C.18: AVL APC to TSI 3790 number comparison with catalytic stripper inserted before instruments on Suite 2.

BIBLIOGRAPHY

[1] *Annex 16 Environmental Protection - Volume II - Aircraft Engine Emissions*. International Civil Aviation Organization, Montreal, Quebec, Canada, second edition, July 1993.

[2] E-31 Aircraft Exhaust Emissions Measurement Committee, editor. *Aircraft Gas Turbine Engine Exhaust Smoke Measurement [ARP1179D]*. SAE International, Warrendale, Pennsylvania, United States, July 2011.

[3] Icao aircraft engine emissions databank. *http://easa.europa.eu/environment/edb /aircraft-engine-emissions.php*, Jan 2012.

[4] Dane Westerdahl, Scott A. Fruin, Phillip L. Fine, and Constantinos Sioutas. The los angeles international airport as a source of ultrafine particles and other pollutants to nearby communities. *Atmospheric Environment*, 42(13):3143–3155, 2008.

[5] Subhasis Biswas, Philip M. Fine, Michael D. Geller, Suzanne V. Hering, and Constantinos Sioutas. Performance evaluation of a recently developed water-based condensation particle counter. *Aerosol Science Technology*, 39(5):419–427, 2005.

[6] Shishan Hu, Scott Fruin, Kathleen Kozawa, Steve Mara, Arthur M Winer, and Suzanne E Paulson. Aircraft emission impacts in a neighborhood adjacent to a general aviation airport in southern california. *Environmental Science Technology*, 43(21):8039–8045, Nov 2009.

[7] Chowen C. Wey, Bruce E. Anderson, Changlie Wey, Richard C. Miake-Lye, Philip Whitefield, and Robert Howard. Overview on the aircraft particle emissions experiment. *Journal Of Propulsion And Power*, 23(5):898–905, Oct 2007.

[8] C Arden Pope, 3rd and Douglas W Dockery. Health effects of fine particulate air pollution: Lines that connect. *Journal of the Air Waste Management Association*, 56(6):709–742, Jun 2006.

[9] Constantinos Sioutas, Ralph J Delfino, and Manisha Singh. Exposure assessment for atmospheric ultrafine particles (ufps) and implications in epidemiologic research. *Environmental Health Perspectives*, 113(8):947–955, Aug 2005.

[10] ICRP. Human respiratory tract model for radiological protection. icrp publication 66. *Annals Of The ICRP*, 24(1-3), 1994.

[11] William C Hinds. *Aerosol Technology: Properties, Behavior, And Measurement Of Airborne Particles*. Wiley, New York, 2nd edition, 1999.

[12] A Nemmar, P H M Hoet, B Vanquickenborne, D Dinsdale, M Thomeer, M F Hoylaerts, H Vanbilloen, L Mortelmans, and B Nemery. Passage of inhaled particles into the blood circulation in humans. *Circulation*, 105(4):411–414, Jan 2002.

[13] Prashant Kumar, Alan Robins, Sotiris Vardoulakis, and Rex Britter. A review of the characteristics of nanoparticles in the urban atmosphere and the prospects for developing regulatory controls. *Atmospheric Environment*, 44(39):5035–5052, 2010.

[14] H. Horvath. Conference on visibility, aerosols, and atmospheric optics, vienna, september 3-6, 2006. *Atmospheric Environment*, 42(11):2569–2570, 2008. Vienna Visibility Conference 2006.

[15] H. Horvath. Atmospheric aerosols, atmospheric optics and visibility. *Journal Of Aerosol Science*, 25, Supplement 1:23–24, 1994. Abstracts of the 1994 European Aerosol Conference.

[16] Mark Z Jacobson. *Fundamentals Of Atmospheric Modeling*. Cambridge University Press, Cambridge, UK, 2nd edition, 2005.

[17] Susan Solomon. *Climate Change 2007: The Physical Science Basis : Contribution Of Working Group I To The Fourth Assessment Report Of The Intergovernmental Panel On Climate Change*. Cambridge University Press, Cambridge, 2007.

[18] Serena H. Chung and John H. Seinfeld. Climate response of direct radiative forcing of anthropogenic black carbon. *Journal Of Geophysical Research*, 110(D11102), June 2005.

[19] John S. Kinsey. Characterization of emissions from commercial aircraft engines during the aircraft particle emissions experiment (apex) 1 to 3. Technical Report EPA-600/R-09/130, United States Environmental Protection Agency, Oct 2009.

[20] Paul A. Baron. Aerosol calculator, November 2001.

[21] Roger L. Wayson, Gregg G. Fleming, Brian Kim, and Julie Draper. Derivation of a first order approximation of particulate matter from aircraft. Technical Report Paper 69970, Federal Aviation Administration, 2003.

[22] D. L. Champagne. Standard measurement of aircraft gas turbine exhaust smoke. *ASME*, 71-GT-88, 1971.

[23] C. D. Hurley. Smoke measurements inside a gas turbine combustor. *AIAA 93-2070*, 29th Joint Propulsion Conference and Exhibit, 1993.

[24] R. B. Whyte. Alternative jet engine fuels. *AGARD Advisory Report No. 181*, Vol. 2, 1982.

[25] Gayle Ratliff, Christopher Sequeira, Ian Waitz, Theodore Thrasher Melissa Ohsfeldt, Michael Graham, and Terence Thompson. Aircraft impacts on local and regional air quality in the united states. Technical Report Partner Project 15 Final Report, Partnership for AiR Transportation Noise and Emissions Reduction, Oct 2009.

[26] E-31 Aircraft Exhaust Emissions Measurement Committee, editor. *Aircraft Exhaust Nonvolatile Particle Matter Measurement Method Development [AIR6037]*. SAE International, Warrendale, Pennsylvania, United States, March 2010.

[27] E-31 Aircraft Exhaust Emissions Measurement Committee, editor. *Nonvolatile Exhaust Particle Measurement Techniques [AIR5892A]*. SAE International, Warrendale, Pennsylvania, United States, 07 2004.

[28] A. Petzold and F. P. Schröder. Jet engine exhaust aerosol characterization. *Aerosol Science and Technology*, 28(1):62–76, 1998.

[29] Andreas Petzold and Markus Schönlinner. Multi-angle absorption photometry—a new method for the measurement of aerosol light absorption and atmospheric black carbon. *Journal of Aerosol Science*, 35(4):421–441, 2004.

[30] David R Snelling, Gregory J Smallwood, Fengshan Liu, Omer L Gülder, and William D Bachalo. A calibration-independent laser-induced incandescence technique for soot measurement by detecting absolute light intensity. *Applied Optics*, 44(31):6773–6785, Nov 2005.

[31] Wolfgang Schindler, Christoph Haisch, Harald A. Beck, Reinhard Niessner, Eberhard Jacob, and Dieter Rothe. A photoacoustic sensor system for time resolved quantification of diesel soot emissions. *SAE Technical Paper*, 2004-01-0968, 2004.

[32] Peter H. McMurry. The history of condensation nucleus counters. *Aerosol Science and Technology*, 33(4):297–322, 2000.

[33] Richard C. Flagan. History of electrical aerosol measurements. *Aerosol Science and Technology*, 28(4):301–380, 1998.

[34] H. Tammet, A. Mirme, and E. Tamm. Electrical aerosol spectrometer of tartu university. *Atmospheric Research*, 62(3-4):315–324, 2002.

[35] Otmar Schmid, Donald E. Hagen, Philip D. Whitefield, Max B. Trueblood, Andrew P. Rutter, and H. V. Lilenfeld. Methodology for particle characterization in the exhaust flows of gas turbine engines. *Aerosol Science And Technology*, 38(11):1108–1122, 2004.

[36] Tami C. Bond, Theodore L. Anderson, and Dave Campbell. Calibration and intercomparison of filter-based measurements of visible light absorption by aerosols. *Aerosol Science and Technology*, 30(6):582–600, 1999.

[37] Paola Massoli, Paul L. Kebabian, Timothy B. Onasch, Frank B. Hills, and Andrew Freedman. Aerosol light extinction measurements by cavity attenuated phase shift (caps) spectroscopy: Laboratory validation and field deployment of a compact aerosol particle extinction monitor. *Aerosol Science and Technology*, 44(6):428–435, 2010.

[38] John T. Jayne, Danna C. Leard, Xuefeng Zhang, Paul Davidovits, Kenneth A. Smith, Charles E. Kolb, and Douglas R. Worsnop. Development of an aerosol mass spectrometer for size and composition analysis of submicron particles. *Aerosol Science And Technology*, 33(1-2):49–70, 2000.

[39] J. D. Andersson. *UK Particle Measurement Programme - Heavy Duty Methodology Development Final Report, Report DP 02/2493*. Ricardo Consulting Engineers, Ltd., Shoreham-By-Sea, West Sussex, UK, 31, July 2002.

[40] UNECE. *Uniform Provisions Concerning The Approval Of Vehicles With Regard To The Emission Of Pollutants According To Engine Fuel Requirements*. Apr 2011. Addendum 82: Regulation No. 83.

[41] Engine-testing procedures. *U.S. Code Of Federal Regulations - Title 40 - Protection Of Environment*, Volume 33(Part 1065), July 2011.

[42] Barouch Giechaskiel, Massimo Carriero, Giorgio Martini, and Jon Andersson. Heavy duty particle measurement programme (pmp): Exploratory work for the definition of the test protocol. *SAE International Journal Of Engines*, 2:1528–1546, 06 2009.

[43] M. Matti Maricq, Richard E. Chase, Diane H. Podsiadlik, and Rainer Vogt. Vehicle exhaust particle size distributions: A comparison of tailpipe and dilution tunnel measurements. *SAE International*, 05 1999.

[44] Barouch Giechaskiel, Leonidas Ntziachristos, and Zissis Samaras. Effect of ejector dilutors on measurements of automotive exhaust gas aerosol size distributions. *Measurement Science and Technology*, 20(4):045703, 2009.

[45] "laser induced incandescence lii". *http://www.artium.com/cgi-bin/DJgallery.cgi?T=products.htmlZONE=LII*, July 2014.

[46] "avl particle counter". *https://www.avl.com/particle-counter*, July 2014.

[47] "avl micro soot sensor". *https://www.avl.com/micro-soot-sensor*, July 2014.

[48] "fast response aerosol size measurements with the dms 500". *http://www.cambustion.com/products/dms500/aerosol*, June 2014.

[49] "minicast series 6200". *http://www.sootgenerator.com/miniCAST_g.htm*, June 2014.

[50] "li-840a co2/h2o analyzer". *http://www.licor.com/env/products/gas$_a$nalysis/LI−840A/*, *July*2014.

[51] Sable Systems International. The sable systems ca–2a carbon dioxide analyzer instruction manual. Las Vegas, NV.

[52] "5012 multiangle absorption photometer (maap)". *http://www.thermoscientific.com/content/tfs/en/product/5012-multiangle-absorption-photometer-maap.html*, July 2014.

[53] "condensation particle counter 3772". *http://www.tsi.com/ProductView.aspx?id=22965*, July 2014.

[54] "condensation particle counter 3775". *http://www.tsi.com/ProductView.aspx?id=22963*, July 2014.

[55] "nano water-based condensation particle counter 3788". *http://www.tsi.com/ProductView.aspx?id=21938*, July 2014.

[56] "engine exhaust condensation particle counter 3790a". *http://www.tsi.com/Engine-Exhaust-Condensation-Particle-Counter-3790/*, July 2014.

[57] Benjamin Y.H Liu and David Y.H Pui. A submicron aerosol standard and the primary, absolute calibration of the condensation nuclei counter. *Journal of Colloid and Interface Science*, 47(1):155 – 171, 1974.

[58] Cambustion. Calibration of dms series fast particulate spectrometers, 2008.

[59] *NIOSH Method 5040, Elemental Carbon (Diesel Particulate)*, volume 3. NIOSH Manual of Analytical Methods, 3003.

VITA

Brian Lowell Catron was born to Kevin and Nila Catron in Jacksonville Florida. He received his B.S. with Honors in Aerospace Engineering in May 2010 from the Missouri University of Science and Technology. He went on to receive his M.S. degree in Aerospace Engineering from Missouri S&T in August 2014. During his schooling, Brian worked for the Missouri S&T Center of Excellence for Aerospace Particulate Emissions Reduction Research. He was inducted into Sigma Gamma Tau in 2005.